Chapter 3

Iron oxide nanocubes as a platform for tumor targeting, oxaliplatin delivery and magnetic hyperthermia

...

3.1. Introduction

Nanotechnology offers the possibility to exploit and modulate materials' properties at the nanoscale providing sustainable and effective cancer therapies. Nowadays, combinatorial therapies *(i.e.* chemotherapy with radiotherapy, combinatorial anti-tumoral drugs, hyperthermia with chemotherapy, *etc.*) are preferably used as clinical treatment against cancer. However, the development of a nanotool gathering different therapeutic properties is still challenging. The present project concern the use of nanocubes (NCs) for the development of a multimodal strategy for cancer treatment.[1, 2] In particular, the here developed project aimed to target ovarian cancer. Epithelial ovarian cancer (EOC) is the leading cause of death from gynecological malignancies due to late diagnosis and high frequency of relapse occurrence.[3, 4] Currently, the standard of care for ovarian cancer is aggressive surgical debulking followed by platinum and taxane based combination chemotherapy.[5] The initial treatment is typically effective in approximately 70% of patients, resulting in a partial or complete response. Tragically, the majority of patients will have a relapse of their disease in less than 5 years.[5] So far, few examples of nanomedicines are known to target ovarian cancer,[6, 7] both in an active or passive manner and using single drugs (Kadcyla® or T-DM1, an antibody-conjugated mertansine) or a drug formulation (*i.e.* Doxil®, loading carboplatin/paclitaxel).[8] Thus, in order to improve the available nanosystems and ameliorate the diagnostic/therapeutic efficiency of nanomedicines against ovarian cancer, more specific drug delivery agents, associated with different therapeutic modalities which are possibly translated in more effective treatments, are needed. Recently, *Quarta et al*. developed a nanosystem based on spherical Fe_2O_3 nanoparticles for targeting ovarian cancer cells.[4] Differently from that study, our project used cubic shaped nanoparticles instead of spherical nanoparticles. The advantage of using nanocubes relies on their higher efficiency as nanoheaters than spherical nanoparticles, as already shown in detail in the introduction.[9] This feature makes nanocubes an appealing choice for hyperthermia treatment, thus adding a therapeutic purpose to the nanosystem. Moreover, by varying the nature of the surface modification of these nanocubes, we were also able to obtain nanoparticles bearing drug delivery functionality, adding further relevance for therapy. The drug delivery ability was obtained by the use of a platinum drug. Platinum drugs represent an important class of anticancer drugs, even taking their severe side effects and intrinsic or acquired resistance to the treatment into account (**Figure 1b**).[10, 11] Multiple cellular events appear to contribute to their cytotoxic effects.[10] Among them, the most crucial step is the platination of DNA leading to the formation of Pt-DNA adducts, which disrupt essential processes of the cell life, like DNA replication or transcription, leading to apoptosis (**Figure 1a**).[10, 12, 13] Cisplatin (**Figure 1**), the first clinically used platinum-based drug, was discovered fortuitously for its anticancer activity in the late 1960s.[12] As first generation of platinum anticancer drug, cisplatin is active against solid neoplasms, including ovarian, testicular, bladder, colorectal, lung and head and neck cancers.[10]

Despite this wide spectrum of activity, its clinical use is limited by its severe toxicity and the existence or development of resistance.[12] For those reasons the second-generation platinum drug carboplatin was developed (*cis*-diamine (1,1-cyclobutane dicarboxylate) platinum(II), **Figure 1b**). Compared to cisplatin, carboplatin possesses low reactivity and, therefore, lower toxicity and is suitable for aggressive dose-dependent chemotherapy. However, its spectrum of activity is more limited compared to that of cisplatin and its efficacy against several kind of cancers is modest. Moreover, carboplatin presents significant problems associated with tumor resistance, which restrict its clinical use.[10] Further improvements in the direction of the synthesis of better platinum-based drugs were achieved with the third-generation drug oxaliplatin (**Figure 1b**).[14] The introduction of the lipophilic 1,2-diaminocyclohexane (DACH) increases passive uptake of the compound compared to cisplatin and carboplatin.[10] Additionally, the bidentate oxalate significantly reduces its reactivity, thus limiting the toxic side effects of oxaliplatin.[10] In combination with 5-fluorouracil and folinate (Leucovorin), this drug is used for an efficient treatment of adjuvant and metastatic colorectal cancer intrinsically insensitive to cisplatin. However, also the oxaliplatin efficacy is compromised by its dose limit toxicity, including peripheral neuropathy and neurotoxicity. Therefore, the broader scientific and pharmaceutical community is in need of novel strategies for selective delivery of chemotherapeutics to tumor tissues. The development of such strategies may lead to enhanced therapeutic efficacy that will directly benefit cancer patients.[15]

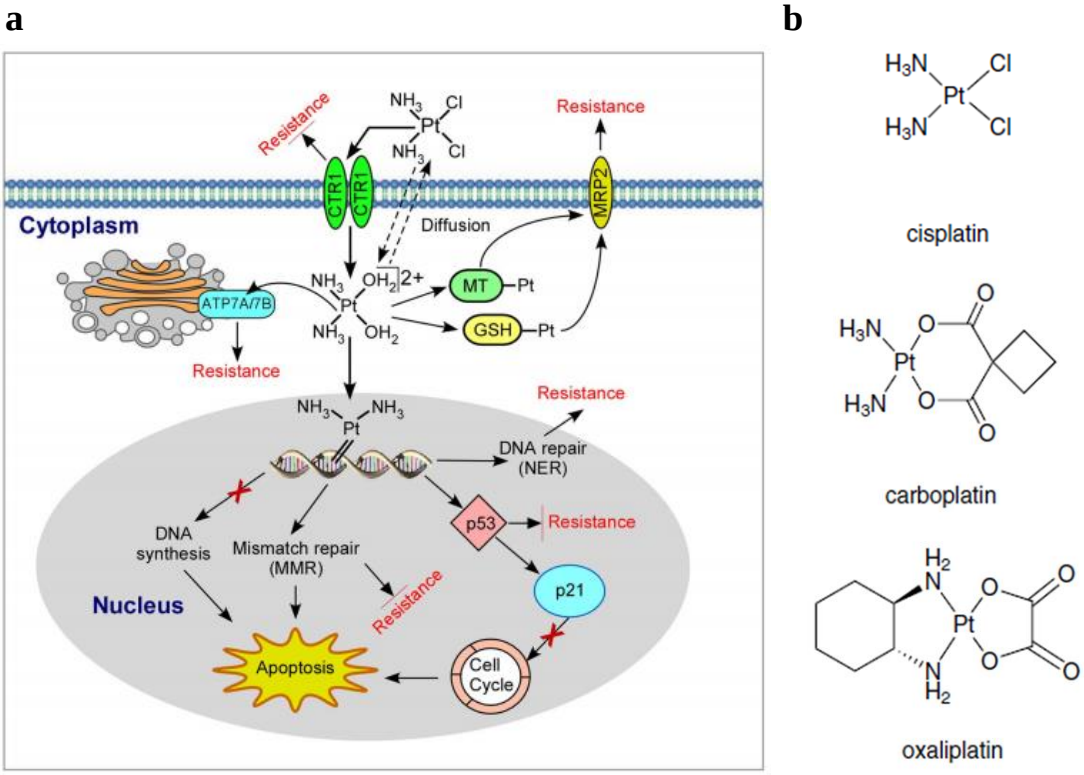

Figure 1. Platinum drugs. **a)** Schematic representation of the action of cisplatin inside the cells. The resistance pathways are also shown. This scheme can be considered as the general route by which platinum-based drug elicit their toxic action.[10] *(a-b) Reprinted from Cancer Chemother Pharmacol, Platinum-based drugs: past, present and future (2016) 77:1103, Dilruba, S. & Kalayda, G.V., with pemission of Springer (© Spinger-Verlag Berlin Heidelberg 2016).*

Taken all these issues into account, the here proposed and developed drug delivery strategy, relies on the use of an oxaliplatin-derived PEG molecule.[16] The molecule was synthetized by our collaborator from the University of Santiago de Compostela (Department of Organic Chemistry and Center for Research in Biological Chemistry and Molecular Materials, CIQUS) and was designed for a pH responsive release of the active oxaliplatin molecules from the PEG scaffold, upon the cleavage of an acid-sensitive functional group. Thus, this modified version of oxaliplatin acquired intrinsic selectivity and a targeting feature, being released selectively at intracellular low pH (or at the site of actively proliferating tumors). In addition to hyperthermia and drug delivery, the third feature introduced to the NCs was the targeting. The nanoparticles developed by Quarta *et al*. were functionalized with a fragment antigen-binding (Fab) of the human folate receptor antibody. Instead, in our study the single-chain fragment variable recombinant antibodies (scFv) version was chosen(kindly provided by Fondazione IRCCS, Istituto Nazionale dei Tumori).[17] Within a size of 25 kDa, significantly smaller than an entire monoclonal antibody (mAb, ca. 150 kDa), scFv is more stable and did not present a high immunogenic profile.[18] Even if it expresses a reduced affinity for its target, the folate receptor alfa (αFR), compared to its parent entire antibody, the binding at high density on the surface of the nanoparticles may result into an increase of the number of the interactions with the target (avidity), compensating the reduction of affinity. The advantage in using scFv compared to other folate receptor ligands (*e.g.* folic acid or folinic acid) derives from its specificity restricted to epithelial ovarian cancer (EOC) cells and not towards other non-cancer cells (*e.g.* macrophages). The antibody binding was reached using the histidine tag chemistry. For this purpose, the scFv antibody was provided with a histidine tag (His-Tag), a peptide sequence of six histidine molecules linked to the polypeptidic chain of scFv. Light variable chains are separated each other by a spacer of Gly-Ser (NCO-serine-glycine-glycine-glycine-glycine-serine-glycine-glycine-glycine-glycine-serine-CON) which ensured a certain degree of freedom and distance from the tag, with respect to the scFv polypeptidic chain. Thanks to this tag, it is possible to bind the antibody to the nanoparticles previously functionalized with *N*,*N*-(carboxymethyl) lysine (Lys-NTA, here named NTA), a derivative of nitrilotriacetic acid. This molecule has three carboxylic groups, which are able to coordinate, together with the ternary amine of the nitrilotriacetic acid, a nickel cation resulting in the formation of a complex with histidine (**Figure 2**).

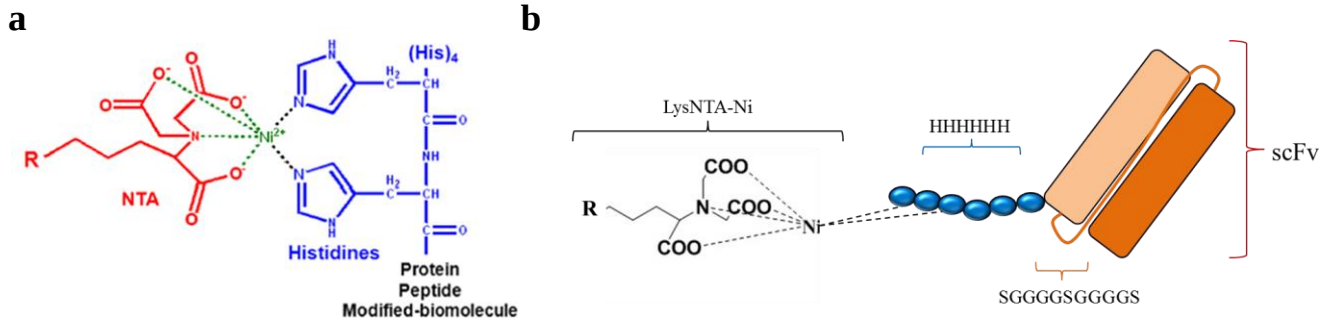

Figure 2. Scheme of the NTA-Ni chemistry [19]. (a) Chemistry of the binding of NTA-Ni to the His-tag. **(b)** Chemistry of the binding of scFv_C4 to the nanocubes. The binding is mediated by NTA-Ni / His-tag interaction. A sequence composed of Gly and Ser (SGGGGSGGGGS) was also cloned in the antibody fragment, in order to confer spacing and mobility to the biomolecule. *(a) Reprinted with permission from Kim E. Sapsford, W. Russ Algar, Lorenzo Berti, Kelly Boeneman Gemmill, Brendan J. Casey, Eunkeu Oh, Michael H. Stewart, and Igor L. Medintz, Chem. Rev.*, 2013, *113 (3), pp 1904–2074. Copyright © 2013 American Chemical Society.*

The binding chemistry chosen not only provides a controlled orientation of the biomolecules on the nanoparticles surface, but also offers the possibility to switch to different antibodies, making these nanoobjects interchangeable and multitasking. In order to equip the nanocubes with the scFv and oxaiplatin molecules, the functionalization procedure schematically shown in **Figure 3** was applied. Briefly, first the functionalization with the drug delivery platinum-based molecules was carried out (**2**), paying attention to avoid the saturation of the free carboxylic groups of the polymeric shell. Afterwards, the PEG-NTA-Ni targeting molecules were bound (**3**). Subsequently, the scFv was added to the nanocubes and bound *via* His-tag (**4**).

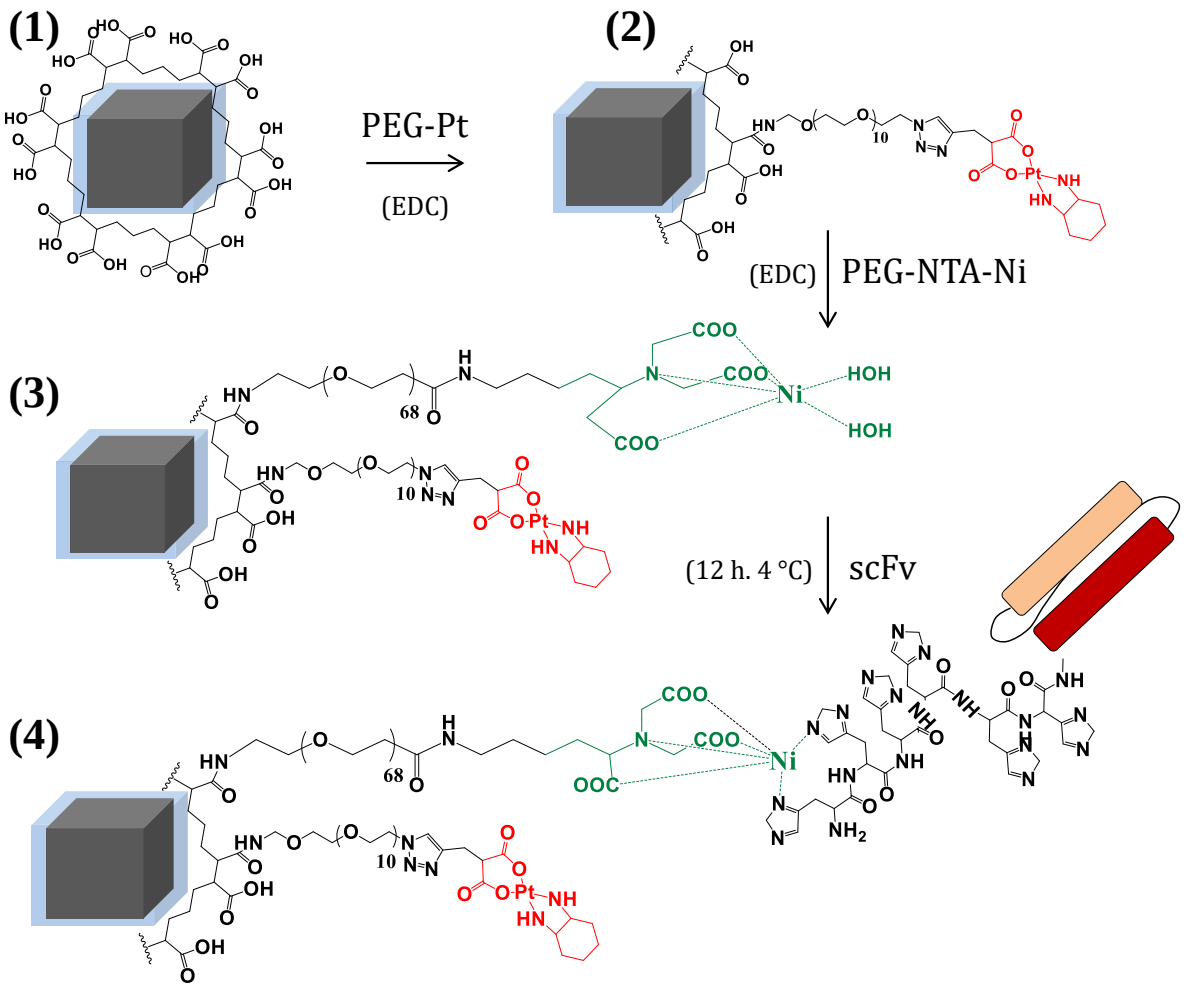

Figure 3. **Scheme of the functionalization strategy of nanocubes**. **(1)** The NCs were transferred in water *via* the polymer coating procedure. **(2)** PEG-Pt drug was bound to the NCs surface. **(3)** PEG-NTA was provided to the nanocubes for the binding of the single chain fragment variable antibody. **(4)** scFv was incubated with the NCs and bound through the interaction of its His-Tag and the NTA-Ni moiety.

By enhancing the intrinsic properties of the material for an efficient hyperthermia and combined targeted drug delivery, the here presented nanocubes become an appealing candidate for a specific and tunable cancer therapy. Until now, only few examples of nanoparticle-based systems able to combine targeting and drug delivery with the intrinsic properties of a material for obtaining a synergistic triple therapeutic effect are reported in literature.[20-23] *Sasikala et al.*[20] presented a system based on spherical iron oxide

nanoparticles for the combinatorial pH-dependent delivery of bertozomib drug and hyperthermia for the treatment of head and neck cancer in mouse model. They successfully demonstrated the combination of the two activities in inducing toxicity, while the single treatments alone were not efficient in killing cancer cells or regressing tumor development. However, as exhaustively explained, nanocubes represent a more interesting and promising choice in term of efficiency for carrying out thermal ablation of cancer, compared to spherical nanoparticles. In addition, they did not bind any targeting agents to the system, a disadvantage compared to our material. *Huang et al.*[21] could functionalize spherical iron oxide nanoparticles with an scFv specific for endoglin, overexpressed on ovarian cancer cells. They also bound on their surface docetaxel for drug delivery purposes. However, the chemistry chosen for the binding of scFv was the EDC. This technique promotes the coupling between amines and carboxylic groups and do not allow governing the binding site and the orientation of the biomolecule on the nanoparticle surface because there is not control over the reactive groups activated on the biomolecule. Moreover, reasonably due to the low heating performance of those nanoparticles, they could not exploit hyperthermia treatment. *Sun et al.*[22] synthesized iron oxide nanoparticles doped with gadolinium for efficient MRI purposes. They also bound folic acid on the nanoparticle surfaces in order to achieve cancer targeting. Furthermore, the encapsulation of cisplatin leaded to the development of a multiple system for targetied drug delivery and imaging. However, the main drawbacks from this work came from the toxicity of the Gd in the nanoparticles shell, the low specificity of folic acid over the folate receptor specimens and the poor solubility of cisplatin for encapsulation purposes. In addition, this kind of nanoparticles was not suitable for hyperthermia treatment. In the last work, *Patra et al.* reached the synthesis of manganese ferrite nanoparticles ($MnFe_2O_4$) able to release curcumin in a thermo-responsive manner and to trigger extremely high heating-mediated hyperthermia. However, they did not test the heating performances on cells. This was probably due to the expected viscosity-dependent behavior of the nanoparticles, which translated to low hyperthermia efficiency in biological environment.

Therefore, the here presented project is an outstanding example of triple-combination for a multi-therapy approach, hitherto not yet pursued by any nanoparticles-based system.

3.2. Results and Discussion

3.2.1 Polymer coating of single nanocubes

As already mentioned, cubic iron oxide nanocubes express interesting magnetic properties in term of magnetic hyperthermia performances. In the here presented project, maghemite (Fe_2O_3) nanocubes (NCs), with an edge size of 14 ± 3 nm, were used **(Figure 4).**

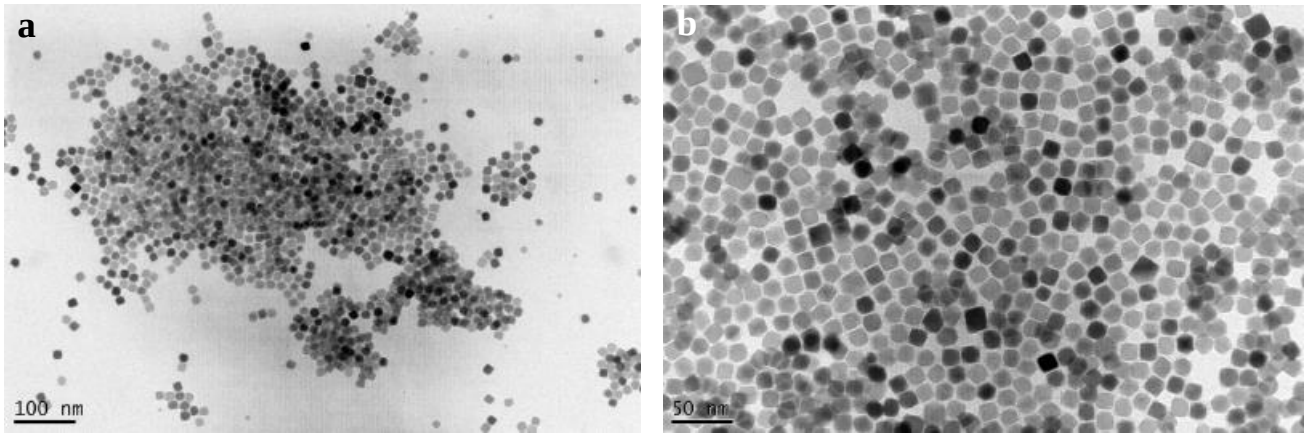

Figure 4. **Transmission Electron Microscopy (TEM) images of 14 nm iron oxide nanocubes in chloroform. a)** Low and high **b)** magnification. The first step to render the iron oxide nanocubes biocompatible is to ensure their solubility and stability in water. As they were synthesized in organic solvents, they are coated with alkyl surfactants molecules, and thus not soluble in aqueous environments. A proper strategy for transferring them in water was required as a first step. For the water transfer of single nanocubes, the polymer coating technique (scheme of **Figure 5**) was applied, following a procedure established in our group and explained in chapter 2.[24-26]

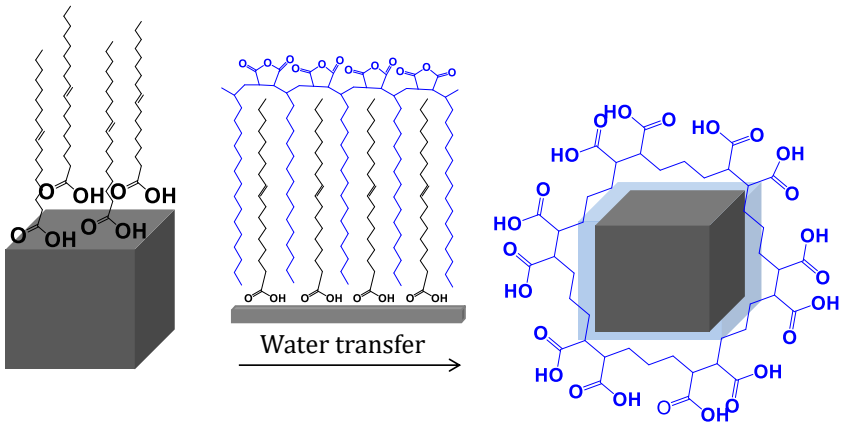

Figure 5. Scheme of the polymer coating procedure. The alkyl-chains of the poly(maleic anhydride-*alt*-1-octadecene) intercalates to the alkyl-chains of the surfactant on the nanocubes. Thus, the hydrophilic region of the polymer points towards the outermost surface of the nanoparticles leading to soluble and stable NCs in aqueous solvent.

The detailed procedure of the polymer coating is shown in materials and methods paragraph. Briefly, after the ultracentrifugation step, set in order to remove the excess of unreacted polymer, gel electrophoresis was carried out to investigate the purity of the obtained sample.[27] The gel image in **Figure 6a** shows that the polymer-coated nanocubes were stable and able to migrate, even if a broad migration band was visible. This indicated a slight degree of aggregation of the sample, which however was not affecting the migration itself and the overall stability of the nanocubes. Moreover, the absence of the fluorescent polymeric band, under irradiation with UV light (in the picture on the right), clearly indicated that the sample is completely clean from the excess of polymer (**Figure 6b**). As further characterization, dynamic light scattering (DLS) analysis was performed. As shown in **Figure 6c**, a number-weighted hydrodynamic diameter of 22 nm was detected. Moreover, a monomodal signal with a narrow size distribution was observed, indicating the presence of stable, single nanoparticles in water and the absence of larger aggregates.

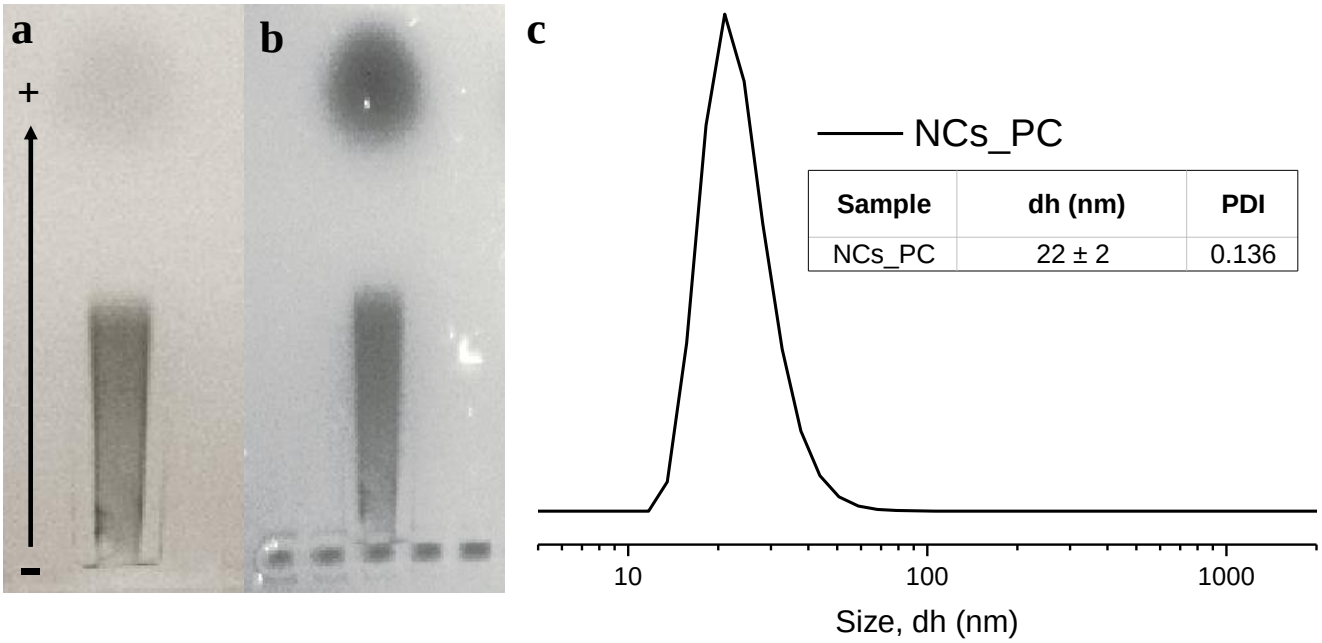

Figure 6. Characterization of nanoparticles after polymer coating procedure. a) and **b)** migration patterns of NCs_PC on an 1% agarose gel. The pictures were acquired under white light (**b**) and under UV light (**c**) with a 430 nm filter, the latter in order to detect the presence of free polymer. The black spot at the top of the gel is due to the presence of orange g solution (the loading buffer), used to trace the migration. **c)** The DLS graph shows the size weighted by number of the nanocubes (NCs) transferred in water using the polymer coating procedure. Table in the inset reports the obtained hydrodynamic diameter (dh) and polydispersity index (PDI).

TEM measurements further confirmed the presence of isolated polymer coated nanocubes. Interestingly, also the polymeric shell was clearly visible (**Figure 7 7**; red arrow).

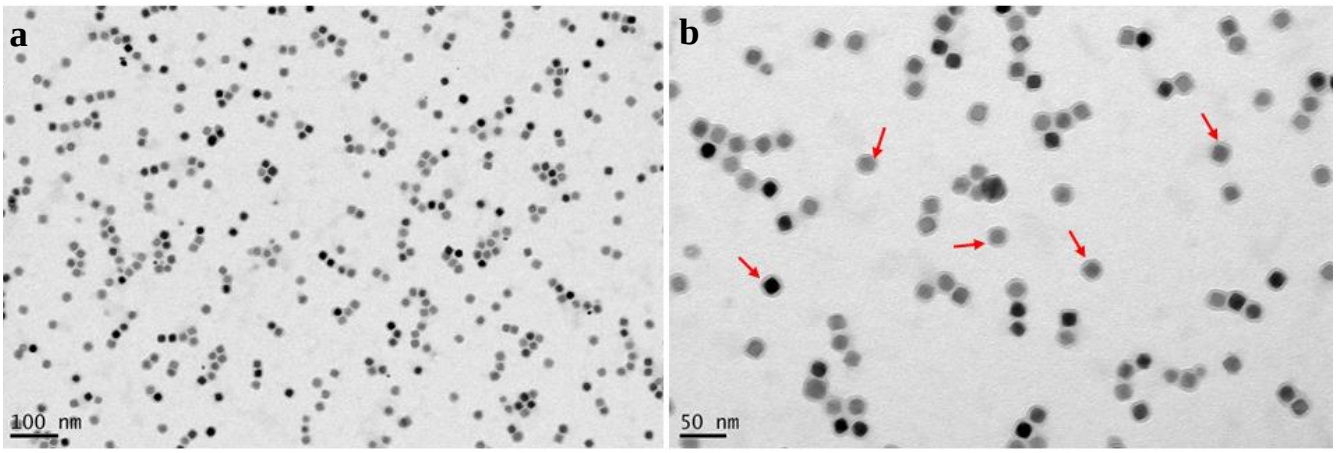

Figure 7 TEM micrographs of polymer coated iron oxide NCs. a) low and **b)** high magnification. The red arrows indicate the presence of the polymeric shell around the nanocubes.

3.2.2 Magnetic characterization of polymer-coated nanocubes

The specific absorption rate (SAR) of the PC-NCs was determined by exposing the NCs in water solution to an alternating magnetic field generated by a coil inside a commercial available device (DM100 Series, nanoScale Biomagnetics Corp.). The SAR values, measured at two different frequencies (110 kHz and 301 kHz) and different magnetic field amplitudes (in the range between 12 and 24 kAm^{-1}), showed linear increase proportional to the strength of the magnetic field applied, as expected for superparamagnetic nanoparticles (**Figure 8a**).[28] The heating performances were also determined in viscous media. The water-glycerol (W:Gly) mixtures were set to 64:36 v%, 32:68 v%, and 19:81 v%, corresponding to a mean η of 3.8, 24, 97.3 mPa.s.[29] Interestingly, the nanocubes kept high SAR values, independently from the media viscosity (**Figure 8b**), making them appealing for exploiting an efficient hyperthermia on cells. In order to further investigate the magnetic relaxation process of the nanocubes AC susceptibility (ACS) measurements were performed in media at different viscosity. The nanocubes were dissolved in water or water-glycerol mixtures at the fixed iron concentration of 1 g/L. As shown in **Figure 9**, the real (χ'_{AC}) and imaginary (χ''_{AC}) parts of AC susceptibility reflected the contribution of the sole Néel relaxation. Indeed, both assuming a cubic shape or a spherical shape of the nanocubes after the polymer coating, the Brownian time constant calculation gave ω equal to 110 kHz and 213 kHz respectively. χ'AC was decaying down to zero at high frequencies and χ"AC exhibited a pronounced maximum at ca. 900 kHz, the latter related to Néel relaxation and its position remained constant regardless of the sample viscosity. The anisotropy constant (K) value obtained was K= 11.9 kJ/m^3, very close to pure magnetite structure (13 kJ/m^3).[29] These data confirmed that the nanocubes relaxed purely via Néel mechanism in a viscosity free manner, as expected.[29] The feature is extremely important for an *in vivo* application, since it was demonstrated that the interaction with cell membranes, when the nanoparticles are bound on the cell surface or internalized, could compromise the heating performance of these nanoobjects, which mainly relax by Brownian.[30] On the opposite, Néel relaxation is insensitive to the viscosity of the surrounding environment, thus allowing the nanoparticles to not lose their heating performance.

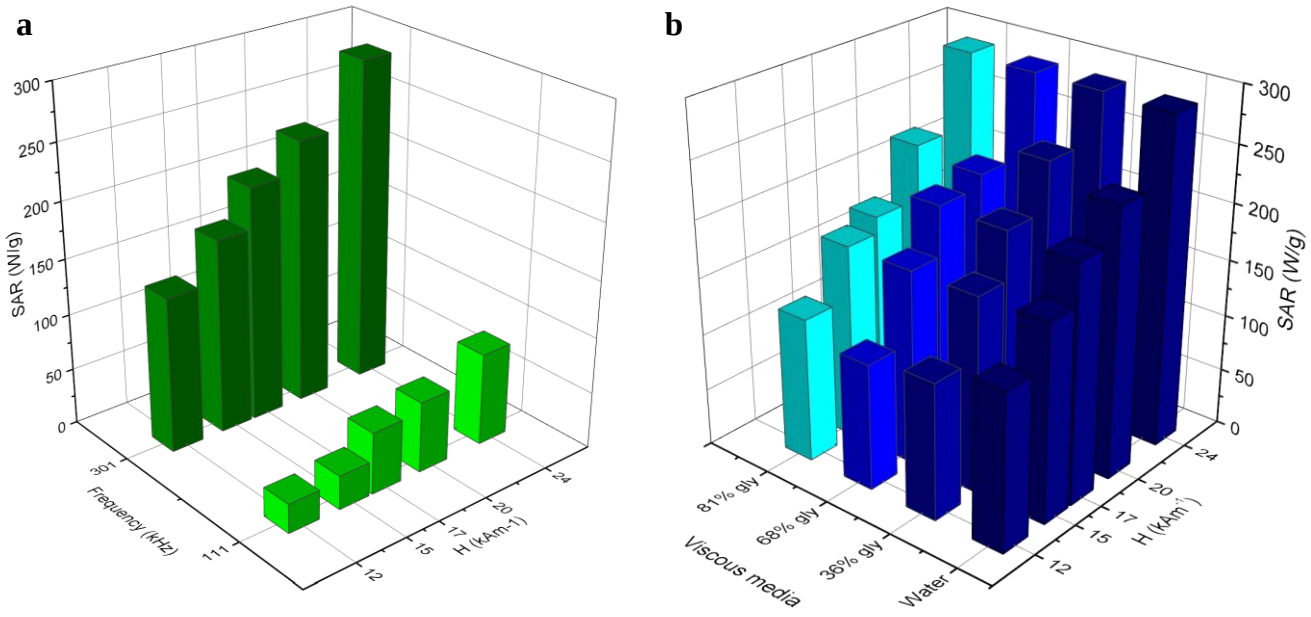

Figure 8. Specific absorption rate (SAR) characterization for the 14 nm nanocubes. a) SAR values as a function of five magnetic field amplitudes (12, 15, 17, 20 and 24 kAm^{-1}) at the frequencies of 111 kHz (light green bars) and 301 kHz (dark green bars). **b)** SAR values plotted as a function of five magnetic field amplitudes (12, 15, 17, 20 and 24 kAm^{-1}) measured in different viscous media (water, 81%, 68% and 36% glycerol), at 301 kHz.

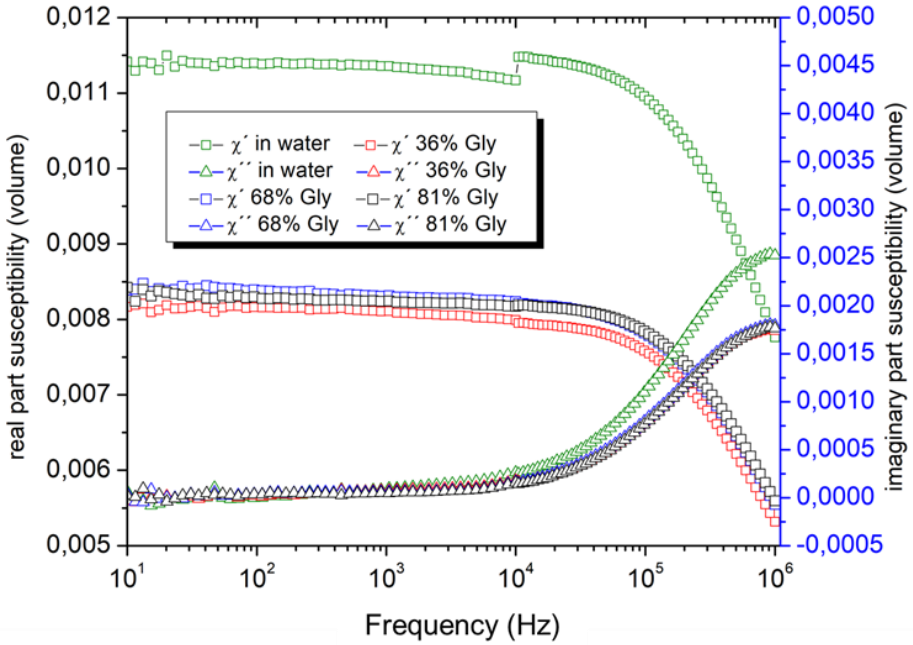

Figure 9. AC susceptibility analysis. Frequency dependence of χ'_{AC} (square dots) and χ''_{AC} (triangle-shaped dots) for 14 nm nanocubes dispersed in water (light green dots), 36% glycerol (red dots), 68% glycerol (blue dots) and 81% glycerol (dark green dots). K = 11.9 kJ/m^3, calculated according to the equation (2) showed in "materials and methods" paragraph.

3.2.3 Deprotection of the PEG-Pt ligand: providing drug delivery feature

The drug delivery strategy here proposed and developed, relies on the use of an oxaliplatin-derived PEG molecules,[16] as explained in the "introduction". The molecule is shown in **Figure 10** (Mn = ~ 1,000 g/mol -NR649 batch-).[16] After the deprotection of the amine group from the triphenylmethane-protecting group (**Figure 11**), the molecule was suitable for the binding to the nanocubes *via* EDC chemistry.

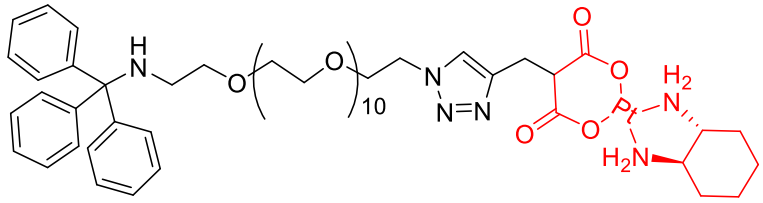

Figure 10 Oxaliplatin-derived PEG molecules (PEG-Pt) used for drug delivery. In red is underlined the oxaliplatin moiety.

The deprotection of the amine group was carried out in methanol, using Amberlite resin (IR-120) (**Figure 11a**). After 12 h of stirring, the obtained mixture was filtered and analyzed *via* thin-layer chromatography (TLC) (**Figure 11b)**. After the deprotection, the triphenylmethane protecting group signal (dark spot) shifted, migrating more (B, black arrow) in comparison to the pristine compound not deprotected (A, red arrow), indicating that it is bound to the PEG (which instead does not migrate). This data demonstrated the removal of triphenylmethane from the PEG compound.

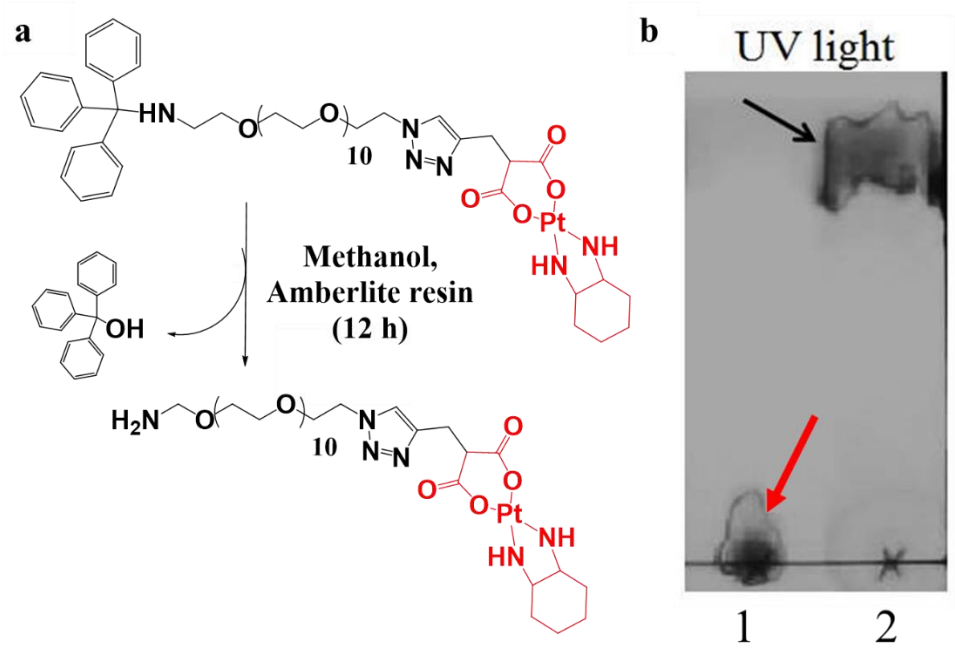

Figure 11 Deprotection scheme of the amine group of the PEG-Pt. **(a)** The compound, dissolved in methanol, was stirred with the Amberlite resin for 12 h. The deprotected compound was recovered by filtration. Thin-layer chromatography (TLC) on silica plate for the protected PEG-Pt (1) and the deprotected product (2). The image was acquired under UV light (254 nm filter). The arrows indicate the signal coming from the aromatic rings of triphenylmethane in the pristine compound (red arrow) and in the deprotected compound (black arrow). Mobile phase: 10% CH_3OH in CH_2Cl_2.

3.2.4 PEG-NTA-Ni synthesis: providing targeting feature

A strategy for developing a targeting chemistry was also planned. To do this, a PEG molecule derivatized with Lys-NTA was synthesized. Given the high affinity of the binding between *N*, *N*'-(carboxymethyl) lysine, Ni and histidine (with a dissociation constant of ca. $K_d = 10^{-13}$ M),[31] the chosen chemistry enables a quasi-covalent attachment of the antibody fragment to the nanocubes. Moreover, this strategy enables to bind biomolecules in a controlled and oriented manner, depending on the position of His-Tag inside the antibody, carefully designed during the cloning, thus resulting in a more precise bioconjugation.[32] In detail, starting from a procedure found in literature,[33] Fmoc-PEG-COOH (Mn = 3,000 g/mol) was reacted with *N*-hydroxysuccinimide (NHS) in DCM at 6 °C using an ice bath, in order to activate the carboxylic group, as depicted in the scheme of **Figure 12**.

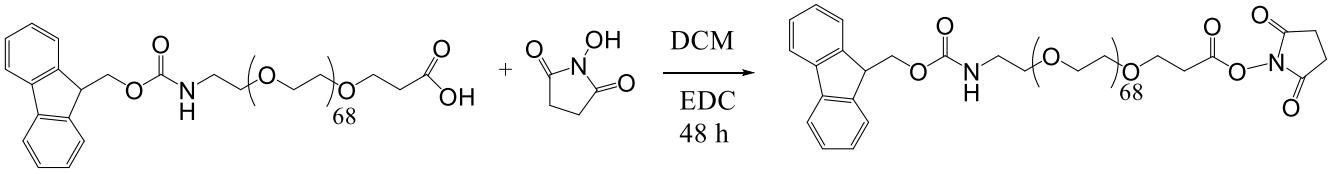

Figure 12 Schematic representation of the activation reaction of the carboxylic group of Fmoc-PEG-COOH with NHS. The reaction was carried out in dichloromethane (DCM), with the addition of EDC. The solution was let to react for 48 h.

The product was analyzed *via* ^{1}H-NMR spectroscopy in DMSO-d_6. The spectrum is reported in **Figure 13**. From the ratio of the integration of the characteristic Fmoc signals and the signal of the PEG backbone a degree of functionalization *f* = 74% could be obtained.

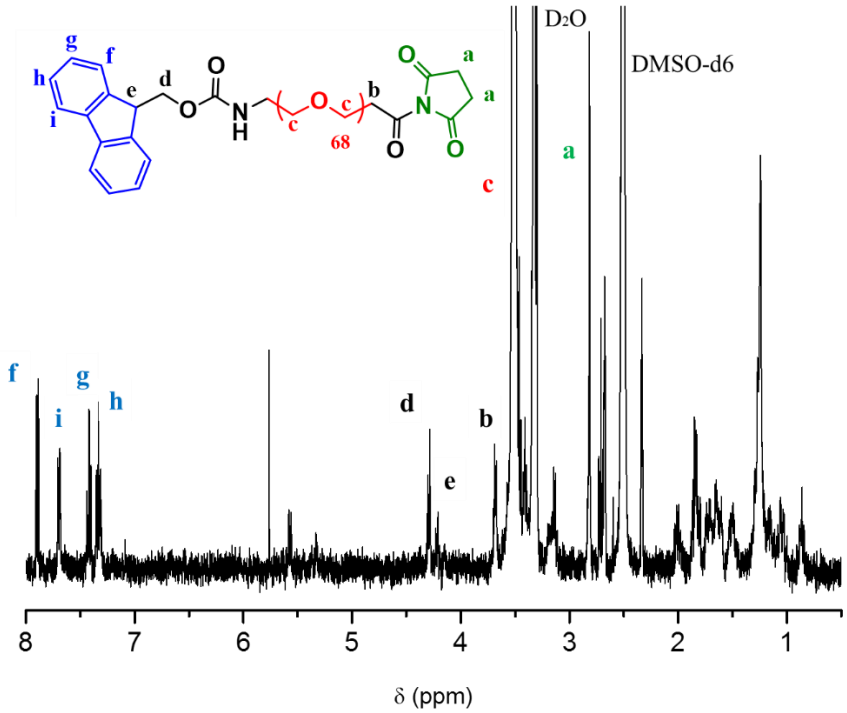

Figure 13. ^{1}H-NMR spectrum of Fmoc-PEG-NHS. δ_H(400 MHz, 128 scans, DMSO-d_6) 7.78 (2 H, **f**, fluor), 7.62 (2 H, **i**, fluor), 7.42-7.30 (4 H, **gh,** fluor), 4.32 (2 H, **d**, CH_2OCO), 4.22 (1 H, **e**), 3.70 (2 H, **b**, CH_2), 3.54 (272 H, **c**, CH_2OCH_2), 2.81 (4 H, **a**, CH_2CH_2).

Then, Fmoc-PEG-NHS was dissolved in a 1:1 mixture of DMSO and water. N_{α},N_{α}-bis(carboxymethyl)-*L*-lysine and EDC were added and the solution was allowed to stir for 12 h, as depicted in the scheme of **Figure 14**). The obtained product was then dialyzed against water using a RC membrane with a cut-off of 1000 g/mol. Subsequently, water was evaporated from the product using a rotary evaporator.

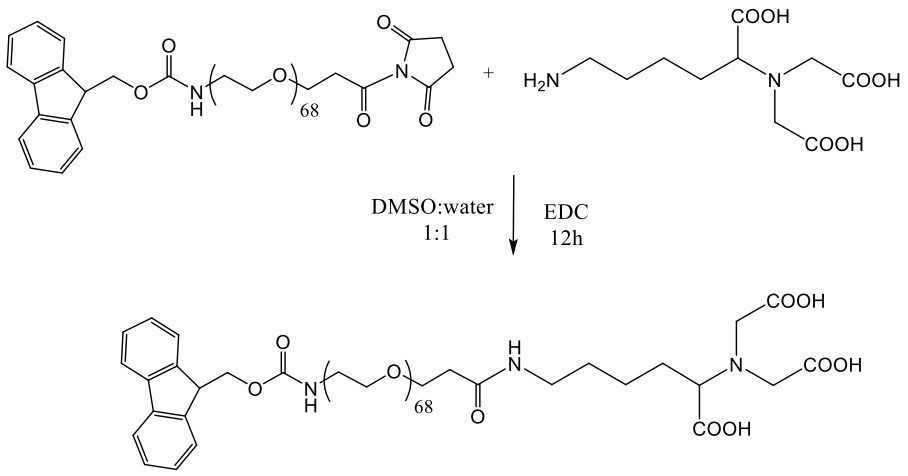

Figure 14. Schematic representation of the reaction of Lys-NTA with Fmoc-PEG-NHS.

Subsequently, Fmoc-PEG-NTA was dissolved in a mixture of dichloromethane : ethanolamine 1:1 and reacted for 12 h, in order to deprotect the amine groups (scheme of **Figure 15**). The deprotected compound was dialyzed, as previously explained, and freeze-dried.

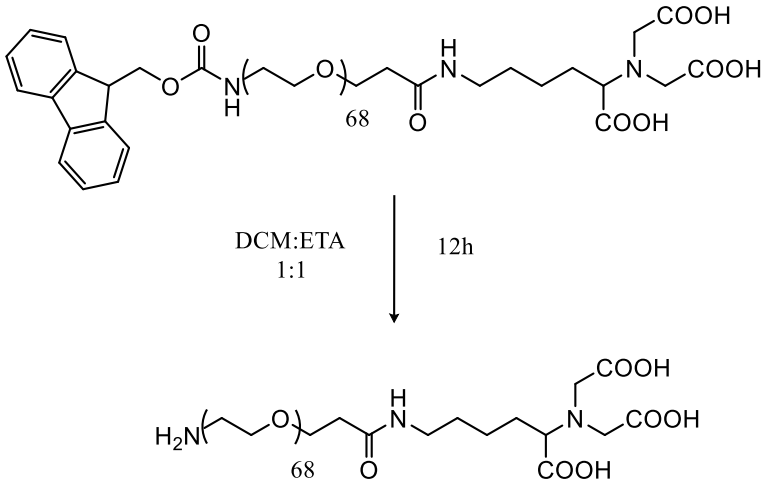

Figure 15. Schematic representation of the deprotection reaction of the amine group of Fmoc-PEG-NTA. The reaction took place in a mixture of DCM and ethanolamine (ETA) 1:1, for 12 h.

The product was then analyzed *via* size exclusion chromatography (SEC) using DMF (dimethyl formamide) containing LiBr as eluent to avoid interactions of the amine groups with the column material. The obtained chromatogram is reported in **Figure 16**. Apart from the amine-PEG-NTA product, signals corresponding to the precursor material amine-PEG-carboxy were still present. As shown in the spectrum, the deprotection of the material led to a change of the elution time of the material in DMF, which does indicate a change in the size of the molecule. Here, the traces of the amine-PEG-carboxy

(black curve, used as reference signal) and the final product amine-PEG-NTA (blue line) are of particular interest. As shown below, the amine-PEG-NTA product is characterized by a bimodal size distribution and therefore the presence of two products can be assumed. Most probably, the final product contains still not reacted amino-PEG-carboxy starting material. This can be explained by the incomplete activation with NHS as shown above and a reaction yield below 100%. To confirm this assumption, the SEC trace of the product was compared to an amino-PEG-COOH polymer used as reference. Indeed, the peak maximum of the reference material at 23 minutes is perfectly overlaying with the second signal of the NTA-PEG-COOH product confirming the above given explanation. Furthermore, the small signal of the amino-PEG-COOH reference at 21.5 min, corresponding to the double molar mass and, therefore, the coupling product of two PEG chains, can be used for the characterization process. Importantly, the signal at lower elution time (21 minutes; blue arrow) and, therefore, higher molar mass, indicates the NTA functionalized material. As this signal is not overlaying with the peak of the coupling product of the reference at 21.5 minutes (black dashed arrow), we can exclude that the second signal of the NTA-PEG-COOH is caused by impurities as coupling products. Indeed, the maximum peak of NTA-PEG-COOH is shifted (blue dashed line) compared to that of NH_2-PEG-COOH (black dashed line). By integration of the peak areas, a degree of functionalization of 45% was estimated.

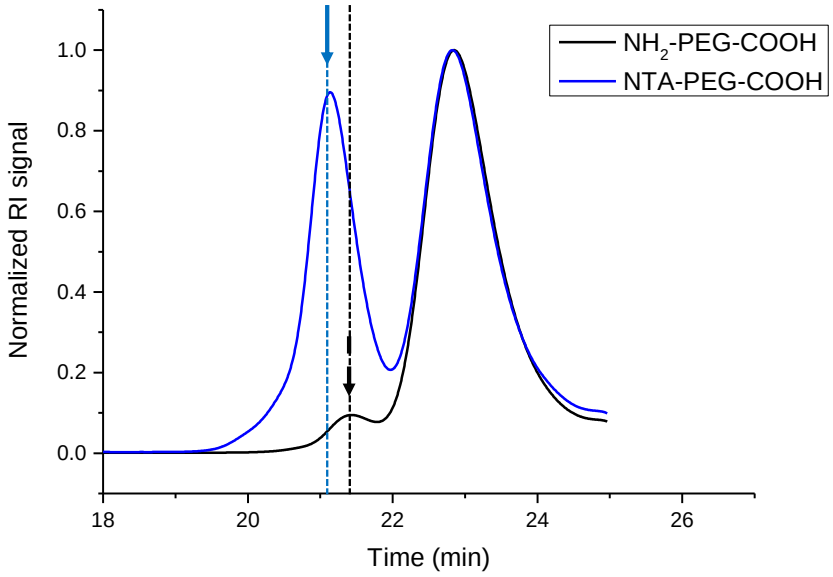

Figure 16. SEC analysis. Chromatogram of synthetized PEG-NTA (blue line) and NH_2-PEG-COOH (black line) used as a reference. The dashed line shows the peak shift of the functionalized NTA-PEG-COOH (blue line) compared to the coupling product present in the NH_2-PEG-COOH reference material (black line).

To enable the complexation of the histidine tag to NTA, Ni ions were necessary. For this purpose, Fmoc-PEG-NTA was dissolved in water with $NiCl_2$ and kept at room temperature for 12 h under magnetic stirring (**Figure 17**). After the incubation, the product was dialyzed in order to remove the excess of Ni and freeze-dried. Change in color of the PEG-NTA towards a slight green color was observed.

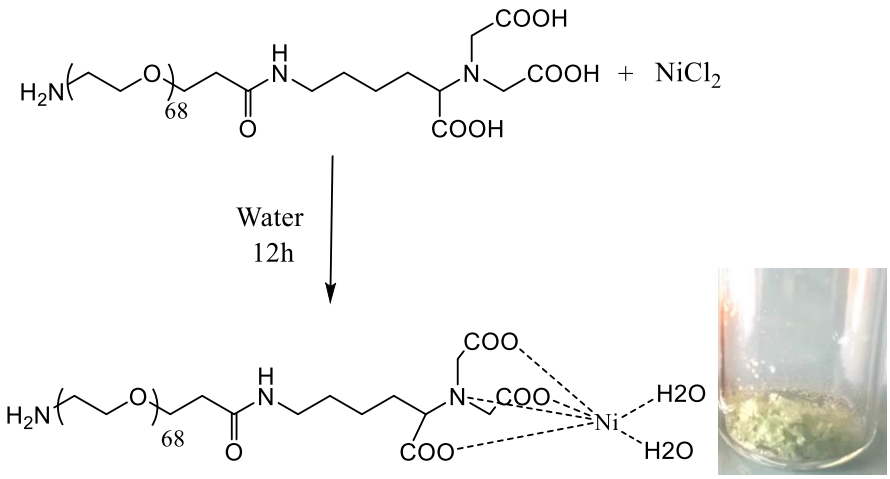

Figure 12. Schematic representation of the complexation of Ni by Lys-NTA PEG. The picture on the right shows the powder obtained after the reaction. The green color indicates presence of Ni.

3.2.5 Functionalization of the nanocubes with PEG-Pt and PEG-NTA-Ni for drug delivery and targeting. Characterization techniques.

The detailed procedure of functionalization is shown in "materials and methods" paragraph. Briefly, PEG-Pt and PEG-NTA-Ni were bound in a two-step reaction as depicted in the schemes of **Figure 18**. PEG-Pt was bound to the carboxylic groups on the polymeric shell of the nanocubes *via* EDC chemistry (**Figure 18**, scheme a). After the functionalization with PEG-Pt, the nanocubes sample was recovered and functionalized with PEG-NTA-Ni, using the same chemistry of PEG-Pt binding (**Figure 18**, scheme b).

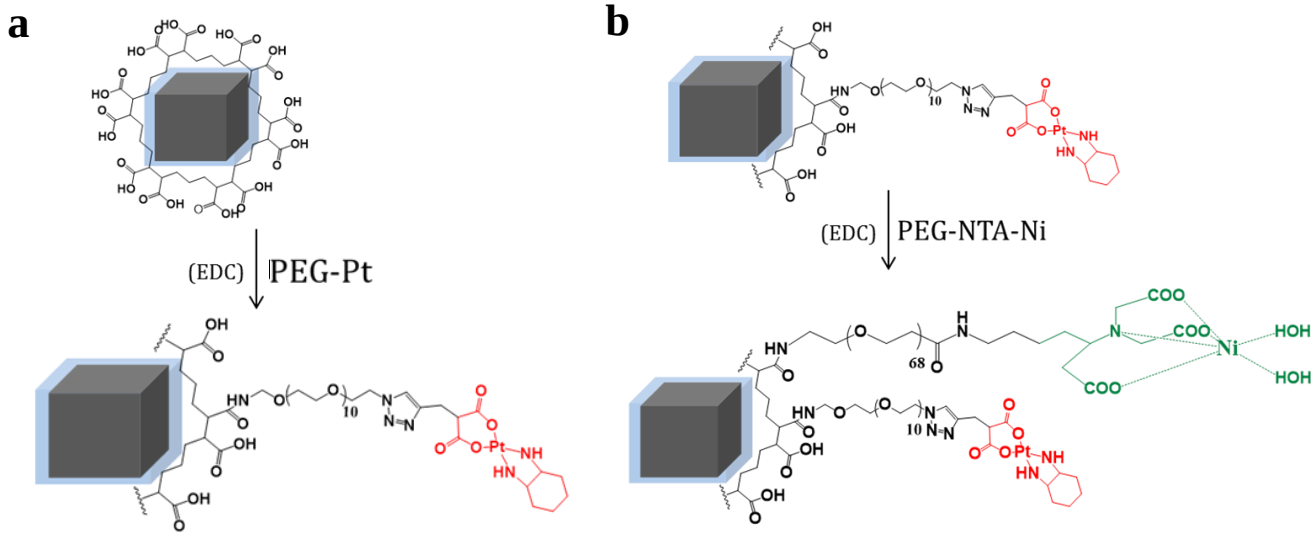

Figure 13. Schematic representation of the functionalization strategy of nanocubes. a) Binding of PEG-Pt *via* EDC chemistry. **b)** Binding of PEG-NTA-Ni *via* EDC chemistry.

After each step of reaction, the samples were analyzed *via* ICP-AES. From the results obtained, it was possible to determine an average amount of Ni cations and Pt (thus the number of OHP molecules) per nanocubes, corresponding to 350 ± 10 for Ni and 260 ± 8 for Pt. After the binding of the functional

ligands, 0.1 μM of NCs were incubated with 2 μM of scFv_C4 antibody. DLS measurements, BCA assay, electrophoresis on agarose and poly-acrylamide gel and dot blot assay were used for characterizing the bioconjugate. **Figure 19** shows the number weighted DLS graph and the zeta potential of the NCs sample after PEGylation (NCs_PEG-NTA) and incubation with the antibody fragment (NCs_scFv or NCs_C4). After the PEGylation with both PEG-Pt and PEG-NTA there was just a slight increase in the nanocubes size, consistent with a wrapped conformation of the ligands around the nanocube surface. However, a consistent size increase occurred after the antibody binding. The table shows the zeta potential values, which indicated the change in the surface charge of the nanocubes after the modifications. In detail, after each step of functionalization, the negative charge of NCs surface shifted toward more positive values due to the saturation of the negative carboxylic groups initially exposed on the nanocubes surface.

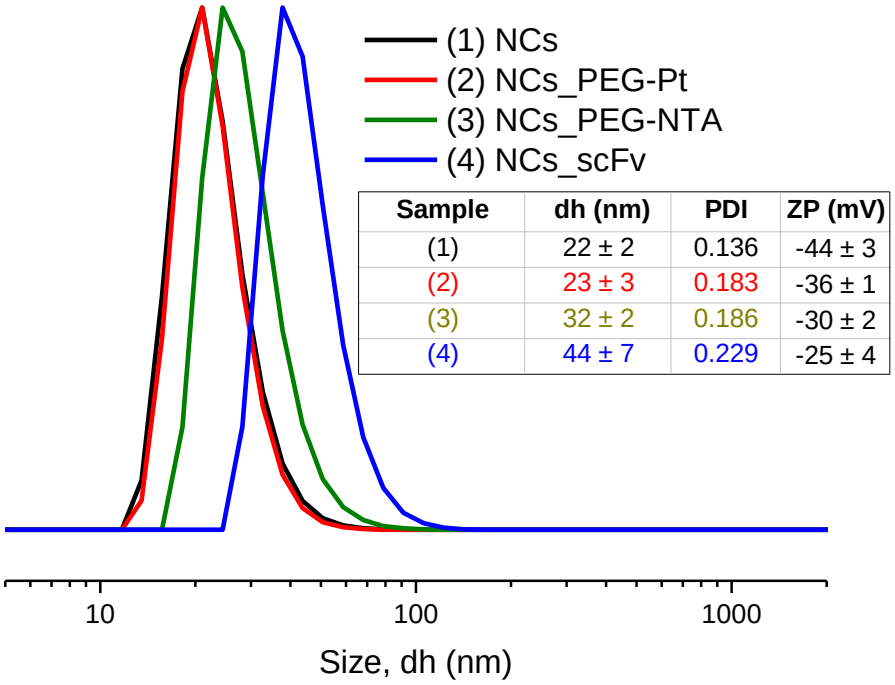

Sample	dh (nm)	PDI	ZP (mV)
(1)	22 ± 2	0.136	-44 ± 3
(2)	23 ± 3	0.183	-36 ± 1
(3)	32 ± 2	0.186	-30 ± 2
(4)	44 ± 7	0.229	-25 ± 4

Figure 14. DLS graph of NCs functionalization. Number weighed hydrodynamic diameter for the nanocubes pristine (NCs), after modification with the drug (NCs_PEG-Pt), PEGylation (NCs_PEG-NTA) and bioconjugation (NCs_scFv). In the table on the right are shown the corresponding charge values measured for each of the functionalization steps.

Bicinchoninic acid (BCA) assay was performed on the nanocubes sample and on the supernatant and washes in order to determine the amount of scFv molecules bound per nanoparticle. The detailed procedure is described in "materials and methods" paragraph. From the assay, an amount of 20 ± 3 molecules for each nanocube has been estimated. As control, BCA was also performed on a sample of nanocubes PEGylated with an amine-PEG-carboxy (Mn = 3000 g/mol, precursor of the PEG-NTA) and incubated with the same amount of antibody. For this sample, 3 ± 1 bound molecules were found, indicating a partial aspecific absorption of PEG molecules. Afterwards, electrophoresis on a 2% agarose gel was performed in order to characterize the migration pattern of the nanocubes before and after the different functionalizations. The binding of each PEG molecule would have given a characteristic migration pattern, with an expected gradual decrease of migration by increasing the size of the molecules grafted on the nanocubes surface. **Figure 20a** shows the gel picture of NCs pristine (line 1), NCs_PEG-Pt (line 2),

NCs_PEG-NTA (line 3) and NCs_scFv (line 4). Migration shift was slightly evident for the sample PEGylated with PEG-Pt, as expected due to the small size of the molecule but it was more pronounced for PEGylation with PEG-NTA-Ni. Interestingly, migration shift further increased for the sample incubated with the antibody. These data well agreed with the size increase measured by DLS (**Figure 19**) and with the zeta potential values recorded, since the electrophoretic mobility is consistent with the size and charge of the nanocubes. Furthermore, SDS-PAGE on a 12.5% poly-acrylamide gel was performed in order to unequivocally determine the presence of the antibody on the nanocube surface. Compared to agarose gels, acrylamide gels allow the fine separation of proteins from the remaining nanocubes components. **Figure 20b** shows the bands obtained on the gel after the staining with Comassie reagent. Line 4, corresponding to the sample of PEGylated nanocubes with PEG-NTA and incubated with the fragment antibody C4 (scFv_C4,) clearly indicates that the scFv was bound to the nanocubes. Finally, to prove the specificity of the antibody binding to the NCs functionalized with PEG-NTA, those nanocubes and a reference batch of particles functionalized with an amine-PEG-carboxy (Mn = 3,000 g/mol), and, therefore, without NTA binding unit, were incubated with scFv_C4 after the treatment with a solution of bovine serum albumin (BSA) at the concentration of 0.4 mg mL^{-1}. The aim of this experiment was to saturate all the possible aspecific sites on the NCs surface, as previously reported.[34] As clearly visible from **figure 20c**, only the sample PEGylated with PEG-NTA showed the band corresponding to the antibody fragment (**3**), while the sample PEGylated with the standard PEG showed only a slight band corresponding to BSA (**2**). These results indicated that the binding of scFv_C4, bearing a histidine tag, was specifically mediated by the PEG-NTA.

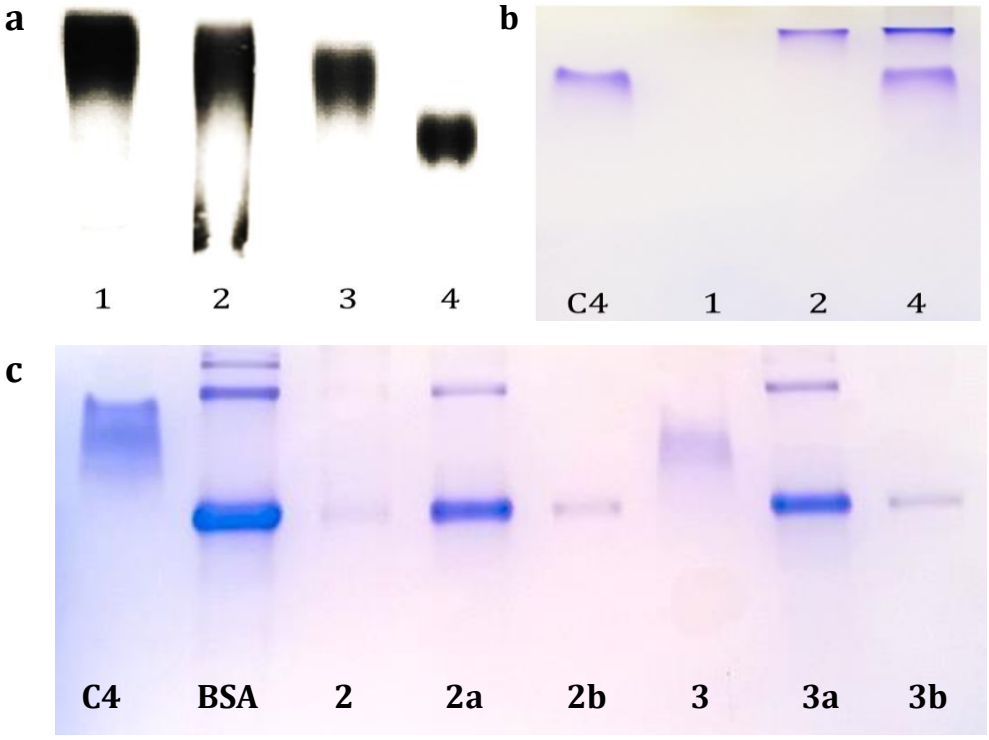

Figure 15. scFv binding characterization. a) Electrophoresis carried out on a 2% agarose gel. Line 1 = NCs pristine; Line 2 = NCs_PEG-Pt; Line 3 = NCs_PEG-Pt_NTA; Line 4 = NCs_PEG-Pt_NTA incubated with scFv. **b)** SDS PAGE carried out on a 12.5% acrylamide gel. M= size marker; C4 = scFv_C4; 1= NCs pristine; 2 = NCs_PEG-NTA; 3 = NCs_PEG-NTA incubated with scFv. **c)** SDS PAGE carried out on a 12.5% acrylamide gel.

C4 = scFv_C4; BSA = bovine serum albumin; 2 = NCs_PEG incubated with scFv and albumin; 2a and 2b = washes of NCs_PEG; 3 = NCs_PEG-NTA incubated with scFv and albumin; 3a and 3b = washes of NCs_PEG-NTA. Both the SDS PAGE gels were stained with Comassie reagent.

After the electrophoresis run on the agarose gel (**Figure 20a**), the nanocubes bands 1, 2 and 3 were cut out, digested (according to the procedure explained in "material and methods" section) and analyzed *via* ICP-AES. The results reported in

Table 1 indicate the presence of Pt in the band 2 and both Ni and Pt in the band 3. All the bands contain iron. These data further confirmed the effectiveness of the functionalization steps.

Table 1. Elemental analysis of Fe, Ni and Pt determined inside the gel after electrophoresis.

Sample	Fe (ppm)	Ni (ppm)	Pt (ppm)
NCs	2.823	/*	/*
NCs_Pt	3.988	/*	0.038
NCs_Pt_NTA	4.028	0.012	0.05

Note 1 *=data below the sensitivity curve of the instrument.

To further prove the binding of scFv on the nanocubes, a dot blot assay was set on the samples of nanocubes functionalized with PEG-Pt and PEG-NTA. **Figure 21** shows the results obtained after the incubation of the nanocubes or scFv with a primary antibody IgG anti-myc (a tag sequence which labeled scFv C4) and a secondary antibody conjugate with Alexa 488 fluorophore, which bind to the Fc (Fragment crystallisable) region of the primary antibody. The samples of nanocubes and the corresponding supernatants and washes are illustrated. As clearly shown in the picture, a fluorescent signal can be detected for both nanocubes functionalized with just PEG-NTA (NCs_scFv) and with the combination of PEG-NTA and PEG-Pt. Moreover, up to 3 μg of nanocubes it was possible to detect the presence of the bound antibody, while just a slight signal comes from the 1.5 μg dot (bottom line, NCs_C4). The obtained data indicate that the antibody fragment was bound on both the samples of functionalized nanocubes.

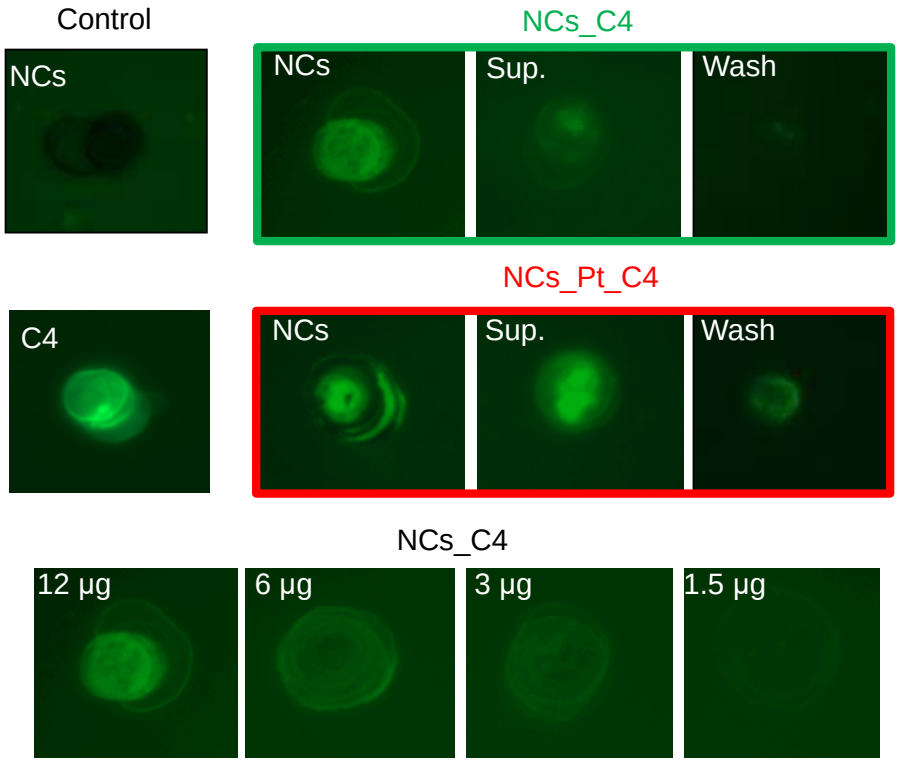

Figure 21. Dot blot assay. NCs and C4 as controls were spotted. 20 µg of NCs_scFv (NCs_C4) or NCs_PEG-Pt_scFv (NCs_Pt_C4) were analyzed, together with their corresponding supernatants and washes (20 µL, Sup. and wash, pictures in the green box and red box respectively). In the bottom line, a serial dilution of NCs_C4 was also studied. Dot blot was carried out on a nitrocellulose membrane. After spotting the samples, the membrane was incubated with a primary antibody specific for the scFv_C4 and a secondary antibody conjugated with Alexa 488. The images were acquired by exciting the membrane with 488 nm laser.

To further confirm that the binding of the antibody fragment was mediated by the interaction of the NTA-Ni and the histidine tag, a wash with imidazole (an antagonist of the histidine for the binding of NTA-Ni) was performed. The presence of the antibody on the particles and in the eluted volume was analyzed *via* dot blot assay. As shown in **Figure 22**, PBS wash was not effective in detaching the antibody fragment from the nanoparticles, as one can see from the absence of the fluorescent signal in the wash spot compared to the fluorescent NCs spot (first and second line, second column, upper and bottom square respectively). However, the wash with imidazole 0.4 M successfully remove the scFv from the nanoparticles and the antibody fragment was detected in the fluorescent spot of the wash, with respect to the non-fluorescent dot of the nanocubes (last column, upper and bottom square respectively). These data indicated that the scFv_C4 antibody fragment was bound on the nanoparticles surface and the binding was directly mediated by the interaction between NTA-Ni and the histidine tag of the antibody fragment.

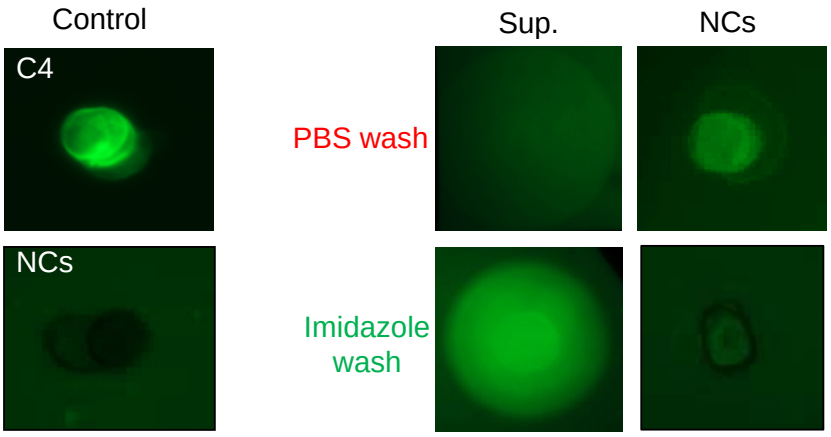

Figure 16. Dot blot assay. NCs and C4 as controls were spotted. NCs and eluted volume after PBS wash are spotted in the second column of the picture. NCs and eluted volume after imidazole wash are spotted in the third column. Dot blot was carried out on a nitrocellulose membrane. After spotting the samples, the membrane was incubated with a primary antibody specific for the scFv_C4 and a secondary antibody conjugated with Alexa 488. The images were acquired by exciting the membrane at 488 nm.

3.2.6 Studies of the biological activity of the bioconjugate

Once demonstrated the binding of the scFv to the nanocubes, functional studies were carried out in order to determine the activity of the antibody fragment and to verify that, once bound, C4 was still able to recognize its target folate receptor α. To do that, two different kinds of experiments were set. In the first one, kinetic analysis, exploiting the SensiQ technique, was done to study the binding of NCs_scFv to the target folate binding protein (FBP) immobilized on the chip surface. This technique is based on the surface plasmon resonance (SPR) for the detection of biomolecular interactions. **Figure 23** shows the curve responses for the NCs_scFv (red line) and a sample of NCs PEGylated with the reference amine-PEG-carboxy. As clearly evident from the resonances unit (RU) values, the binding to the chip of the NCs_scFv sample was significantly higher than that of PEGylated sample. Thus, it was possible to conclude that the nanocubes bioconjugated with scFv_C4 were able to recognize the sensor-chip immobilized FBP. Noteworthy, despite the several attempts done, it was not possible to regenerate the chip. This case was already reported in the work of *Stella et al.*[35] Due to that, was not possible to calculate the K_d as ratio of K_{on} / K_{off}.

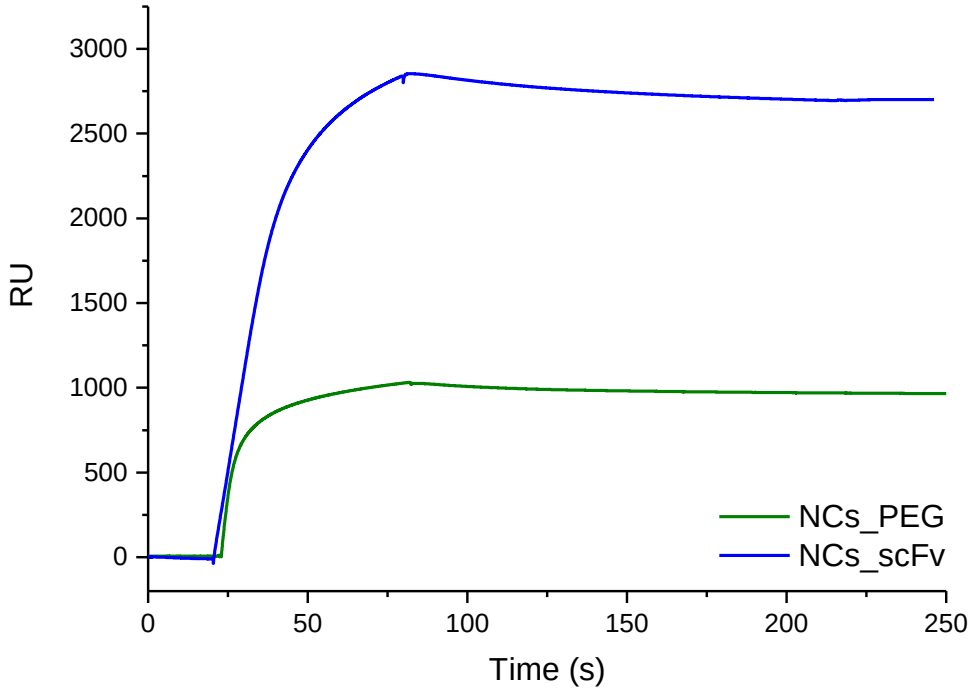

Figure 17. SPR analysis of binding of NCs_scFv on immobilized FBP. These experiments were conducted with 8 nM of both nanocubes functionalized with antibody fragment C4 or just PEGylated with an amine-PEG-carboxy (Mn = 3,000 g/mol). 25 μL of sample at a rate of 25 μL min^{-1} were injected. It has to be mentioned that chip regeneration was not possible in any tested regeneration conditions (see "materials and methods" paragraph).

In a second series of experiments, the binding ability of the nanocubes for their target was tested on different kinds of cell lines, expressing different folate receptors levels. This kind of analysis was carried out by means of a flow cytometer (FACS instrument, Fluorescent Activating Cell Sorting). To perform this experiment, 0.025 mg mL^{-1} of nanoparticles were incubated with 500,000 cells of the desired line. Four cell lines were studied. KB and IGROV-1 (cells with natural high expression of folate receptor), A431-FR (A431 cells transfected with a vector containing the αFR gene) and A431-MOCK (A431 cells transfected with the empty vector, which do not express folate receptors). As shown in the graphs of **Figure 24**, binding was demonstrated for IGROV-1, KB and A431-FR cells, while no binding occurred toward A431-MOCK cells that does not express folate receptors. We could conclude that the obtained nanoparticles were able to recognize specifically their target, expressing also a broad specificity toward different cell lines.

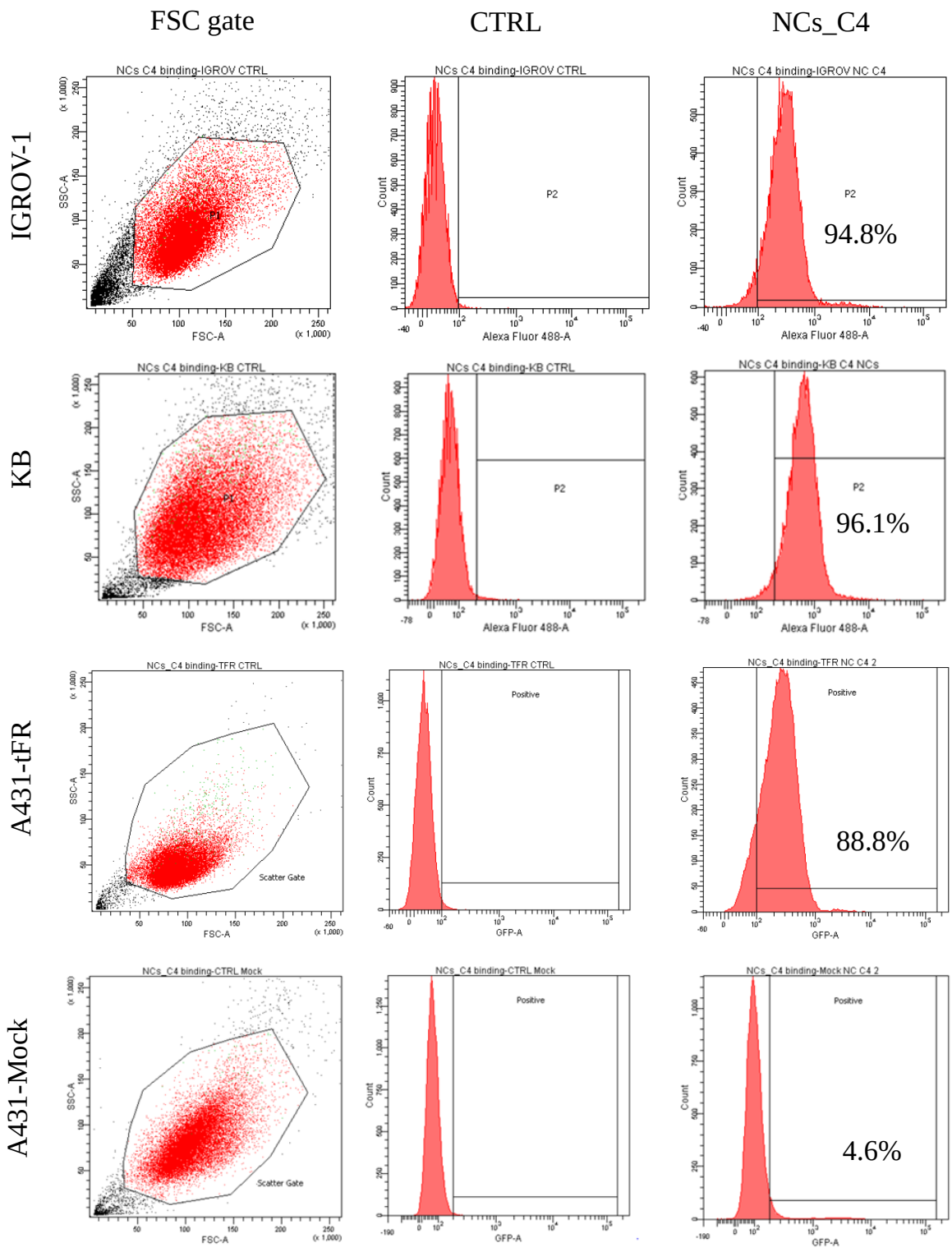

Figure 18. Flow cytometer analysis. Four cell lines were analyzed. KB, IGROV-1 and A431-FR are positive for the expression of folate receptor, while A431-MOCK is the negative cell line. The fluorescence was detected using a secondary antibody conjugated with Alexa-488.

Further, to confirm the binding ability of the functionalized nanocubes and also for evaluating the possibility to track them once they are bound to and internalized by the cells, confocal microscope images were acquired after 2 h of incubation of nanoparticles with IGROV-1 cells. The nanocubes were labeled using a secondary fluorescent antibody against C4. As shown in **Figure 25**, the green signal coming from labeled NCs is clearly visible on the cell membranes, indicating that the binding effectively occurred and was easily detectable.

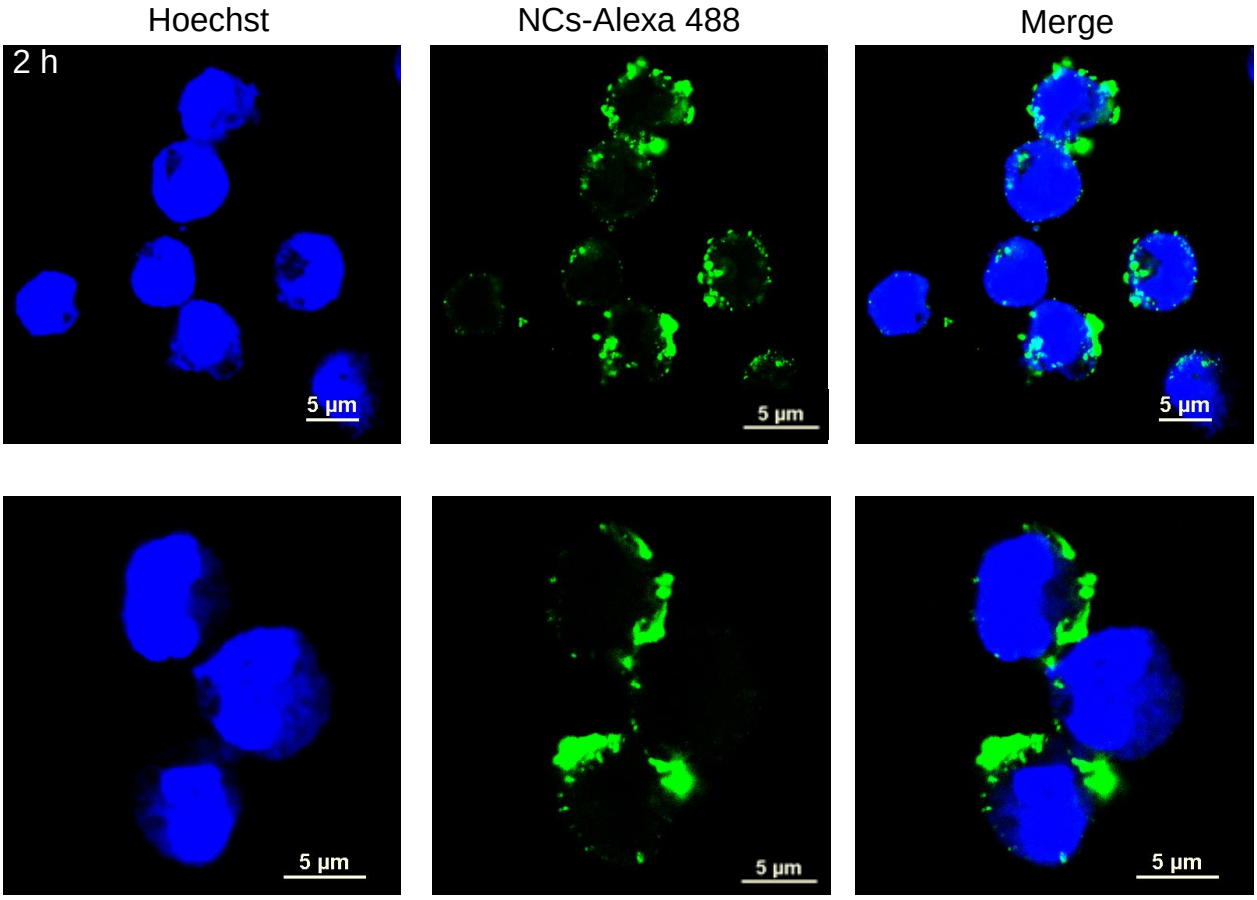

Figure 19. Confocal laser scanning microscopy (CLSM) images. IGROV-1 cells incubated with 21.8 nM (0.15 g_{Fe}/L) of NCs_C4 for 2 h at 37 °C were analyzed. The blue signal indicates the nuclear staining Hoechst (excitation wavelength of 405 nm), while the green signal indicates the nanocubes labeled with Alexa-488 secondary antibody (excitation wavelength of 488 nm). Merge image of all individual single channels is shown. Scale bar 5 µm.

3.2.7 Nanocubes cytotoxicity studies

Once demonstrated the specificity of the functionalized nanocubes, their toxicity toward the target cells was tested. Since the nanocubes should express the ability to deliver platinum in a controlled and specific manner, it was important to assess the biocompatibility and non-toxicity of the starting material. These tests were required given the presence of Ni as possible toxic cation. Indeed, it was reported that this metal is toxic at mM concentration and chronic exposures.[36] For that reason, it was important to define the amount of Ni bound to the nanocubes before performing the cytotoxicity test with cells. Additionally, it was important to determine the concentration of oxaliplatin, which was delivered within the NCs, in order to investigate at which concentration they were affective in killing cells. Three doses of nanocubes

(expressed in Fe amount) for the incubation with the cells were chosen. **Table 2** reports the values expressed as molar concentration for Ni cations, oxaliplatin drug and for nanocubes at the different doses tested on cells (0.05 g/L, 0.1 g/L, 0.15 g/L). As shown in **Table 2**, even at the highest concentration the amount of Ni was below the toxic threshold.[36] Instead, the OHP amount bound was in the range of the doses usually tested for toxicity.[11] From now on, the nanocubes functionalized with PEG-Pt will be referred as NCs_OHP for indicating the presence of the cytotoxic compound.

Table 2. Concentrations of Ni, OHP and NCs used for the cell studies.

Conc. (Fe)	Ni (µM)	OHP (µM)	NCs (nM)
0.05 g/L	2.3±0.06	1.3±0.05	7.26
0.1 g/L	4.5 ±0.1	2.6±0.1	14.52
0.15 g/L	6.8±0.2	3.9±0.15	21.79

Once defined the concentration of reagents involved during the treatment of the cells with the nanocubes, the cytotoxicity of the particles functionalized with PEG-NTA alone and conjugated to the scFv was tested on IGROV-1 cells line derived from ovarian carcinoma. Presto blue assay was chosen to determine the viability of the cells.[37] This assay is based on the reduction of the resazurin reagent into resorufin, red in color and highly fluorescent. This reduction activity is expressed in the mitochondria of living cells, but it is not catalyzed in dead cells. The cells where then incubated with NCs_PEG-NTA_C4 for 24, 48 and 72 h at 7.3, 14.5 and 21.8 nM (corresponding to 0.05, 0.1 and 0.15 g_{Fe}/L), and their viability assessed. As shown in the graph of **Figure 26**, up to 72 h and at the highest dose of nanoparticles incubated, the viability of the cell line was not affected. It was possible to conclude that the particles themselves were non-toxic, and that the Ni amount on their surface was present at non-toxic level.

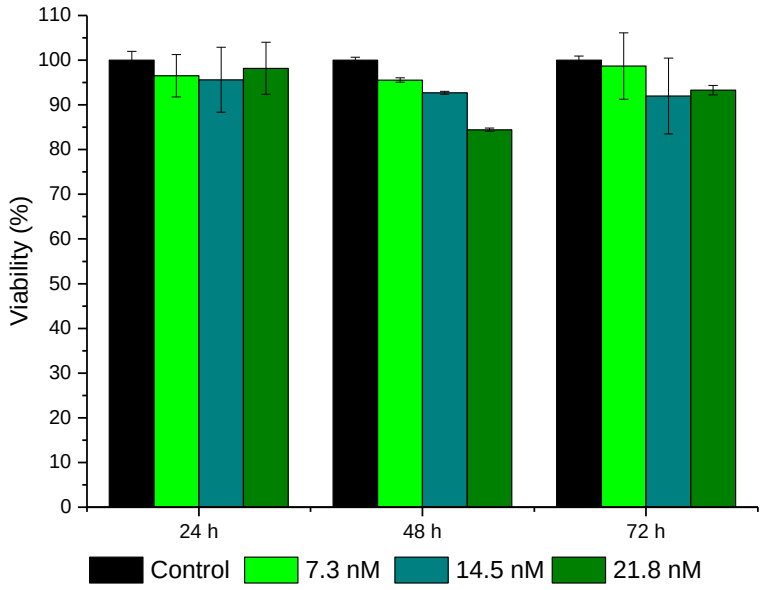

Figure 20. Presto blue assay. Viability assessed on IGROV-1 cells incubated with the nanocubes sample functionalized with PEG-NTA (NCs_C4) for 24, 48 and 72 h at the concentrations of 7.3, 14.5 and 21.8 nM (corresponding to 0.05, 0.1 and 0.15 g_{Fe}/L).

On the opposite, the nanocubes also functionalized with PEG-Pt compound, already at 48 h of exposition presented severe toxicity, which increased after 72 h of incubation (**Figure 27a**). Because the action of platinum-based drugs involves their cross-linking of purine bases of the DNA of the cells, the adverse effects of the treatment should have been still visible at different times post exposition. Thus, it was decided to monitor the toxicity of the nanocubes post incubation. Then, after 24 h, 48 h or 72 h of treatment, the supernatant containing the nanocubes was removed and replaced with fresh media. The viability was investigated after 24, 48 and 72 h. As shown in **Figure 27b**, the viability decreased after the 24 h treatment for the successive 24 h, for then recover viability again after 48 and 72 h post incubation. Instead, for the treatment at 48 h the viability still decreased for the successive 72 h, indicating that Pt compounds were still active inside the cells (**Figure 27c**). In the case of 72 h treatment, the toxic effect post incubation was even more severe (**Figure 27d**).

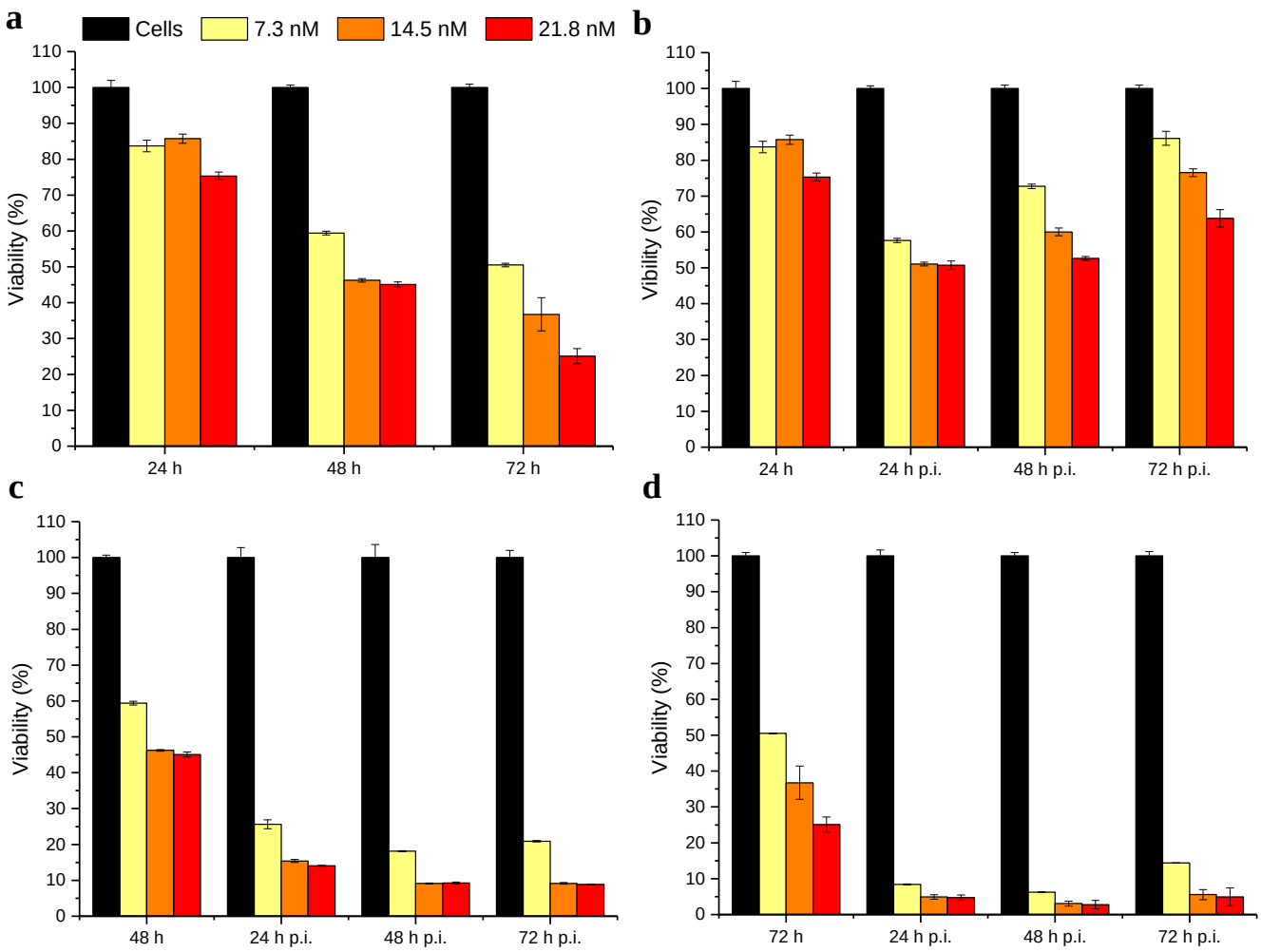

Figure 21. Presto blue assay. Viability assessed on IGROV-1 cells incubated with nanocubes sample functionalized with PEG-NTA , PEG-Pt and scFv-C4 (NCs_OHP_C4) at the concentrations of 7.3, 14.5 and 21.8 nM (corresponding to 0.05, 0.1 and 0.15 g_{Fe}/L). **a)** Viability after the treatment for 24, 48 and 72 h. **b)** Viability after the treatment for 24 h and 24, 48 and 72 h post incubation (p.i.). **c)** Viability after the treatment for 48 h and 24, 48 and 72 h post incubation. **d)** Viability after the treatment for 72 h and 24, 48 and 72 h post incubation.

In addition, the toxicity of the drug alone was also evaluated. OHP was administered to the cells for 24 h, 48 h and 72 h at the concentration corresponding to the amount loaded on the nanocubes. As visible

in the graph of **Figure 28**, the free drug had moderate toxicity at the tested concentration, as expected from previous reported studies.[38] Noteworthy, the toxicity of free oxaliplatin was lower than that found for the drug conjugated to the nanocubes. This could be explained with the role that the nanocubes exerted in concentrating the amount of drugs inside the cells at the same time, thus significantly limiting their ability to repair the damages induced by oxaliplatin.

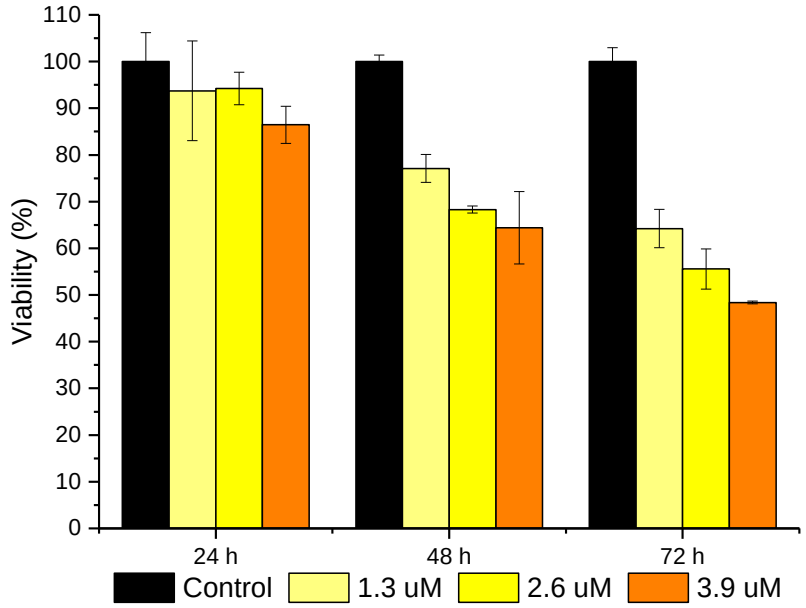

Figure 22. Presto blue assay. Viability assessed on IGROV-1 cells incubated with oxaliplatin at the concentrations of 1.3, 2.6 and 3.9 μM, the same loaded on 7.3, 14.5 and 21.8 nM of NCs (corresponding to 0.05, 0.1 and 0.15 g_{Fe}/L respectively).

3.2.8 Study of the evolution of the nanocubes-cells interaction

With the aim to investigate the interaction between the nanocubes and the cells, a series of uptake experiments were carried out at different time points. NCs functionalized with scFv C4 were incubated with IGROV-1 cells for 2 h, 4 h or 12 h at 37 °C. In these experiments, the cells were also labeled with Lysotracker for monitoring the evolution of the interaction between the nanoparticles and the cells. As clearly visible in **Figure 29**, while at 2 h most of the NCs were localized at the cells membrane (as already highlighted in **Figure 25**) at 4 h of incubation, the progressive internalization of the nanoparticles in an endocytosis-dependent manner was indicated by the co-localization of the green signal of the NCs and the red signal of the Lysotracker (originating a yellow signal). After 12 h there was the completely co-localization of nanocubes and lysosomes.

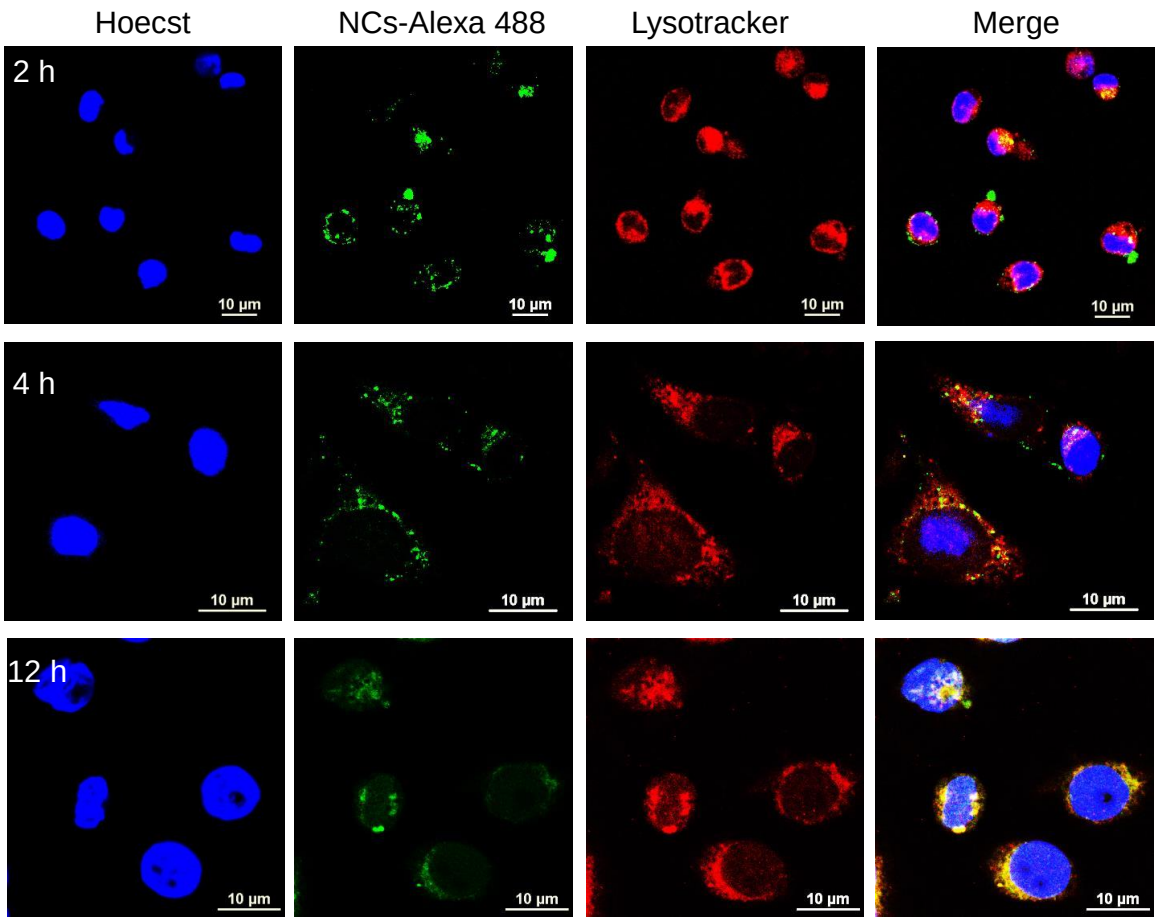

Figure 29. Confocal laser scanning microscopy (CLSM) images. IGROV-1 with NCs at 2 h, 4 h and 12 h of incubation were analyzed. Images were obtained on a single channel of nuclear stain (Hoechst, excitation wavelength of 405 nm), nanoparticles fluorescence (Alexa-488, excitation wavelength of 488 nm), lysosomes (lysotracker, excitation wavelength of 570 nm). Merge images of all individual single channels are shown. Scale bar 10 µm.

Furthermore, three dimensional reconstructions (3D) images acquired at 2, 4 and 12 h supported further the gradual internalization of the nanocubes inside the cells (**Figure 30**).

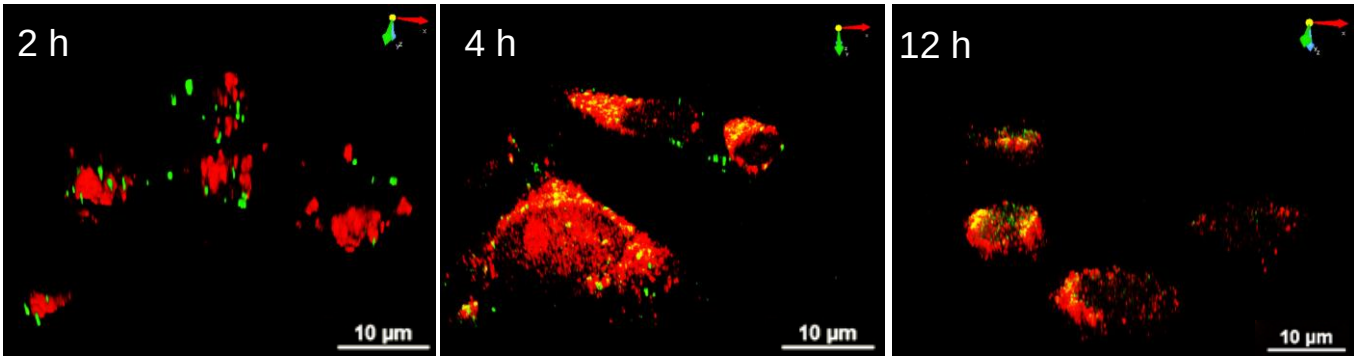

Figure 30. 3D reconstructions of confocal images. NCs with cells at 2h, 4h and 12 h of incubation were analyzed. Images were obtained on a single channel of nanoparticles fluorescence (Alexa-488, excitation wavelength of 488 nm), lysosomes (lysotracker, excitation wavelength of 570 nm) and then merged. Scale bar 10 µm.

In **Figure 31**, Y and Z projections of the three dimensional (3D) reconstruction underline the localization of the NCs with the cells. At 2 h (**Figure 31a**), most of the nanoparticles did not co-localize with lysosome, indicating that they were still bound to the cell membrane or just internalized. After 4 hours (**Figure 31b**) it was possible to observe more co-localization events, even if nanocubes outside the lysosome were still present. Interestingly, after 12 hours (**Figure 31c**) the nanocubes co-localized with lysosomes and no free nanoparticle signals were further detected. This indicated the efficient internalization of the NPs inside the cells.

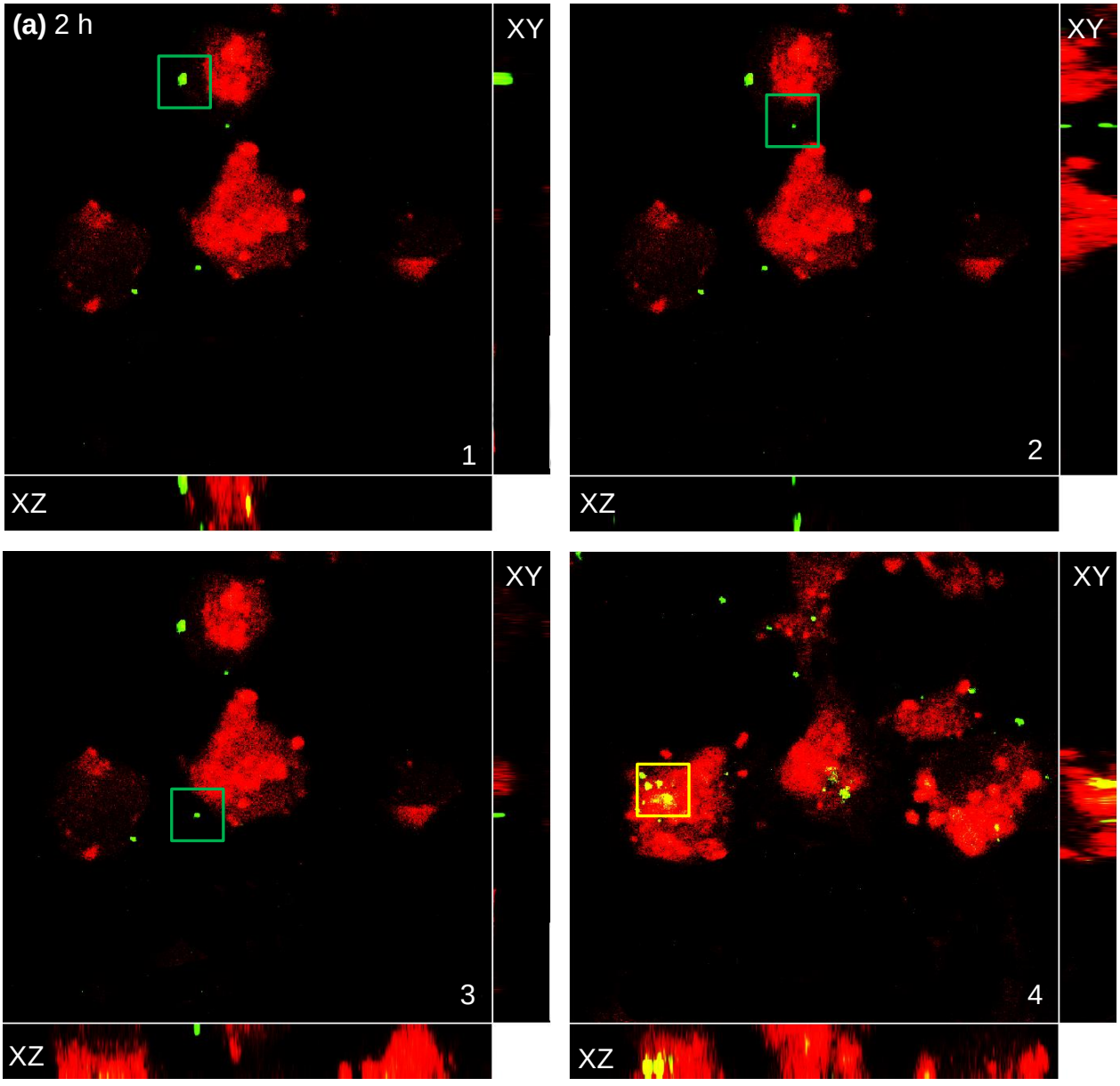

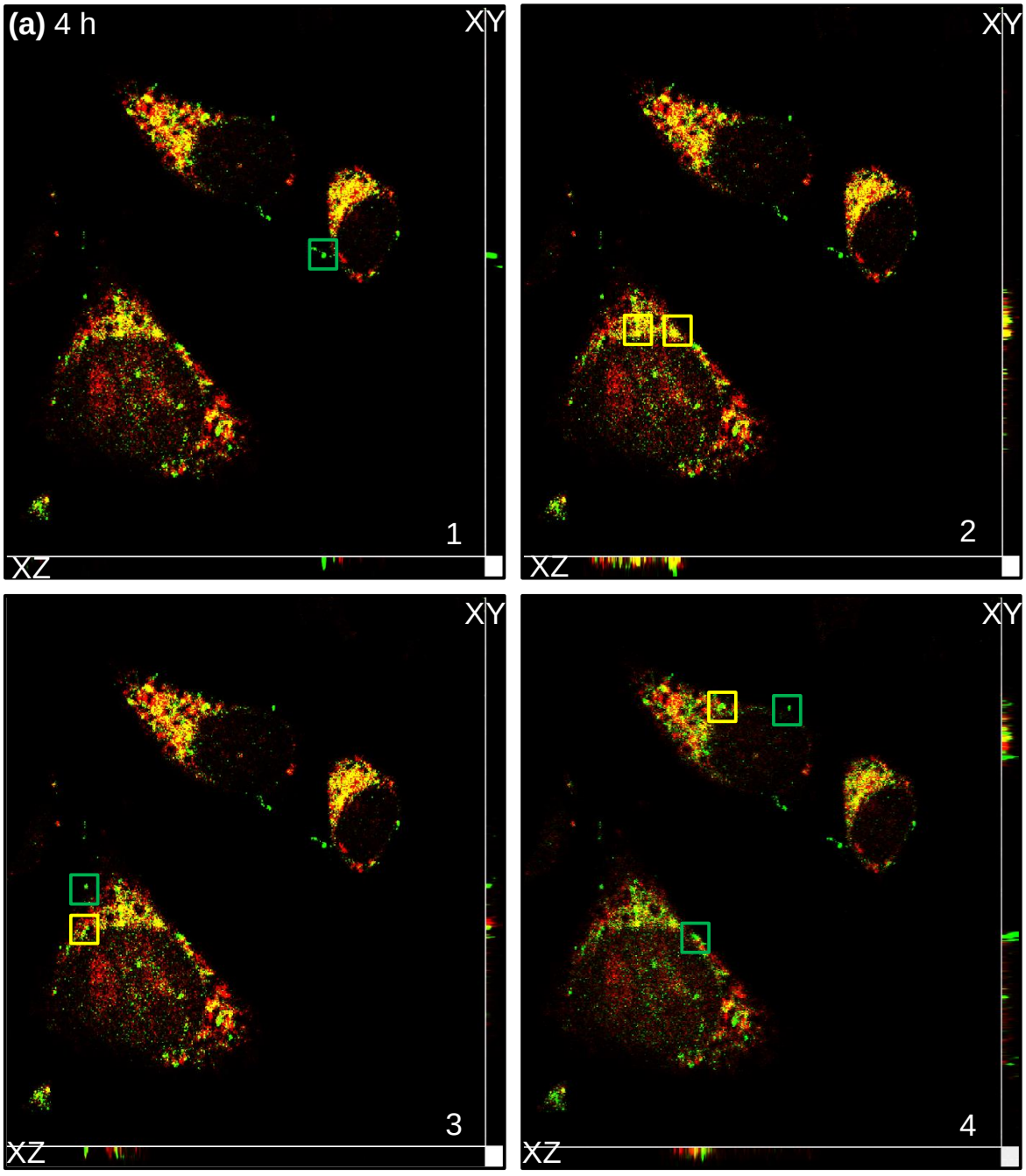
(a) 4 h
XY
XZ
1
2
3
4

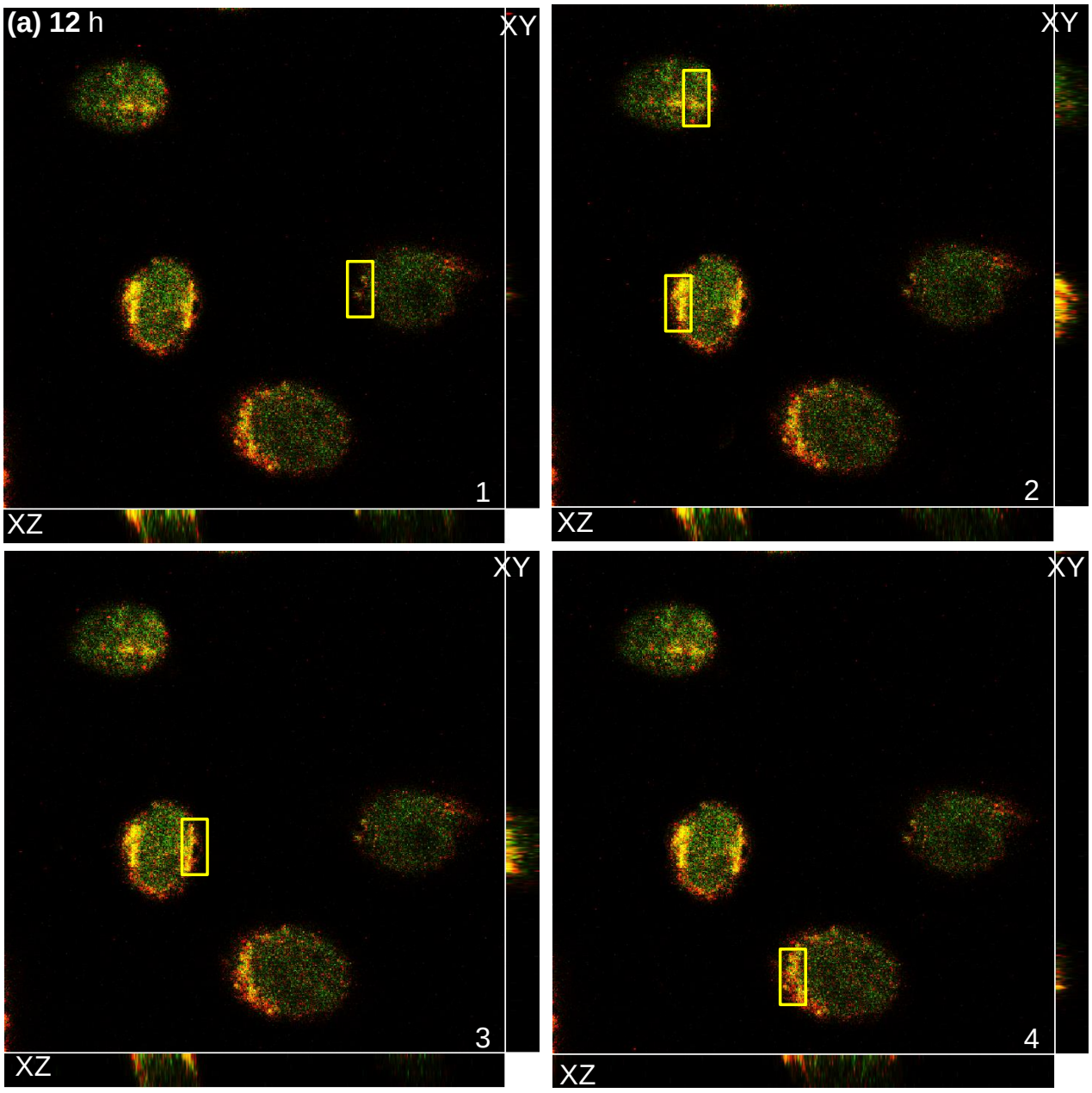

Figure 31. Y and Z projections of the three dimensional reconstruction. NCs with cells at 2 h (**a**), 4 h (**b**) and 12 h (**c**) of incubation. Images were obtained on a single channel for nanoparticles fluorescence (Alexa-488, excitation wavelength of 488 nm), lysosomes (lysotracker, excitation wavelength of 570 nm) and then merged. Scale bar 10 μm. Green box indicates the nanoparticles alone, yellow box indicates the co-localization of nanoparticles and lysosomes. Scale bar 10 μm.

The internalization of the nanoparticles was also followed at different resolutions, using transmission electron microscopy (TEM). After 48 h of incubation with NCs_OHP_C4 (0.15 g/L of iron) the nanocubes were found inside the cells cytoplasm, as shown in **Figure 32**. Noteworthy, numerous nanocubes clustered together inside late endosomes, indicating a high uptake rate (details in **Figure 32**, pictures **d** and **e**). Folate receptor internalization is expected to follow the endocytic pathway, clathrin independent.[39] Some single particles were also found in small vescicles, in proximity of the cell membrane (detail in **Figure 32**, picture **f**). These results further confirm the endocytosis mechanism

proposed and already underlined above with the confocal microscopy experiments. However, further analysis at low incubation time will be conducted in the future to understand the internalization mechanism in detail *via* TEM microscopy.

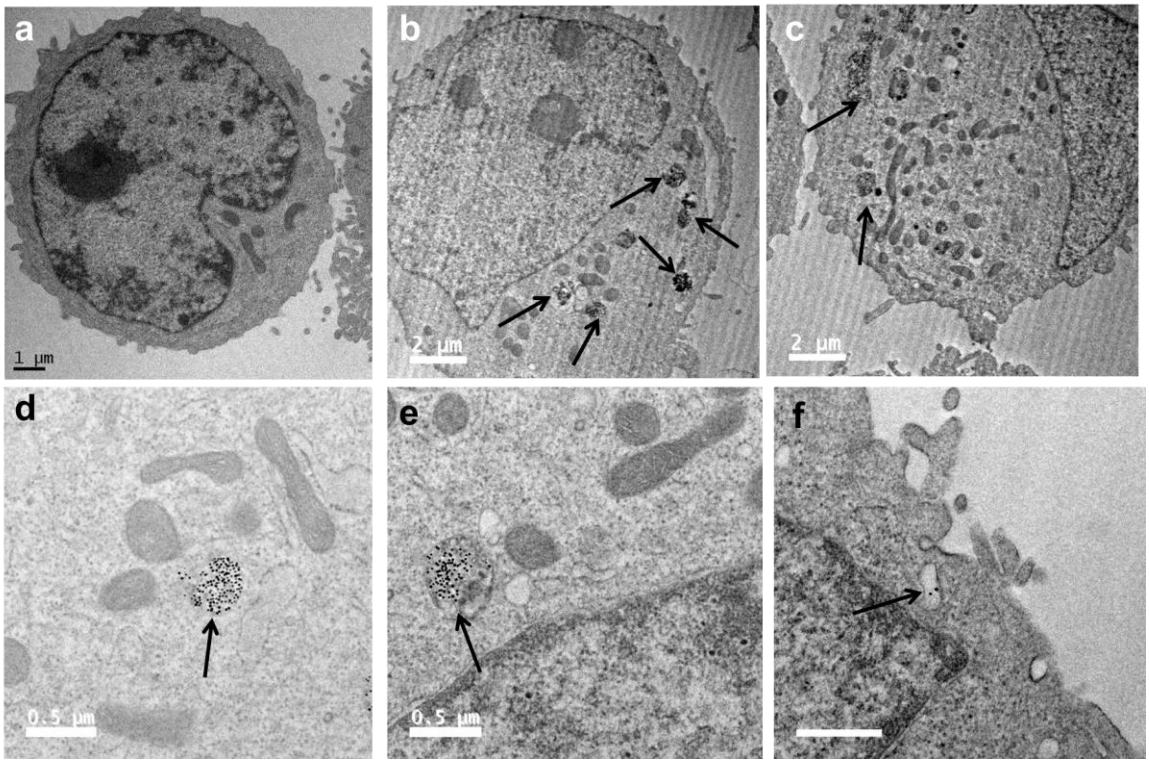

Figure 23. Thin-section TEM images of IGROV-1 incubated with NCs_OHP_C4 for 48 h at the concentration of 0.15 g/L of iron. Black arrows indicate the presence of nanoparticles. **(a)**, **(b)** and **(c)** low magnification. **(d)**, **(e)** and **(f)** high magnification.

3.2.9 Drug delivery efficiency: determination of Pt amount inside the cells

To determine the amount of Pt inside the cells, ICP-AES was performed on a cell sample treated for 48 h with 0.15 g/L of nanocubes. After the incubation, approximately $1.3x10^6$ cells were collected and digested (according to the procedure explained in "materials and methods" section). **Table 3** shows the results obtained for untreated cells and cells treated with nanocubes functionalized with platinum and antibody fragment (NCs_OHP_C4). As expected, Pt was detected inside the treated cells. Surprisingly, no nickel was found. This can indicate either that the amount of metal is below the detection limit of the instrument or that it is possibly removed from inside the cells according to an unknown mechanism.

Table 3. Elemental analysis of Fe, Ni and Pt with the relative concentrations found per cell.

Sample	Fe (µg)	Ni (µg)	Pt (µg)	µmol Fe / 10^6 cells	nmol Pt / 10^6 cells
Cells	0.023	/*	/*	0.000322	/*
NCs_OHP_C4	6.3	/*	0.12	0.086	0.6

Note 2 *=data below the sensitivity curve of the instrument.

The amount of Pt and Fe was also evaluated in the cells incubated with 0.15 g/L of NCs_OHP_C4 for 48 h, and grew in fresh medium for the successive 96 h. Then, $1.3x10^6$ cells were collected and digested. **Table 4** reports the obtained results. While Pt was still present inside the cells at amount comparable to those shown in table 3, the amount of Fe was significantly decreased. This data suggested that while the nanocubes were starting to be degraded (a decrease in the Fe amount of 28% was detected), Pt was better retained inside the cells (decrease in the Pt amount of 17.5% was detected). This not only indicated that NCs and Pt followed a different pathway inside the cells, but also that it was reasonable to suppose that Pt was indeed released efficiently from the nano-carriers.

Table 4. [Fe] and [Pt] found inside the cells following the 96 h after the exposure with NCs for 48 h.

Sample	µmol Fe / 10^6 cells	nmol Pt / 10^6 cells
NCs_OHP_C4 (p.i. 96 h)	0,0621	0,495

As the toxicity of oxaliplatin occurs through the generation of Pt-DNA adducts, [11, 40] also the presence of Pt was investigated inside the DNA. Cells were incubated with NCs for 48 h and grown in fresh medium for the successive 72 h. Then, the cells were collected ($1.3x10^6$ cells) and the DNA isolated. After the digestion with HCl, the sample was analyzed by ICP-MS (Inductively Coupled Plasma-Mass Spectroscopy), a more sensitive analytical technique compared to ICP-AES, since we would expect to find a significantly lower fraction of platinum inside the DNA compared to the entire cell. By the comparison of untreated cells and cells treated with NCs_OHP_C4 (Table 5), Pt was not found in DNA of control cells. Instead, in DNA of the cells treated with the nanoparticles bearing Pt, the metal was detected in a relevant amount. This clearly indicated that not only Pt reached the DNA of the cells, but that it is also accumulated inside the nuclei, thus exploiting its toxicity for long period.

Table 5. Pt Amount found inside the cells and DNA following 72 h after the exposure with NCs for 48 h.

Sample	Pt (ng)	pmol Pt / µg DNA	pmol Pt / 10^6 cells
Cells	/*	/*	/*
NCs_OHP_C4	0.23	0.17	1.13

Note: 3 *=data below the sensitivity curve of the instrument.

3.2.10 Study of the Pt release mechanism

Furthermore, the release of the drug was evaluated. Since the nanoparticles were uptaken according to the endocytic way, we expected the release of oxaliplatin at the level of endosome/lysosome. To simulate the organelles environment, citrate buffer solutions at different pH (5.5, 5 and 4.5) were prepared.[41, 42] The nanoparticles were dissolved in each buffer and kept at 37 °C for 24 h, before being re-collected using an amicon centrifuge filter (cut-off 100,000 g/mol). The amount of iron and Pt within the solution of nanoparticles and in the supernatant was evaluated *via* ICP-AES. As shown in the graph of **Figure 33**, the percentage of drug release increased by decreasing the pH of the solution in which the nanoparticles were dissolved, reaching a maximum at the pH characteristic of the lysosomes. Noteworthy, at pH = 7.4 (were the nanocubes were usually stored) release was not detected.

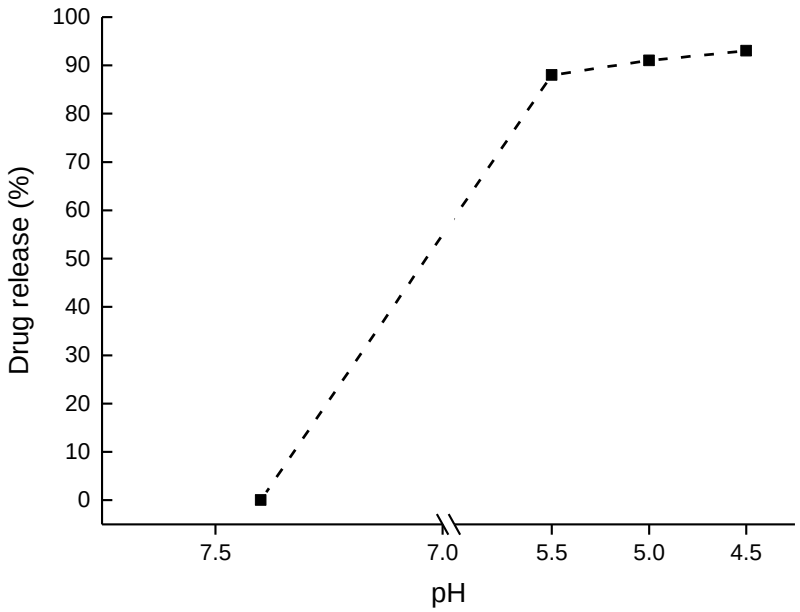

Figure 24. **Release profile of oxaliplatin from nanocubes**. Release experiments were performed at 37 °C in citrate buffer solutions (10 mM) at pH 5.5, 5 and 4.5, for 24 h.

In particular, the here proposed mechanism relies on the acidic hydrolysis of the PEG-Pt compound with the subsequent biotrasformation of oxaliplatin in its active compound dichloro-1-cyclohexanediamine platinum (Pt[dach]Cl_2, **a**) and eventually its hydration to form the aquated compound (b) (**Figure 34**).[13, 43, 44]

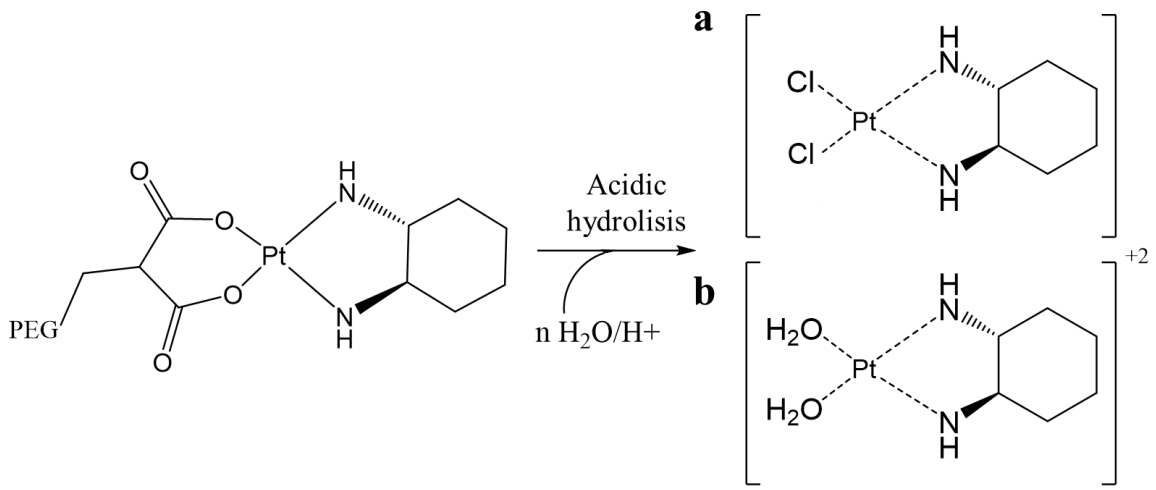

Figure 25. **Scheme of the proposed mechanism release of oxaliplatin from PEG-PT and NCs.** The displacement of the oxalate ligand generates active complexes, such as those here shown, dichloro-1-cyclohexanediamine platinum (**a**) and diaquo-1,2-cyclohexanediamine platinum (**b**).[13, 44, 45]

3.2.11 Study of the activity of Pt drug inside the cells

A further experiment was also set for evaluating the formation of Pt-DNA adducts. Alkaline comet assay was reported to be a sensitive method for the detection of a variety of DNA lesions.[46] The assay involves the lysis of agarose-embedded cells to generate a nucleoid body composed of supercoiled nuclear DNA. These nucleoid bodies are then subjected to electrophoresis that causes the damaged DNA to migrate

slower than the undamaged DNA generating a characteristic smeared spot on the agarose know as "comet", in which the "head" is composed by the undamaged DNA and the "tail" by the damaged DNA. Therefore, the more damaged a cell's DNA is, the greater the amount of DNA in the tail.[46] The extent of the damage can be indicated with the term Olive tail moment (OTM), which is expressed as the product of the tail length and the fraction of total DNA in the tail. To carry this assay out, control cells, cells incubated with NCs_C4 and cells incubated with NCs_OHP_C4 for 24, 48 and 72 h, were treated or not with hydrogen peroxide which is able to induce single and double strand breaks in DNA.[47] The cells treated with H_2O_2 should have presented a long "comet" due to the high DNA damaged induced by ROS (Reactive Oxygen Species). However, the presence of Pt-DNA adducts, which crosslink the DNA strands, would have retarded the electrophoretic mobility of DNA, thus leading to a decrease of the mean OTM compared to the control cells exposed to hydrogen peroxide.[46] As shown in **Figure 35a**, almost no difference in OTM for all the samples not exposed to oxidative damage (black lines) was visible. Instead, in the case of H_2O_2 treated samples, a significant decrease in the Olive tail moment occurred over the time for the sample treated with NCs_OHP (blue line with circle), compared to the other samples for which the OTM did not vary. Confocal microscopy images acquired for all the samples, treated or not with hydrogen peroxide, at 24, 48 and 72 h (**Figure 35b**, **c** and **d** respectively) clearly showed the decrease of the tail moment for the cell samples treated with oxaliplatin.

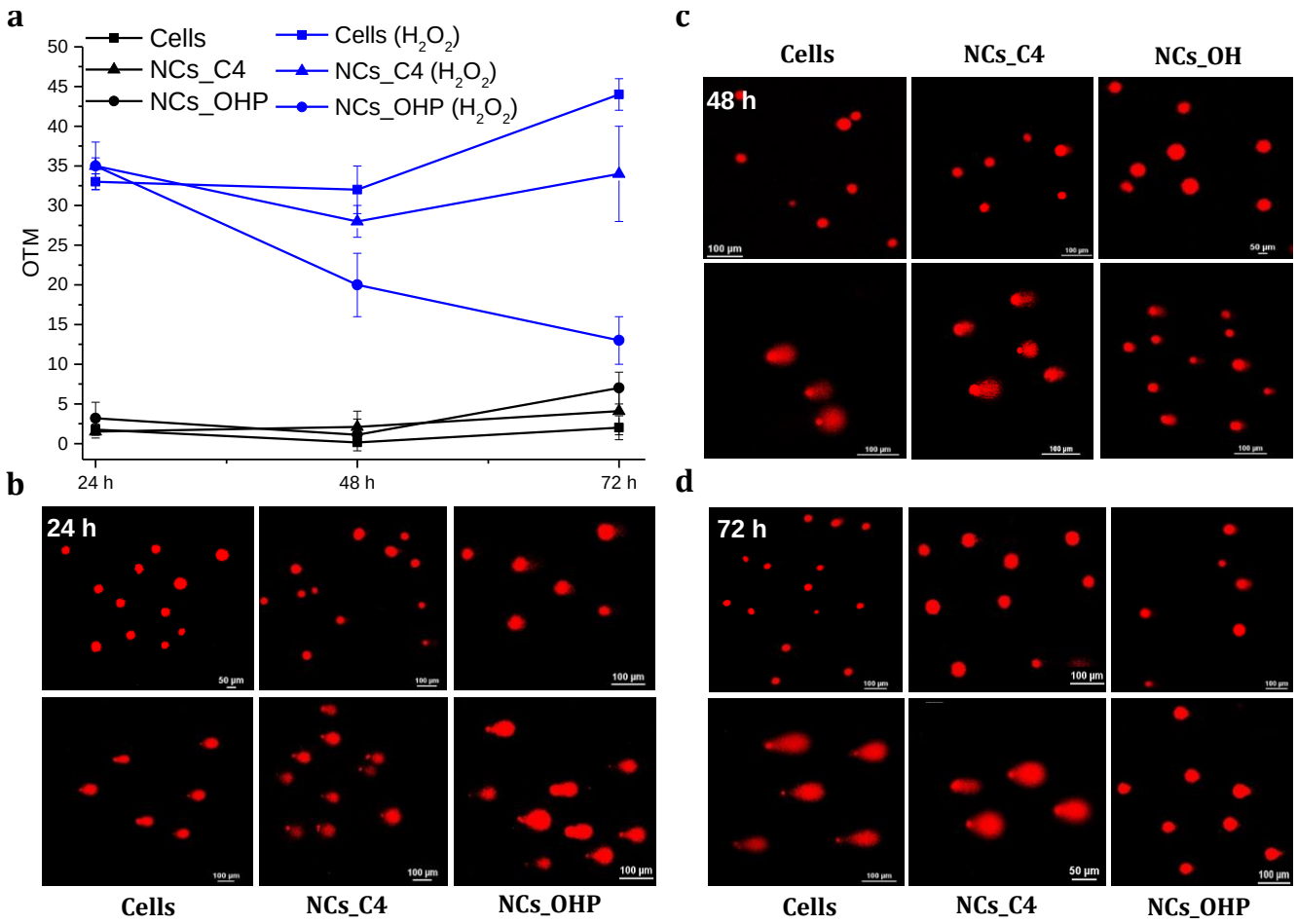

Figure 26. **Alkaline comet assay performed on IGROV-1 cells. a)** Mean Olive tail moment of IGROV-1 cells untreated (black lines) or exposed to 20 μM of H_2O_2 (blue lines). The data from control cells are shown as square, those from cells treated with NCs as triangle and those from NCs_OHP incubated cell as circles. **b)**, **c)** and **d)**

typical comet images obtained with confocal microscopy, showing the nucleoid body of the cells untreated (up pictures) or exposed to hydrogen peroxide (bottom picture) at 24 h **b)**, 48 h **c)** and 72 h **d)** of culturing (cells) or incubation with nanoparticles (NCs_C4 and NCs_OHP). The DNA was stained with propidium iodide (excitation wavelength at 590 nm). Scale bar 100 μm.

In detail, **Figure 36** shows typical comet pictures obtained for the cells incubated with NCs for 24, 48 and 72 h and treated or not (H_2O_2 and control respectively) with hydrogen peroxide. It was observed that, while for the cells incubated with NCs_C4 the comet remained unchanged after different times of exposition to the nanocubes, for the cells incubated with NCs_OHP_C4 the comet progressively reduced over time, reaching a comet pattern profile similar to that of the cells not treated with H_2O_2 (first line, last picture on the right). These data indicated that oxaliplatin delivered by our nanocubes-based system was able to crosslink the DNA of the cells and that the toxicity observed could be related to these platination events.

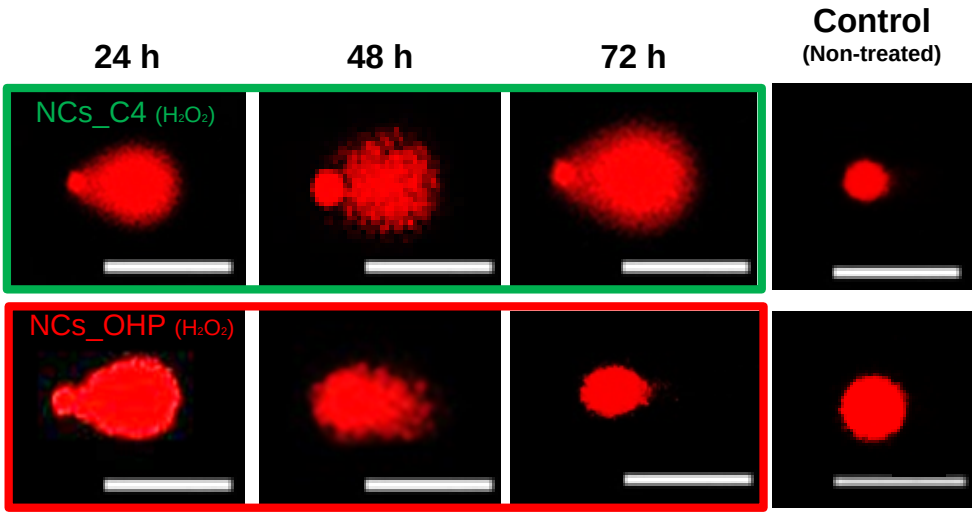

Figure 27. **Detail of the confocal microscopy images of comet assay.** Cell samples incubated with NCs_C4 (green box) and NCs_OHP_C4 (red box) for 24, 48 and 72 h and then treated with hydrogen peroxide. As control, typical comet images obtained for the cells incubated with the nanoparticles but not treated with H_2O_2 are also shown. Scale bar 100 μm.

3.2.12 Evaluation of the NCs-mediated hyperthermia efficiency on cells: intratumoral simulating injection

The choice of the nanocubes as vectors for drug delivery was primarily determined by their outstanding magnetic hyperthermia performances. Indeed, hyperthermia experiments were carried out on the cells treated with NCs, in order to monitor the efficiency of the nanoparticles in killing cancer cells by heat and in improving the toxicity mediated by oxaliplatin release. Two different strategies were followed. The first strategy aimed to simulate the intratumoral injection of nanoparticles, while the second the intravenous injection. The scheme of **Figure 37** sums up the first concept. IGROV-1 cells were grown at confluence. Once detached, $3x10^6$ cells were transferred in a small vial to a final volume of 100 μL. The collected cells, which simulate a tumor mass,[48] were incubated with NCs_PEG-Pt_C4 and exposed to an alternating magnetic field. After treatment, the cells were washed from the excess of nanoparticles and aliquots were collected for trypan blue, LDH, presto blue assays and ICP-AES analysis.

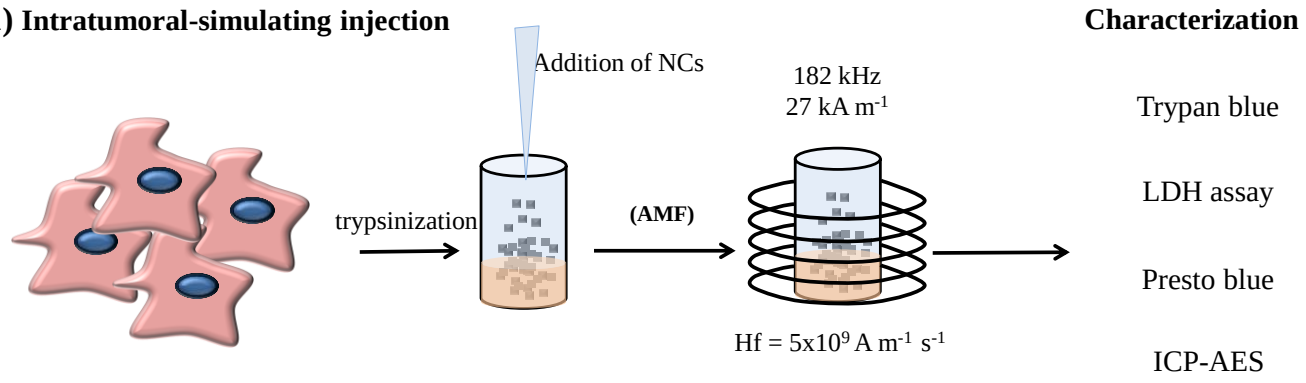

Figure 28. **Scheme of the first procedure used for exposing the cells incubated with the nanocubes to hyperthermia treatment.** With this strategy **(1)**, which simulates an intratumoral injection, the cells were detached and the nanoparticles added at high concentration to the cells just before starting the treatment.

According to the first strategy (scheme in **Figure 37**), $3x10^6$ IGROV-1 cells were incubated with 5.5 g/L of NCs_PEG-Pt_C4. Subsequently, they were exposed to a magnetic field of 27 kA m^{-1} at the frequency of 182 kHz, in order to not exceed the biological limit (Hf = $5x10^9$ A m^{-1} s^{-1}).[31] Two consecutive treatments of 30 min each were done. The maximum temperature ($T_{max)}$ was set at 42 °C. **Figure 38** shows the hyperthermia plot presenting the parameters used during the experiment. As control, also not treated cells, cells incubated with NCs_C4 (exposed to hyperthermia treatment or not) and cells incubated with NCs_OHP_C4 (not exposed to hyperthermia) were studied. A further control experiment was done by incubating the cells with free OHP at the same amount of drug loaded on the nanocubes (140 μM).

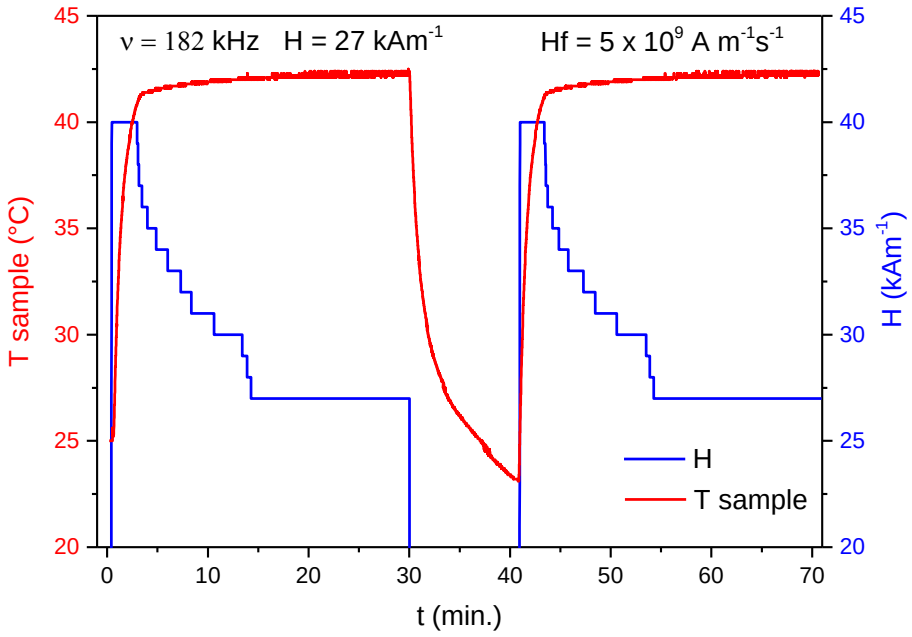

Figure 29. **Hyperthermia plot.** The parameters temperature (T), field (H), time (t) and the biological condition (Hf) used during the treatment of the cells with the nanocubes are shown. The parameter were chosen by keeping the product Hf within the limit regarded as safe for the treatment (Hf = 5 x 10^9 Am^{-1} s^{-1}). T_{max} was set at 42 °C.

3.2.12.1 Toxicity studies after the treatment

For trypan blue test, cells were collected, opportunely diluted, mixed with trypan blue dye and counted using optical microscopy. This test evaluates the cell viability by assessing the membrane integrity. This dye exclusion test is based on the principle that living cells have intact cell membranes which exclude some dyes such as trypan blue, whereas dead cells do not.[49] As a consequence, a viable cell has a clear cytoplasm, while a dead cell present a blue cytoplasm. **Figure 39** shows the percentage of blue dead cells, which became permeable to the trypan blue stain. With this test, no toxicity was observed for the cells treated with the free oxaliplatin or for the cells incubated with NCs_C4 and NCs_OHP_C4 but not exposed to hyperthermia cycles. Instead, ca. 20% of mortality was observed for the cells incubated with both nanocubes and treated with hyperthermia. These data indicated that the heat treatment induced cell damages and that the nanocubes obtained were able to kill cell by efficiently responding to an alternating magnetic field.

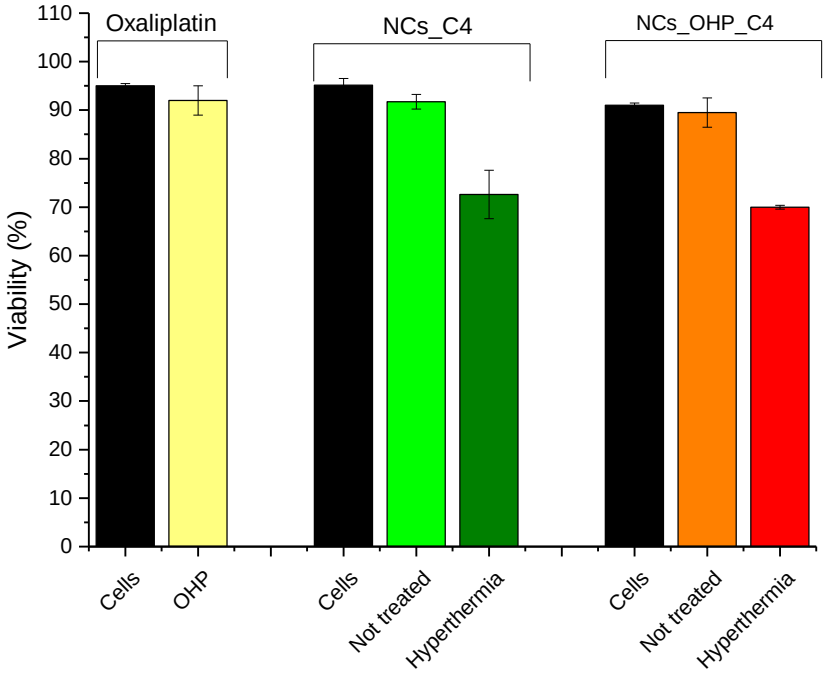

Figure 30. **Trypan blue assay.** Test performed after the cells exposition to the free oxaliplatin drug (light yellow bar) and incubated with NCs_C4 (green bars) or NCs_OHP_C4 (orange and red bars), exposed or not to hyperthermia (hyperthermia and not treated, respectively).

For the LDH viability assay, 50,000 cells from each sample were put in a vial with 200 µL of serum free media and incubated for 1 h at 37 °C. Then, the cells were pelleted in centrifuge and the supernatant collected and used for the test. This test measures the cells death using lactate dehydrogenase (LDH) release as a marker of membrane integrity.[50] LDH is a cytosolic enzyme which, when released in the supernatant of the cells, generates a colorimetric reaction by converting the lactate to pyruvate, via reduction of NAD+ to NADH. Then, diaphorase enzyme uses NADH to reduce a tetrazolium salt (INT) to a red formazan product. Therefore, the level of formazan formation is directly proportional to the amount of released LDH in the medium. The obtained results are shown in **Figure 40**. As also observed with trypan blue assay, the higher toxicity came from the cells incubated with both NCs and exposed to

hyperthermia. This was another clear indication that heat treatment efficiently induced toxicity in the treated cells.

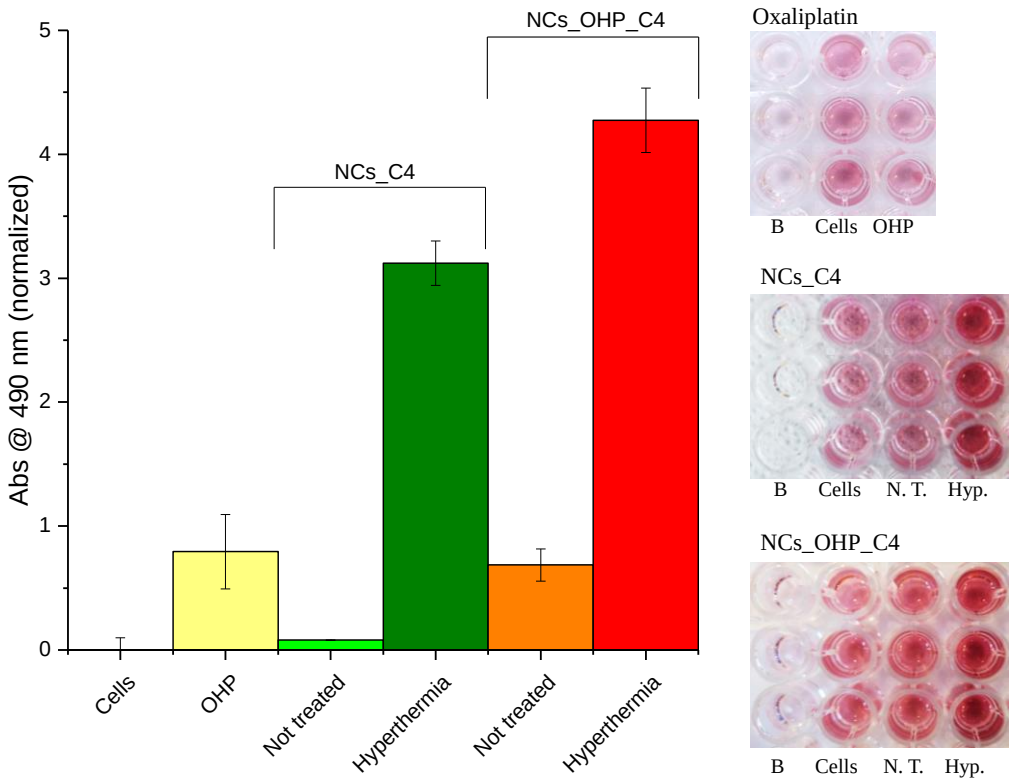

Figure 40. LDH assay. **a)** Test performed on IGROV-1 cells untreated, treated with NCs_C4 or NCs_OHP_C4 for 1 h at the concentrations of 5.5 g/L. The analysis was done on the supernatants collected after the 1 h hyperthermia treatment. The absorbance values are normalized with respect to the control. **b)** The pictures of the wells indicates the change of color for the sample with the higher amount of enzyme release.

Presto blue[37] was done starting from 24 h up to 120 h following the treatment, by re-incubating the cells from each sample, at the same number, in fresh medium. 50,000 cells in triplicate for each sample and time were used. The results obtained are shown in **Figure 41**. The viability of the cells treated with free oxaliplatin or NCs_C4, in presence or not of hyperthermia, or even NCs_OHP_C4 without heat treatment, after 120 h was comparable to that of the control cells (**Figure 41**). On the opposite, hyperthermia significantly affected the viability of the cell. Here, also in the case of cells treated with NCs_C4 moderate toxicity was observed after hyperthermia. However, 120 h after the treatment, the cells recovered their viability. Instead, the viability of the cells treated with NCs_OHP_C4 was significantly compromised even after 120 hyperthermia.

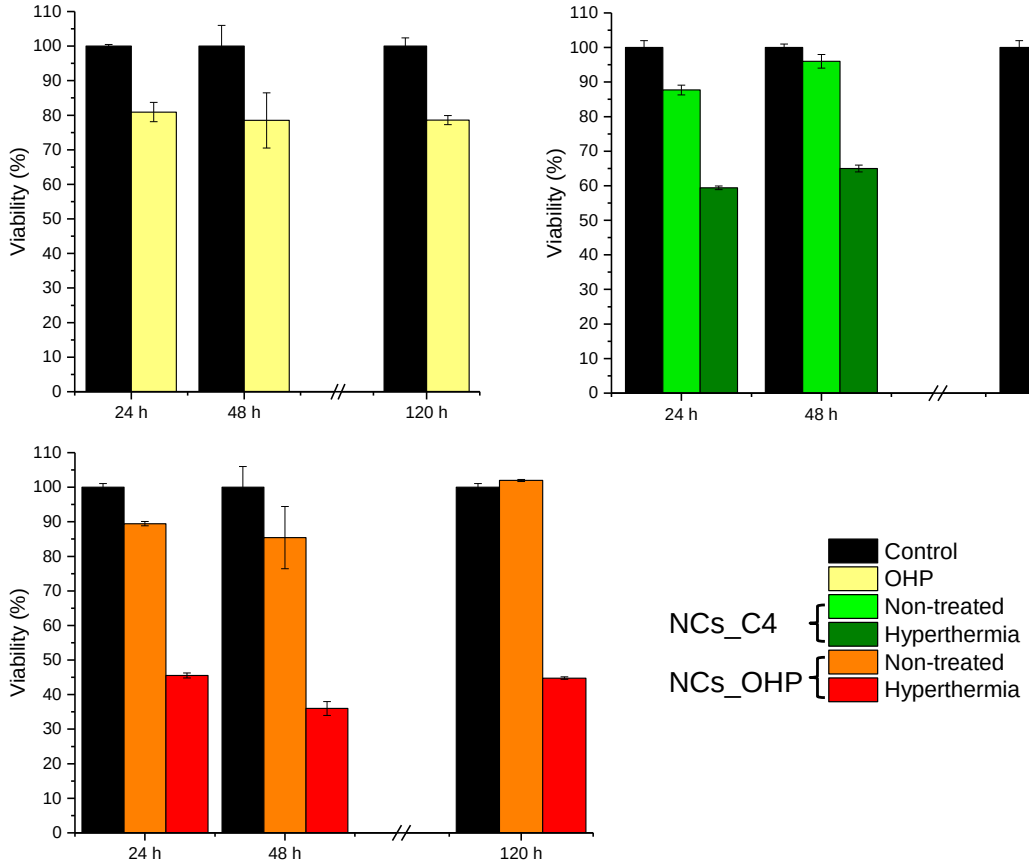

Figure 41. **Presto blue viability assay**. Test performed on IGROV-1 cells treated with free oxaliplatin (top left), with NCs_C4 (top right) or NCs_OHP_C4 (bottom left) for 1 h at the concentrations of 5.5 g/L. The viability of the cells was checked after 24, 48 and up to 120 h, at the confluency of the untreated control cells.

3.2.12.2 Determination of intracellular Pt after the treatment

Afterwards, $2x10^6$ cells were collected for the quantification of Fe and Pt. The amount of the two elements was determined *via* ICP-AES. In both cases Pt was detected inside the cells after the treatment (**Table 6**). Surprisingly, the cells treated additionally with hyperthermia contained an amount of the elements (Fe and Pt) five times higher than that of a not-treated sample. This could explain the difference in the toxicity found for the two samples. Noteworthy, this data also indicated that hyperthermia treatment could enhance the internalization of the NCs inside the cells, possibly according to a membrane-disruption process (confirmation also from LDH data in **Figure 40**).

Table 6. Concentrations of Fe and Pt per 10 millions cells after hyperthermia.

Sample	µmol Fe / 10^6 cells	nmol Pt / 10^6 cells
Cells	0.00055	/*
NCs_OHP n. t.	0.08	2.3
NCs_OHP hyp.	0.4	10.7

Note 4: *=data below the sensitivity curve of the instrument.

3.2.13 Evaluation of the NCs-mediated hyperthermia efficiency on cells: intravenous simulating injection

In the second strategy, (**Figure 42**) the cells were incubated with NCs_OHP_C4. Then, the cells were detached and $3x10^6$ cells were transferred in a small vial to a final volume of 100 µL. Subsequently, they were exposed to an alternating magnetic field. After the treatment, the cells were washed from the excess of nanoparticles and aliquots were collected for trypan blue, LDH, presto blue assays and ICP-AES analysis.

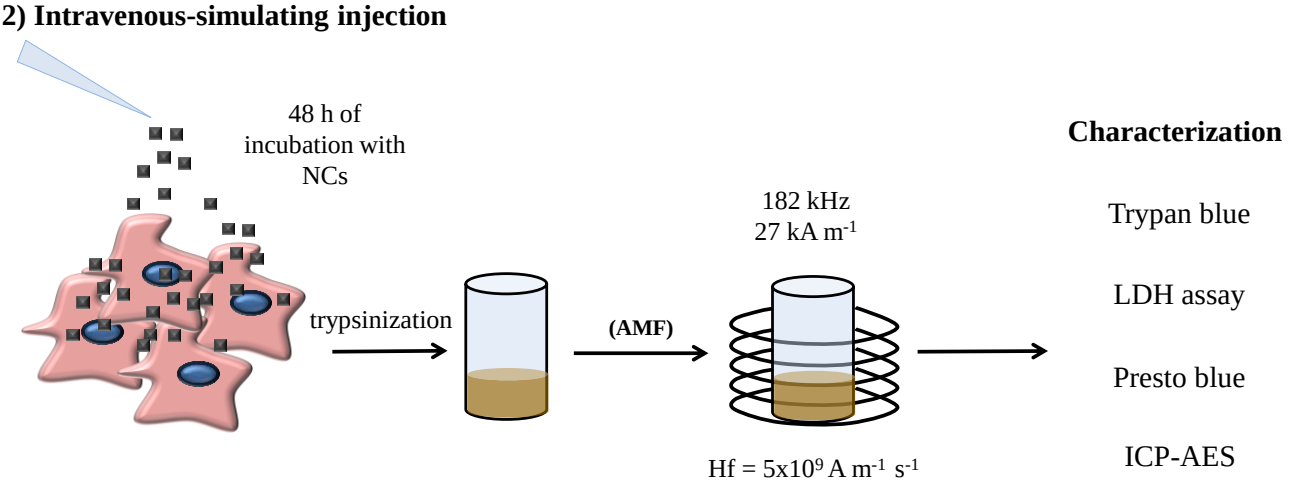

Figure 31. **Scheme of the second procedure used for exposing the cells incubated with the nanocubes to hyperthermia treatment.** In the second case **(2)**, the nanocubes, at lower concentration of incubation, were let to accumulate for 48 h inside the cells. Here, just the nanoparticles directly interacting with the cells participated to hyperthermia treatment. This second procedure mimics a targeted accumulation of the nanoparticles at the tumour site, subsequent a not localized intravenous injection.

According to the second strategy, the treated cells were exposed to a magnetic field of 27 kA m^{-1} at the frequency of 182 kHz, in order to not exceed the biological limit (Hf = $5x10^9$ A m^{-1} s^{-1}). Two consecutive treatments of 30 min each were done. **Figure 43** showed the hyperthermia plot presenting the parameters and their range, using during the experiment. It is clear from this graph that the temperature of 42 °C was reached after a longer time (compare to the case of the first strategy) of exposition of the cells at a field higher than 27 kA m^{-1}, which exceed the limit of Hf, at least at the beginning of the treatment. Just one third of the treatment was done according to the biological limit. This was due to the lower dose of NCs used for the treatment, compared to the first strategy. Differently from the first case, non-treated cells and cells incubated with NCs_PEG-Pt_C4 (not exposed to hyperthermia) were studied. Indeed, there was not significant toxicity for the NCs_C4, even with hyperthermia (**Figure 39**, **40** and **41**). As in the first strategy, a control experiment using free oxaliplatin at the loaded concentration (3.9 µM) was done.

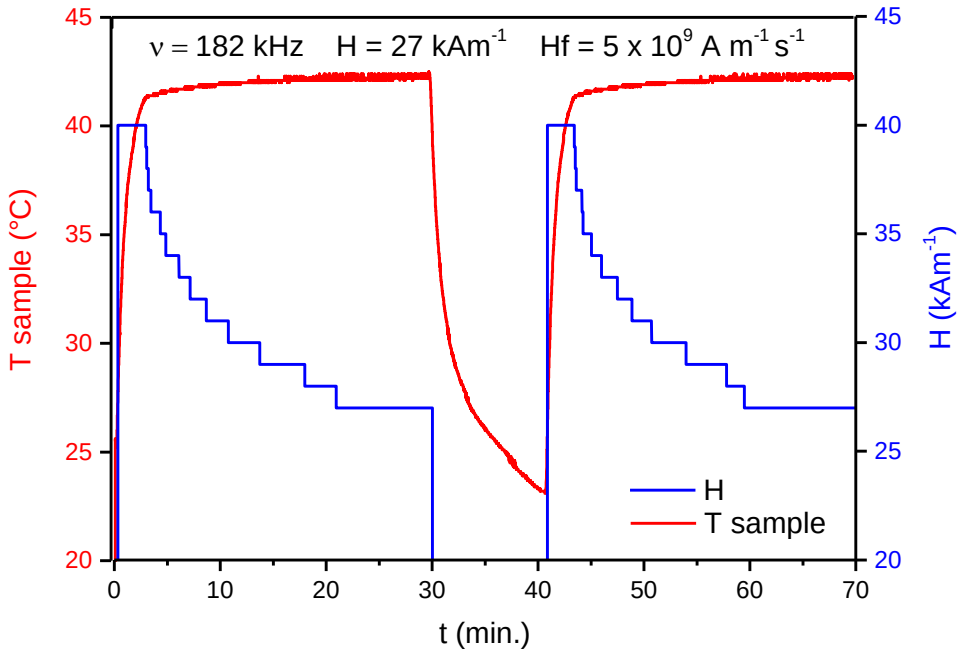

Figure 32. **Hyperthermia plot.** The parameters temperature (T), field (H), time (t) and the biological condition (Hf) used during the treatment of the cells with the nanocubes are shown. The parameters were chosen by keeping the product Hf within the limit regarded as safe for the treatment (Hf = 5 x 10^9 Am^{-1} s^{-1}). T_{max} was set at 42 °C. It has to note that just one third of the treatment time was done according to these conditions. Indeed, the magnetic field amplitude is stabilized at 27 kAm^{-1} just 20 minutes after the beginning of the treatment, while in the first experiment (**Figure 38**) after 10 minutes.

3.2.13.1 Toxicity studies after the treatment

Trypan blue test (**Figure 44)** indicated a slight mortality for the cells treated with hyperthermia, suggesting that, even after being up-taken by the cells, the nanocubes were able to heat the surrounding environment (as also verify by reaching the temperature of 42 °C in the graph of **Figure 43**) and to affect the viability of the "tumor-like" mass.

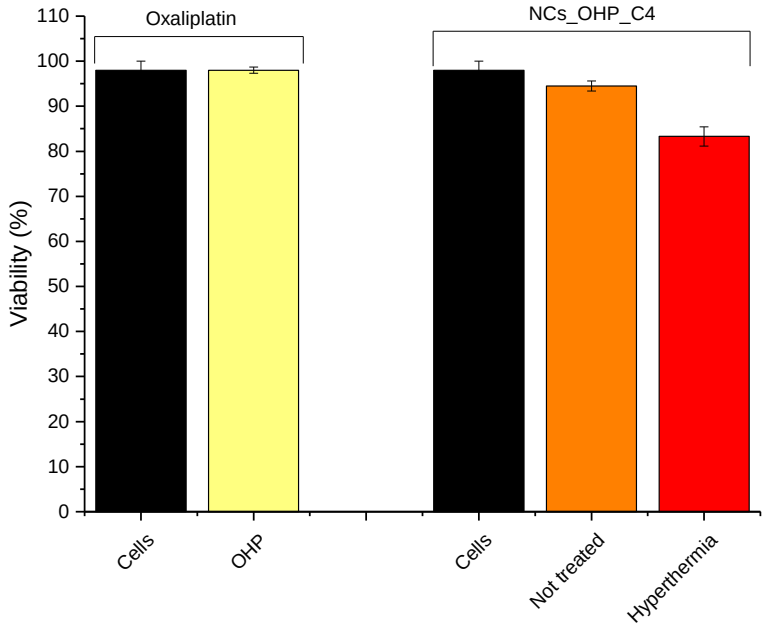

Figure 33. **Trypan blue assay**. Test performed after the cells exposition for 48 h to free oxaliplatin drug (left) and incubated with NCs_OHP_C4 (right), exposed or not to hyperthermia (hyperthermia and not treated, respectively).

Subsequently, LDH viability assay was performed, according to the above shown procedure. As one can observed in **Figure 45**, hyperthermia treatment produced the higher cell damage, inducing a high LDH release.

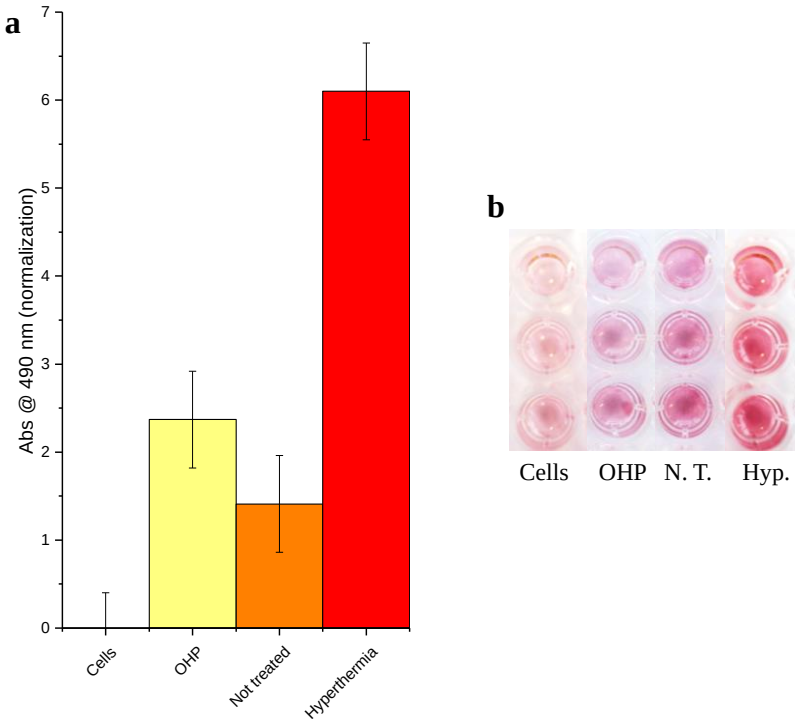

Figure 34. LDH assay. **a)** Test performed on IGROV-1 cells untreated, treated for 48 h with free drug and NCs_OHP_C4, exposed or not to hyperthermia (hyperthermia and not treated, respectively). The analysis was done on the supernatants collected after the 1 h hyperthermia treatment. The absorbance values are normalized

with respect to the control. **b)** The pictures of the wells indicates the change of color for the sample with the higher amount of enzyme release.

Viability assay *via* presto blue was done starting from 24 h up to 120 h following the treatment, by re-incubating the cells from each sample, at the same number, in fresh medium. 50,000 cells in triplicate for each time were used. Presto blue assay in **Figure 46** indicated that the viability of cells treated with NCs_OHP_C4 and also exposed to the hyperthermia treatment was significantly affected. On the other side, the toxicity of the nanocubes in absence of hyperthermia was comparable to that of free oxaliplatin. These data indicated that the combination of oxaliplatin release and hyperthermia treatment affected irreversibly the cell viability.

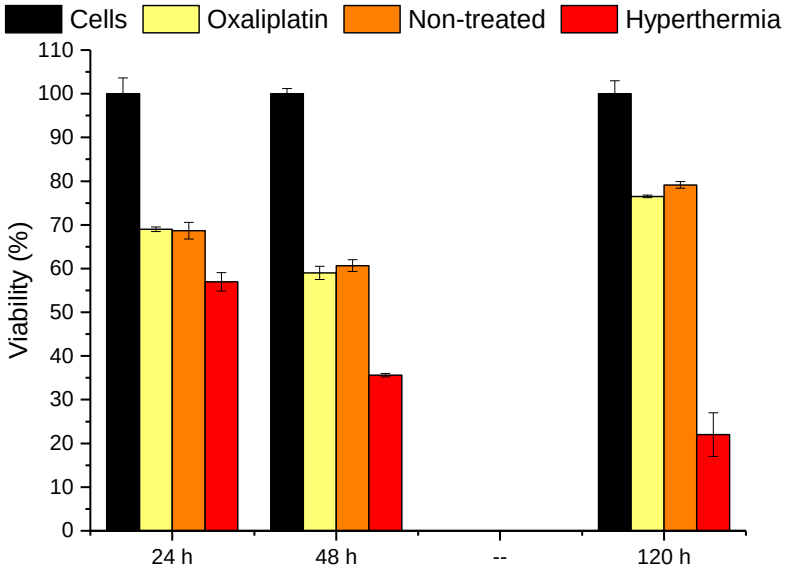

Figure 35. **Presto blue viability assay**. Test performed on IGROV-1 cells untreated, treated for 48 h with free drug and NCs_OHP_C4, exposed or not to hyperthermia (hyperthermia and not treated, respectively). The viability of the cells was checked after 24, 48 and up to 120 h, at the confluency of the untreated control cells.

3.2.13.2 Determination of intracellular Pt after the treatment

Subsequently, the amount of Fe and Pt inside the cells was determined *via* ICP-AES. **Table 7** shows the values collected. Pt was found both in the sample treated with hyperthermia and not-treated, confirming, also in this second case, that the toxicity resulted from a combination of hyperthermia treatment and oxaliplatin delivery. Differently from the previous experiment, the values of intracellular Pt were similar for both the samples. This can be explained with the assumption that in this second case just the NCs already internalized or bound to the cells participated to the heating process and no membrane disruption process, which force the nanocubes inside the cells, occurred as happened in the case of the first strategy.

Table 7. Concentrations of Fe and Pt per 10 millions cells after hyperthermia.

Sample	µmol Fe / 10^6 cells	nmol Pt / 10^6 cells
Cells	0.00055	/*
NCs_OHP n. t.	0.118	3.33
NCs_OHP hyp.	0.113	3.17

Note 5: *=Data below the sensitivity curve of the instrument.

3.3 Conclusions and perspectives

In this project, cubic iron oxide nanoparticles (NCs) were investigated in detail and applied for multiple purposes. The main result obtained was the double functionalization of these nanocubes, which made them suitable for a combinatorial drug delivery and targeting approach. To reach the drug delivery aim, the nanocubes were first functionalized with oxaliplatin-derived PEG molecules (PEG-Pt). To enable an active targeting of tumor cells, the iron oxide NCs were successfully functionalized with PEG- *N*,*N*-(carboxymethyl) lysine (PEG-NTA) to bind an his-tagged scFv antibody, specific for folate receptor α (FRα). It could be demonstrated that the antibody fragment attached on the nanocubes was r active and able to recognize its target, either immobilized on synthetic substrates or expressed on the cell membrane. Subsequently, the toxicity of the material conjugated with the antibody and functionalized with the PEG-Pt compound, as well as the non-functionalized material was assessed. It could be shown that while the nanocubes without the PEG-Pt compound did not show toxicity, confirming the safety of the reagents and materials used for the synthesis of the nanoparticles, the NCs with attached PEG-Pt significantly affected the viability of the treated cells. The drug release of oxaliplatin (OHP) from the nanocubes was investigated in *in vitro* conditions using citrate buffer at different pH values, according to the values characteristic for endosome, late endosome and lysosome (pH= 5.5, 5 and 4.5 respectively). It could be demonstrated that the release of OHP was pH dependent and that the maximum release was obtained at the lowest pH, representing the lysosome environment. Consequently, the release efficiency of the drug in cells was tested. Once released, the toxicity of oxaliplatin was induced by coordinating to the DNA and thus blocking the replication and transcription of the genetic material of the cell. Indeed, it was demonstrated that Pt was able to form crosslinks with the DNA. The stability in aqueous solvent plays a crucial role for the exploitation of these nanomaterials in biological applications. Thus, iron oxide magnetite nanocubes were efficiently covered with an amphiphilic polymer using the polymer coating procedure. After the efficient water transfer using a published technique,[24, 25] the nanocubes exhibited good stability and monodispersity. The investigation of the magnetic properties of the nanocubes revealed a viscosity independent behavior of the heating performance. Indeed, even at the highest viscosity (81% glycerol, 97.3 mPa.s), conditions which simulate the tumoral environment, the SAR value did not vary significantly compared to the value calculated in water as the relaxation process is exclusively determined by the Néel mechanism. This is crucial for the hyperthermia application, since these nanocubes have to heat in a highly viscous environment as the cells mass. Indeed, the performed hyperthermia tests demonstrated the efficient heating of the treated cells up to the hyperthermia temperature window (42 °C). Besides promoting the cell death with the thermal treatment, the presence of PEG-Pt further increased the toxicity of the nanocubes. The toxicity arose in combination with the release of OHP, which was efficiently found inside the cells. In conclusion, we developed a triple-therapy strategy for cancer treatment, by combining targeting, drug delivery and hyperthermia. The nano-platform designed is able to efficiently recognize its target, can be loaded with drugs and kill the desired cells by a powerful combination of drug release and hyperthermia, in the *in vitro* model studied. This combination represents a result so far not yet reached in literature. Further developments of this project will exploit the properties of the nanocubes in *in vivo* studies, in order to prove the efficiency of our material on animal models consisting of ovarian cancer-xenografted mice.

3.4 Materials and methods

Nanocubes synthesis

Maghemite (Fe_2O_3) nanocubes (NCs), with an edge size of 14 ± 3 nm were synthetized according to a procedure previously set in our group.[2] Briefly, in a 50 mL three neck flask, 0.353 g (1 mmol) of iron(III) acetylacetonate, 0.69 g (4 mmol) of decanoic acid and 2 mL of dibenzyl ether (DBE) were dissolved in 23 mL squalane. After degassing for 120 min at 65 °C, the mixture was heated up to 200 °C (heating ramp was 3 °C min^{-1}) and kept at this temperature for 2.5 h (a shorter "aging time" at 200 °C led to lower reproducibility as well as to broadening of the size and shape distributions of the final particles). The temperature was then increased at a heating rate of 7 °C min^{-1} to 310 °C or reflux temperature and maintained for 1 h. After cooling down to room temperature, 60 mL of acetone were added and the solution was centrifuged at 8500 rpm. The supernatant was then discarded and the black precipitate was dispersed in 2–3 mL of chloroform: this washing procedure was repeated at least two more times. Finally, the collected particles were dispersed in 15 mL of chloroform. The concentration of the final nanocubes was determined by ICP analysis.

Polymer coating on single nanoparticles

Polymer coating on single nanocubes (called PC-NCs) was obtained using the following established method.[24-26] The procedure is based on the coating of single nanoparticles with an amphiphilic polymer, poly(maleic anhydride-*alt*-1-octadecene). The hydrophobic side-chains of the polymer intercalate into the alkyl chains of the pristine NC`s ligand while the hydrophilic maleic anhydrides are exposed to the water phase, thus solubilizing the hydrophobic nanoparticles in polar media. To ensure a single particle polymer coating it is crucial to use an excess of polymer monomer, fixed at 500 monomer units of polymer per nm^2 of nanoparticle surface, as already reported in our previous works.[25, 26] In detail, iron oxide nanocubes were mixed with an excess of 500 monomer/nm^2 of poly(maleic anhydride-*alt*-octadecene) in $CHCl_3$. Then, the solvent evaporation was carried out using a rotary evaporator. The applied vacuum was slowly decreased to 600 mbar. The entire evaporation step took 5 h. In this step, the slow evaporation of the solvent is crucial. After the complete evaporation of chloroform, borate buffer was added and the mixture sonicated for 2 h at 50 °C. Nanocubes were concentrated using an amicon centrifuge filter and separated from the excess of polymer by ultracentrifugation, using a discontinuous sucrose gradient with the following composition (sucrose : water v%): 20%, 40% and 60%, layered from the top to the bottom of the ultracentrifuge tube. After 45 min centrifugation at a speed of 25,000 rpm, the nanocubes were collected in the middle fraction, while the free polymer remained in the top layer of the gradient. The recovered nanoparticles were washed several times in order to remove the excess of sucrose. Dynamic light scattering DLS, gel electrophoresis and transmission electron microscopy (TEM) characterizations were performed to ensure that the NPs were obtained in a single, stable and not aggregated state and free from the excess of polymer.

Low-resolution Transmission electron microscopy (TEM).

Low resolution TEM micrographs were taken using a JEOL JEM-1011 microscope operated at 100 kV. The samples were prepared by drying a drop of diluted particle suspensions on 400 mesh ultra-thin carbon

coated TEM copper grids. The particle size distribution was analyzed using the automatic particle size analysis routine of ImageJ software on a low magnified TEM micrograph.

Calorimetric measurements of the specific absorption rate (SAR)

Magnetic hyperthermia studies on nanocubes were carried out using a nanoScale DM1 Series (Biomagnetics Corp.). Alternating magnetic fields with a frequency of 111 kHz and 301 kHz and with a magnetic field amplitudes of 12, 15, 17, 20 and 24 kAm^{-1} were used. The sample concentration was kept at 3 g/L and 1 g/L for the viscosity studies. The Specific Absorption Rate (SAR) value was determined by measuring the initial slope of the temperature vs. time curve (within the first seconds). The measurements are normalized to the concentration of iron taking into account the water heat capacity. All the reported SAR values and error bars were calculated from the mean and standard deviation of at least three experimental measurements. SAR values were calculated according to the following equation:

$$SAR = \left(\frac{W}{g}\right) = \frac{C}{m}\ x\ \frac{dT}{dt} \qquad (1)$$

where C is the specific heat capacity of the solvent (C_{water} = 4185 J L^{-1} K^{-1}; $C_{gly36\%}$ = 3550 J L^{-1} K^{-1}; $C_{gly68\%}$ = 2850 J L^{-1} K^{-1}; $C_{gly81\%}$ = 2580 J L^{-1} K^{-1}) and m is the concentration (g L^{-1} of Fe) of magnetic material in solution. Note that the final values are reported as (W/gFe). The measurements were carried out in non-adiabatic conditions, thus the slope of the curve dT/dt was measured by taking into account only the first few seconds of the curve.[28]

AC-susceptibility measurements

The complex AC-susceptibility (ACS) measurements were carried out using two set-ups operating form 10 Hz to 10 kHz and 1 kHz to 1 MHz at magnetic field amplitude of 0.46 kAm^{-1} and 0.07 kAm^{-1}, respectively. The ACS measurements at lower frequencies (2 Hz to 9 kHz) were performed using a fluxgate-based rotating magnetic field setup at 0.16 kAm^{-1} magnetic field amplitude. The sample concentration was kept at 1 g/L. The anisotropy constant was calculated according to the following equation: [29]

$$\tau_N = \frac{\sqrt{\pi}}{2\sqrt{KV/TK_B}}\ \tau_0\ e^{-KV/TK_B} \qquad (2)$$

where τ_N is the Néel relaxation time, τ_0 is the inverse attempt frequency, K is the magnetic anisotropy constant, V is the nanoparticle volume, K_B is the Boltzmann constant and T is the temperature.

Characterization of NCs: DLS and gel electrophoresis

The hydrodynamic diameter and zeta potential of the nanoparticles were measured using a Malvern Zetasizer operated in the 173° backscattered mode on highly diluted aqueous solutions. The measurements were performed at 20 °C. Gel electrophoresis was run on 1%-2% agarose gel at a voltage of 100 V for 1 h. This technique was used just for single nanocubes.

Synthesis of PEG-NTA

1. Fmoc-PEG-NHS synthesis

Fmoc-PEG-COOH (Mn=3000 g/mol) was reacted with N-hydroxysuccinimide (NHS) in order to activate the carboxylic group. Briefly, 200 mg of PEG (0.07 mmol) were dissolved in anhydrous dichloromethane (DCM) under nitrogen flow. 1-ethyl–3-(3-dimethylaminopropyl) carbodiimide (EDC) (0.35 mmol; 5 eq.) and NHS (0.35 mmol; 5 eq.) were added and the mixture was stirred under nitrogen atmosphere for 1 h at 6 °C. Afterwards, the reaction was allowed to proceed for 48 h at room temperature. The product was extracted with water and analyzed *via* ^{1}H-NMR spectroscopy ^{1}H NMR spectra were recorded on a Bruker AV-400 NMR spectrometer (Rheinstetten, Germany) operating at 400 MHz (128 scans) in deuterated dimethyl sulfoxide (DMSO-d_6). ppm: δ: 7.89 (**f**), 7.69 (**i**), 7.41 (**g**), 7.33 (**h**), 4.28 (**d**), 4.2 (**e**), 3.68 (**b**), 3.51 (**c**), 2.81 (**a**), as reported in figure 14 of the results and discussion paragraph.

2. Fmoc-PEG-NTA synthesis

Fmoc-PEG-NHS (200 mg; 0.07 mmol) was dissolved in a mixture of DMSO and water 1:1 (20 mL final volume). N_{α},N_{α}-Bis(carboxymethyl)-L-lysine (0.14 mmol; 2 eq.) and EDC (1.3 mmol; 20 eq.) were added and the solution was stirred for 12 h. The obtained product was then dialyzed for 72 h against water using a RC membrane with a cut-off of 1000 g/mol. Subsequently, water was evaporated from the product using a rotary evaporator.

3. Fmoc-PEG-NTA deprotection

The yielded polymeric material was dissolved in a mixture of DCM : ethanolamine 1:1 to deprotect the amine group. Therefore, the mixture was stirred for 12 h and the final product was purified by dialysis against water using a RC membrane (cut-off 1000 g/mol), for 72 h.

4. NH2-PEG-NTA-Ni synthesis

NH_2-PEG-NTA (200 mg; 0.07 mmol) was dissolved in 20 mL of water and incubated with $NiCl_2$ (0.7 mmol; 10 eq.) for 2 h. Subsequently, the product was dialyzed for 72 h against water using a RC membrane (cut-off 1000 g/mol). The final product was obtained, as greenish powder after freeze-drying and stored at -20 °C.

Deprotection of PEG-Pt compound

The PEG-Pt compound (NR649 batch), provided by our collaborator Prof. Juan Granja of the University of Santiago de Compostela (Department of Organic Chemistry and Center for Research in Biological Chemistry and Molecular Materials, CIQUS), was dissolved in methanol at a concentration of 2 mg/mL. The deprotection of the amine group from the triphenylmethane group was carried out according to a procedure set by Alessandra Quarta. Briefly, 1 mg of compound in methanol was incubated with 1 g of Amberlite resin IR-120, under vigorous shaking. After 12 h of stirring, the obtained compound was filtered and analyzed *via* thin-layer chromatography (TLC). The final product was dissolved in methanol at the concentration of 1 mg/mL. Importantly, before use, the Amberlite resin was washed several times with methanol in order to remove the excess of not polymerized polystyrene sulfonate. Since this product is highly fluorescent, we checked the purity of the supernatant of each wash under an UV lamp (365 nm filter).

Functionalization of NCs with PEG-Pt

NCs (0.1 μM), dissolved in 500 μL of a mixture 1:3 of borate buffer (BB; pH=9) and water, were incubated with 12.7 mM of EDC (127,000 molecules per iron nanoparticles) for 10 min. Then, 0.05 mM of amine-PEG-Pt (Mn= 1,000 g/mol) (500 molecules per nanoparticle) were added and the mixture reacted for 4 h. The nanocubes were washed five times with borate buffer using an amicon filter tube (cutoff 100,000 g/mol) until the supernatant was clean from the excess of reagents.

Functionalization of NCs with PEG-NTA

NCs (0.1 μM), dissolved in a mixture 1:3 of borate buffer (BB; pH=9) and water, were incubated with 12.7 mM of EDC (127,000 molecules per iron nanoparticle) for 10 min. Then, 0.55 mM of amine-PEG-NTA (Mn= 3262 g/mol) (5,500 molecules per nanoparticles) was added and the mixture reacted for 4 h. A sample functionalized with amine-PEG-carboxy was synthetized to be used as a control. The nanocubes were washed five times with borate buffer using an amicon filter tube (cutoff 100,000 g/mol) until the supernatant was clean from the excess of reagent.

ICP-AES analysis of Fe, Ni and Pt

For treatment of the nanoparticles samples the following procedure was used: an aliquot of NCs_PEG-Pt-NTA or NCs_PEG-NTA was digested in 1 mL of aqua regia solution (HCl:HNO_3 3:1). The digestion proceeded over-night at room temperature. The solution was diluted to 10 mL with milliQ water and filtered with a PVDF filter (0.45 um) before the analysis. The intracellular Fe, Ni or Pt concentration was measured by inductively coupled plasma atomic emission spectrometry (ICP-AES, Thermofisher ICAP 6300 duo) and with the preparation of a Fe, Ni or Pt calibration curve (0.01 - 10 ppm). **For treatment of cell samples the following procedure was used:** the cell samples incubated with NCs_PEG-Pt-NTA or NCs_PEG-NTA were digested with 250 μL of a concentrated H_2O_2/HNO_3 (1/2) solution for 3 h in a water bath at 55 °C under sonication (in order to ensure the complete digestion of the cells components). After this step, which lead to the complete evaporation of H_2O_2, concentrated HCl was added (3/1 volume ratio respect to HNO_3) to reach a final volume of 500 μL. The digestion proceeded over-night at room temperature. The solution was diluted to 5 mL with milliQ water and filtered with a PVDF filter (0.45 um) before the analysis. The intracellular Fe concentration was measured by inductively coupled plasma atomic emission spectrometry (ICP-AES, Thermofisher ICAP 6300 duo) and with the preparation of a Fe calibration curve (0.01 - 10 ppm).

ICP-MS analysis

For treatment of cell/DNA samples the following procedure was used: the cell/DNA samples incubated with NCs_PEG-Pt-NTA were digested with 200 μL of concentrated HCl. The digestion proceeded over-night at room temperature. The solution was diluted to a final concentration of 5%HCl with milliQ water and filtered with a PVDF filter (0.45 um) before the analysis. **The intracellular Pt concentration** was measured by inductively coupled plasma mass spectrometry (ICP-MS) and with the preparation of a Fe calibration curve (0.01 - 10 ppb).

scFv binding to nanocubes

0.1 μM of NCs_PEG-Pt-NTA or NCs_PEG-NTA were incubated with 4 μM scFv (50 μg) in 500 μL of 0.1 M PBS, pH = 7.4 at 4 °C for 12h under gently shaking. After the incubation time, NCs were washed

with PBS using an Amicon filter tube (cutoff 100,000 g/mol) until the supernatant was free from the excess of reagent.

Quantification of bound protein (BCA assay)

Both the supernatant and the washing solutions were analyzed with BCA, a colorimetric protein assay. It is a spectroscopic procedure used for the quantification of the protein in solution, regarding to a calibration curve made with a standard protein at known concentration. BCA is based on the absorbance shift of the dye Comassie Brilliant Blue G-250 at 560nm, which take place when the reagent interact with the ionizable protein groups. For setting the calibration curve, an aliquot of antibody was used.

SDS-PAGE

12.5% of polyacrylamide gel (12.5%) run at 100 V for 1h. Before running, samples was heated with a solution of denaturing agents (SDS 0.1%, DTT 100 mM) at 90°C for 5 min. In this way, all the proteins, eventually bound by the nanobeads, were eluted prior to run the gel. As control, 5 μg of scFv were run on the gel.

Dot blot assay

Dot Blot assay was carried out on pre-activated nitrocellulose membrane. Typically, 20 μg of nanoparticle were spotted on the membrane and left to dry thoroughly. Next, the membrane was gently shaken in 20 mL suspension of PBS-T20-dried milk powder (100:4 w/w%) for 30 min to block non-specific binding sites. Afterwards, the membrane was washed three times with 30 mL PBS-T20 and finally soaked in 20 mL PBS-T20 containing 4 mL of solution containing the primary antibody (from mouse) specific for the scFv C4. The mixture was gently shaken for 2 h in darkness and then the membrane was rinsed 3 times with 30 mL PBS-T20 to remove unbound antibody counterparts. Subsequently, the membrane was soaked in 20 mL PBS-T20 containing 5 μL goat anti-mouse IgG secondary antibody conjugated to Alexa fluor 488 (1:4000 dilution). The mixture was gently shaken for 1 h in darkness and then the membrane was rinsed 3 times with 30 mL PBS-T20 to remove unbound antibody. The membrane was imaged using Bio-Rad ChemiDoc MR imaging system at 488 nm wavelength.

Surface plasmon resonance (SPR) analysis

Kinetic analysis of NCs_C4 was done by means of SensiQ Pioneer (SensiQ Technologies). Soluble recombinant human folate binding protein (Abcam, UK) was covalently bound to a COOH2 (purchased from SensiQ Technologies) sensor chip using the EDC/NHS chemistry (0.1 M and 0.4 M respectively, flow rate 20 μL min^{-1}) at a ligand concentration of 70 μg/ml in 10 mM sodium acetate, pH=7. The injection rate was 25 μL min^{-1}. The injection of 1.0 M ethanolamine atpH = 8.5 (flow rate 20 μL min^{-1}) was used to block the residual activated groups. The concentration of nanocubes used for the binding proofs was 8 mM. the injection rate was 20 μL min^{-1}. NCs-C4 and NCs_PEG-COOH, as negative control, were used for the analysis. Importantly, the regeneration of the chip (flow rate 50 μL min^{-1}, 25 μL min^{-1} in the case of ethylene glycol) was not possible in any conditions tested (glycine 100 mM, pH = 2; NaCl 1-5 M; glycine 10 mM, pH = 2; glycine 10 mM, pH = 1.5; glycine 20 mM, pH = 1.5; NaOH 10-50 mM; ethylene glycol 50%; ethylene glycol 100%; MgCl 1 M; NCl 10 mM; SDS 0.05%; SDS 0.1%; KSCN 3 M). This case was already reported by *Stella et al*.[35]

Cell Culture

A431-tFR and A431-MOCK cells (provided by Fondazione IRCCS, Istituto Nazionale dei Tumori, Milano, IT) were cultured in Dulbecco's Modified Eagle Medium (DMEM, Merck, Kenilworth, USA). IGROV-1 cells (ATCC, UK) were cultured in RPMI-1640 medium (RPMI-1640, Merck, Kenilworth, USA). KB cells (ATCC, UK) were cultured in RPMI-1640 without folic acid (RPMI-1640 no folic acid, Merck, Kenilworth, USA). All the media were supplemented with 10% Fetal Bovine Serum Inactivated (FBS), 1% Penicillin Streptomycin (PS) and 1% Glutamine at 37 °C, 95% humidity with 5% CO_2. Cells were split every 3-4 days before reaching confluency.

Fluorescence Activating Cell Sorting (FACS)

For the cytofluorimetric analysis, 5 x 10^5 cells were incubated in PBS at 4 °C for 1 h with the nanocubes conjugated with the antibody or functionalized with just carboxy-PEG as negative control. After three washes, the cells were incubated with the primary antibody anti-myc tag of C4 for 1 h and 30 min, at 4 °C. Subsequently, after three washes, the cells were incubated with the secondary antibody conjugated to Alexa-488 for 1 h at 4 °C. After three more washes, the cells were analyzed with a FACSAria II (Becton-Dickinson, San Jose, CA). In detail, first the forward scattering profile (FSC) vs. the side scatter profile (SSC) graphs were recorded. In order to compare always the same cell populations for all the different samples, a physical gate, the area P1, was selected. On all the cells which belong to the area P1, the Alexa-488 fluorescence intensity vs. the number of counts was measured and plotted.

Nanocubes labeling for CLSM analysis

NCs_C4 were labeled using primary antibody specific for scFv C4 (from mouse) and a goat anti-mouse IgG secondary antibody conjugated to Alexa-488. In detail. 0.15 g/L of NCs_C4 were incubated for 1 h with primary antibody, in a 1.5 mL vial, at 4 °C. The nanoparticles were washed once with PBS in order to remove the unreacted antibody, using an amicon tube (cutoff 100,000 g/mol). Afterwards, secondary antibody was added (1:5,000 dilution) and the mixture was let to react for 1 h at 4°C. Finally the NCs were washed once with PBs and incubated with the cells.

Cellular Uptake Studies-Confocal imaging-

40,000 IGROV-1 cells well were plated in 12 mm coverslip in a 24 multiwell plates and allowed to adhere for 24 h. The cells were then incubated with labeled NCs_C4 at the concentrations of iron of 0.15 g/L, in growth medium, for the indicated time. At the same time, LysoTrackerRed DND-99 (Life Technologies, Carlsbad, CA, USA) was added at the concentration of 100 nM. Afterwards, the doping medium was removed and the cells were washed once with Phosphate Buffered Saline Solution (PBS, 10 mM). Hoechst (Thermo Fisher Scientific, Waltham, USA) was added to the cells, in PBS at 37 °C for 15 min. The media was removed, the cells washed twice with PBS, fixed with 4% (w/v) paraformaldehyde (PFA) at room temperature (RT) for 20 min and washed three times with 1 PBS. The samples were then mounted using Equitt quick-hardening mounting medium (Merck, Kenilworth, USA) and stored at 4 °C. To test the membrane crossing 40,000 HeLa cells/well were plated and incubated for 30 min at 4 C with Cu-clusters at 800 nM Cu concentration, fixed with 4% (w/v) PFA at RT, washed three times in PBS and analized by confocal miscoscopy.

Cellular Uptake Studies-TEM imaging-

40,000 IGROV-1 cells well were plated in a 24 multiwell plates and allowed to adhere for 24 h. Alternatively, 3,000,000 IGROV-1 cells were plated in a T25 flask and allowed to adhere for 24 h. The cells were then incubated with NCs_OHP_C4 at the concentrations of iron of 0.15 g/L, in growth medium, for the indicated time. Cells were incubated in growth medium supplemented with glutaraldeyde (2%), for 45 min at room temperature (RT). Cells were then centrifuged at 14,000 rpm for 10 min. The obtained pellet was then dissolved in Na-cocodylate buffer (0.1 M, pH 7.4) supplemented with glutaraldeyde (2%) and mixed for 1 h at room temperature (RT). Afterwards, cells were centrifuged at 14,000 rpm for 10 min. 3 washes of 10 min each were repeated in Na-Cacodylate buffer (0.1 M). Subsequently, the pellet was incubated with Na-Cacodylate buffer (0.1 M) supplemented with OsO_4 (1%) for 1 h, at RT. 3 washes of 10 min each in Na-Cacodylate buffer (0.1 M) followed. Then, the pellet was washed three times for 5 min with mQ water and incubated overnight (O.N.) in Uranyl acetate buffer 1% (in water). Then, the sample was gradually dehydrated in ethanol (EtOH), at increasing concentration of 70%, 90%, 96% and 100%. Then, pellet was washed three times for 15 min with propylen oxide. Afterwards, samples was incubated in a solution of Spurr and propylen oxide (1:3) and 3 h in Spurr and propylene oxide solution (1:1). Finally, the pellet was incubated for 3 h in Spurr and included into it by curing at 70°C O.N. Thin section of 70 nm of selected zones were observed with JEOL Jem1011 electron microscope operated at 100 keV.

Confocal laser scanning microscopy (CLSM)

Confocal imaging was performed using a Nikon A1 laser scanning confocal microscope, all samples were imaged avoiding pixel saturation to not interfere with further analysis. Z-stack imaging was performed with a step size of 200 nm. Images were analyzed with ImageJ (http://rsb.info.nih.gov/ij/).

Cell viability test by presto blue

The cell viability was studied using the PrestoBlue (PB) assay commercially available according to the manufacturer's protocol (Invitrogen, Carlsbad, CA, USA). Cytotoxicity assays were performed at different time points of cell treatment using the desired concentration of Fe or oxaliplatin. The viability studies were performed on cells seeded on 24 multiwell plates. For the experiment at 24 h, 100,000 cells were seeded, for 48 h 80,000 and for 72 h 70,000 cells. Each experiment was measured in triplicate. After the incubation time, the medium was replaced by fresh medium supplemented with 10% Presto Blue reagent and the cells incubated at 37 °C for 2 h in 5% CO_2. After, the medium of each experiment was transferred to a 96 well-plate and the absorbance of the solutions measured for 570 nm and 600 nm. The viability of each experiment was estimated considering the values measured for the control untreated cells.

DNA extraction

1 mL of DNAzol reagent (Thermo Fisher Scientific, Waltham, USA) was added to adherent or in suspension cells, agitating and pipetting gently. Then, the sample was centrifuge at 10,000 g for 10 min at RT. The supernatant was transferred in a new tube. Subsequently, 0.5 mL of 100% EtOH were added. The mixture was gently shaken for 1-3 min at room temperature. The white DNA precipitate was spool by swirling it onto a pipette tip and then transferred in a clean tube. DNA was washed with 1 mL of 75% EtOH and stored in 95% EtOH before the digestion. An aliquot of the extracted DNA was diluted in 8

mM of NaOH and the absorbance measured at 260 and 280 nm. The A_{260}/A_{280} value calculated was 1.9, and can be considered acceptable as indicated on the protocol of the kit. The amount of the isolated DNA was determined by the following formula:

$$\mu g\ DNA/mL = A_{260}\ X\ dilution\ X\ 50 \qquad (3)$$

Drug release experiment

The release of the oxaliplatin from the nanocubes was estimated *via* ICP-AES by analyzing the supernatants and the samples, after the incubation of the nanoparticles in different solutions. PBS 10 mM, pH=7.4 was used as physiological pH, at which no release is expected. The endosome, late endosome and lysosome environment was reproduce with citrate buffer 10 mM, pH=5.5, 5 and 4.5 respectively. Nanocubes were dissolved in 500 µL of the interesting buffer, at the concentration of 2 g/L, in an amicon (cutoff 100,000 g/mol), for 24 h at 37 °C. Afterwards, the nanoparticles were centrifuged for 12 min at 2,800 rpm and the excluded volume and sample collected for the analysis.

Comet assay

Single-cell gel electrophoresis assay was carried out accordingly to a procedure found in literature.[47] For the assay, IGROV-1cells were seeded on 24 multiwell plates. For the experiment at 24 h, 100,000 cells were seeded, for 48 h 80,000 and for 72 h 70,000 cells. Afterwards, 0.15 g/L of NCs was added to the cells. Then, the doping medium was removed and cells wash with PBS, 10 mM, pH=7.4. The cells were trypsinized and counted. 20,000 cells were dissolved in 400 µL of PBS and added to 1.2 mL of agarose low melting point (Eppendorf, Hamburg, DE) at 37 °C. The solution was gently mixed and 600 µL poured on frosted-end microscope slides pre-coated with 1% agarose low melting point. Alternatively, before pouring, 20,000 cells in 400 µL of PBS were treated with 20 µM of freshly prepared H_2O_2 for 1 h, at 37 °C.[46] The agarose was left dried and the slides submerged in freshly prepared alkaline lysis solution (1.2 M NaCl, 100 mM Na_2EDTA, 0.1% T20, 0.26 M NaOH, pH > 13), O.N. at 4 °C. Subsequently, the slide was wash three times in alkaline rinse solution (0.03 M NaOH, 2 mM Na_2EDTA , pH ~12.3) and submerged, within the same fresh buffer, in an electrophoretic chamber. Electrophoresis was run for 20 min at 15 V. The slides were removed from the electrophoretic chamber and washed three times with 200 mL of distilled water. Afterwards, DNA was staining with 2.5 µg/mL of propidium iodide (PI, Merck, Kenilworth, USA), for 20 min. The slides were washed three times with 200 mL of distilled water, in order to remove the excess of PI. After the staining, the comet images were immediately acquired using a Nikon A1 laser scanning confocal microscope, with a 10X objective. The experiment for each sample was repeated four times. At least 30 comets images were acquired. Comet images were analyzed and the Olive Tail Moment (OTM) determined using OpenComet for ImageJ (http://rsb.info.nih.gov/ij/).

Magnetic hyperthermia cell studies

For magnetic hyperthermia analyses of biological samples, approximately $3x10^6$ cells were trypsinized and resuspended in 100 µL of medium, inside a small glass vial. A nanoScale DM100 Series (Biomagnetics Corp.) generated the alternating magnetic field. The frequency was set at 182 kHz and the field was adjusted by the instrument in order to reach the user set temperature of 42 °C. Two consecutive cycles of 30 min each, separated by 10 min of pause, were repeated.

Trypan blue viability assay

Cells viability was estimated *via* Trypan Blue solution (Merck, Kenilworth, USA) in equal volume with a solution of cells opportunely diluted (usually 1:10). The count of the cells was done using Bright-line hemacytometer **(**Merck, Kenilworth, USA) and Motic AE31 microscope.

LDH viability assay

The cell membrane damages and the consequent release of LDH enzyme was estimated using Lactate Dehydrogenase Activity Assay Kit (Merck, Kenilworth, USA). To do that 50,000 IGROV-1 cells, from the control experiments or incubation/hyperthermia experiments, were diluted in 200 μL of serum-free RPMI medium for 1 h. Subsequently, the cells were pelleted at 1,000 rpm for 5 min and the supernatant collected. 50 μL of supernatant were added to 100 μL of reagent mixture in a 96 well-plate and incubated for 15 min at 37 °C. The absorbance of the solutions were measured at 490 nm and 690 nm. The LDH release of each experiment was estimated considering the values measured for the control untreated cells.

3.5 References

1. Guardia, P., et al., *Water-Soluble Iron Oxide Nanocubes with High Values of Specific Absorption Rate for Cancer Cell Hyperthermia Treatment.* Acs Nano, 2012. **6**(4): p. 3080-3091.
2. Pablo Guardia, A.R., Simone Nitti, Giammarino Pugliese, Sergio Marras, Alessandro Genovese, Maria Elena Materia, Christophe Lefevre, Liberato Manna and Teresa Pellegrino, *One pot synthesis of monodisperse water soluble iron oxide nanocrystals with high values of the specific absorption rate.* J. Mater. Chem. B, 2014. **2**: p. 4426-4434.
3. *Stat bite: Relative survival rates of ovarian cancer by stage, 1992-1999.* J Natl Cancer Inst, 2004. **96**(2): p. 96.
4. Quarta, A., et al., *Targeting FR-expressing cells in ovarian cancer with Fab-functionalized nanoparticles: a full study to provide the proof of principle from in vitro to in vivo.* Nanoscale, 2015. **7**(6): p. 2336-51.
5. Foster, R., R.J. Buckanovich, and B.R. Rueda, *Ovarian cancer stem cells: working towards the root of stemness.* Cancer Lett, 2013. **338**(1): p. 147-57.
6. Scarberry, K.E., et al., *Magnetic nanoparticle-peptide conjugates for in vitro and in vivo targeting and extraction of cancer cells.* J Am Chem Soc, 2008. **130**(31): p. 10258-62.
7. Scarberry, K.E., et al., *Selective removal of ovarian cancer cells from human ascites fluid using magnetic nanoparticles.* Nanomedicine, 2010. **6**(3): p. 399-408.
8. Leung, A.W., et al., *Harnessing the potential of lipid-based nanomedicines for type-specific ovarian cancer treatments.* Nanomedicine (Lond), 2014. **9**(3): p. 501-22.
9. Kolosnjaj-Tabi, J., et al., *Heat-Generating Iron Oxide Nanocubes: Subtle "Destructurators" of the Tumoral Microenvironment.* Acs Nano, 2014. **8**(5): p. 4268-4283.
10. Dilruba, S. and G.V. Kalayda, *Platinum-based drugs: past, present and future.* Cancer Chemotherapy and Pharmacology, 2016. **77**(6): p. 1103-1124.
11. Martelli, L., et al., *Different accumulation of cisplatin, oxaliplatin and JM216 in sensitive and cisplatin-resistant human cervical tumour cells.* Biochemical Pharmacology, 2006. **72**(6): p. 693-700.
12. LaRocca, R.V., et al., *Compassionate-use oxaliplatin with bolus 5-fluorouracil/leucovorin in heavily pretreated patients with advanced colorectal cancer.* Southern Medical Journal, 2004. **97**(9): p. 831-835.
13. Joanne Graham, M.M.a.P.K., *Oxaliplatin.* Nature Reviews, 2004. **3**.
14. Perego, P. and J. Robert, *Oxaliplatin in the era of personalized medicine: from mechanistic studies to clinical efficacy.* Cancer Chemother Pharmacol, 2016. **77**(1): p. 5-18.
15. Liu, D.M., et al., *Self-assembled nanoscale coordination polymers with trigger release properties for effective anticancer therapy.* Nature Communications, 2014. **5**.
16. Rodriguez-Vazquez, N., et al., *cis-Platinum Complex Encapsulated in Self-Assembling Cyclic Peptide Dimers.* Org Lett, 2017. **19**(10): p. 2560-2563.
17. Figini, M., et al., *Panning phage antibody libraries on cells: Isolation of human Fab fragments against ovarian carcinoma using guided selection.* Cancer Research, 1998. **58**(5): p. 991-996.
18. Mazzucchelli, S., et al., *Multiple Presentation of Scfv800E6 on Silica Nanospheres Enhances Targeting Efficiency Toward HER-2 Receptor in Breast Cancer Cells.* Bioconjugate Chemistry, 2011. **22**(11): p. 2296-2303.

19. Sapsford, K.E., et al., *Functionalizing nanoparticles with biological molecules: developing chemistries that facilitate nanotechnology.* Chem Rev, 2013. **113**(3): p. 1904-2074.
20. Sasikala, A.R.K., et al., *A smart magnetic nanoplatform for synergistic anticancer therapy: manoeuvring mussel-inspired functional magnetic nanoparticles for pH responsive anticancer drug delivery and hyperthermia.* Nanoscale, 2015. **7**(43): p. 18119-18128.
21. Huang, X., et al., *Magnetic Fe3O4 nanoparticles grafted with single-chain antibody (scFv) and docetaxel loaded beta-cyclodextrin potential for ovarian cancer dual-targeting therapy.* Materials Science & Engineering C-Materials for Biological Applications, 2014. **42**: p. 325-332.
22. Sun, X., et al., *A pH-Responsive Yolk-Like Nanoplatform for Tumor Targeted Dual-Mode Magnetic Resonance Imaging and Chemotherapy.* Acs Nano, 2017. **11**(7): p. 7049-7059.
23. Patra, S., et al., *Dual-Responsive Polymer Coated Superparamagnetic Nanoparticle for Targeted Drug Delivery and Hyperthermia Treatment.* ACS Applied Materials & Interfaces, 2015. **7**(17): p. 9235-9246.
24. Di Corato, R., et al., *Water solubilization of hydrophobic nanocrystals by means of poly(maleic anhydride-alt-1-octadecene).* Journal of Materials Chemistry, 2008. **18**(17): p. 1991-1996.
25. Pellegrino, T., et al., *Hydrophobic nanocrystals coated with an amphiphilic polymer shell: A general route to water soluble nanocrystals.* Nano Letters, 2004. **4**(4): p. 703-707.
26. Quarta, A., et al., *Multifunctional nanostructures based on inorganic nanoparticles and oligothiophenes and their exploitation for cellular studies.* Journal of the American Chemical Society, 2008. **130**(32): p. 10545-10555.
27. Sperling, R.A., et al., *Electrophoretic separation of nanoparticles with a discrete number of functional groups.* Advanced Functional Materials, 2006. **16**(7): p. 943-948.
28. Casula, M.F., et al., *Manganese doped-iron oxide nanoparticle clusters and their potential as agents for magnetic resonance imaging and hyperthermia.* Physical Chemistry Chemical Physics, 2016. **18**(25): p. 16848-16855.
29. Cabrera, D., et al., *Unraveling viscosity effects on the hysteresis losses of magnetic nanocubes.* Nanoscale, 2017. **9**(16): p. 5094-5101.
30. Cabrera, D., et al., *Influence of the aggregation, concentration, and viscosity on the nanomagnetism of iron oxide nanoparticle colloids for magnetic hyperthermia.* Journal of Nanoparticle Research, 2015. **17**(3).
31. Sapsford, K.E., et al., *Functionalizing Nanoparticles with Biological Molecules: Developing Chemistries that Facilitate Nanotechnology.* Chemical Reviews, 2013. **113**(3): p. 1904-2074.
32. De, M., S. Rana, and V.M. Rotello, *Nickel-Ion-Mediated Control of the Stoichiometry of His-Tagged Protein/Nanoparticle Interactions.* Macromolecular Bioscience, 2009. **9**(2): p. 174-178.
33. Hauptmann, N., et al., *Ni(II)-NTA Modified Poly(ethylene imine) Glycopolymers: Physicochemical Properties and First In Vitro Study of Polyplexes Formed with HIV-Derived Peptides.* Macromolecular Bioscience, 2013. **13**(5): p. 531-538.
34. Galbiati, E., et al., *Peptide-nanoparticle ligation mediated by cutinase fusion for the development of cancer cell-targeted nanoconjugates.* Bioconjug Chem, 2015. **26**(4): p. 680-9.
35. Stella, B., et al., *Design of folic acid-conjugated nanoparticles for drug targeting.* Journal of Pharmaceutical Sciences, 2000. **89**(11): p. 1452-1464.
36. D'Anto, V., et al., *Effect of nickel chloride on cell proliferation.* Open Dent J, 2012. **6**: p. 177-81.
37. Boncler, M., et al., *Comparison of PrestoBlue and MTT assays of cellular viability in the assessment of anti-*

proliferative effects of plant extracts on human endothelial cells. J Pharmacol Toxicol Methods, 2014. **69**(1): p. 9-16.
38. Erba, E., et al., *Isolation and characterization of an IGROV-1 human ovarian cancer cell line made resistant to Ecteinascidin-743 (ET-743).* Br J Cancer, 2000. **82**(10): p. 1732-9.
39. Rothberg, K.G., et al., *The Glycophospholipid-Linked Folate Receptor Internalizes Folate without Entering the Clathrin-Coated Pit Endocytic Pathway.* Journal of Cell Biology, 1990. **110**(3): p. 637-649.
40. Woynarowski, J.M., et al., *Oxaliplatin-induced damage of cellular DNA.* Molecular Pharmacology, 2000. **58**(5): p. 920-927.
41. Levy, M., et al., *Degradability of superparamagnetic nanoparticles in a model of intracellular environment: follow-up of magnetic, structural and chemical properties.* Nanotechnology, 2010. **21**(39): p. 395103.
42. Gutierrez, L., et al., *Degradation of magnetic nanoparticles mimicking lysosomal conditions followed by AC susceptibility.* Biomed Tech (Berl), 2015. **60**(5): p. 417-25.
43. Jerremalm, E., et al., *Oxaliplatin degradation in the presence of chloride: identification and cytotoxicity of the monochloro monooxalato complex.* Pharm Res, 2004. **21**(5): p. 891-4.
44. Han, C.H., et al., *Predicting effects on oxaliplatin clearance: in vitro, kinetic and clinical studies of calcium- and magnesium-mediated oxaliplatin degradation.* Sci Rep, 2017. **7**(1): p. 4073.
45. Reardon, J.T., et al., *Efficient Nucleotide Excision Repair of Cisplatin, Oxaliplatin, and Bis-aceto-ammine-dichloro-cyclohexylamine-platinum(IV) (JM216) PlatinumIntrastrand DNA Diadducts.* Cancer Research, 1999. **59**(16): p. 3968-3971.
46. Almeida, G.M., et al., *Detection of oxaliplatin-induced DNA crosslinks in vitro and in cancer patients using the alkaline comet assay.* DNA Repair, 2006. **5**(2): p. 219-225.
47. Olive, P.L. and J.P. Banath, *The comet assay: a method to measure DNA damage in individual cells.* Nature Protocols, 2006. **1**(1): p. 23-29.
48. Di Corato, R., et al., *Magnetic hyperthermia efficiency in the cellular environment for different nanoparticle designs.* Biomaterials, 2014. **35**(24): p. 6400-11.
49. Strober, W., *Trypan blue exclusion test of cell viability.* Curr Protoc Immunol, 2001. **Appendix 3**: p. Appendix 3B.
50. Cummings, B.S. and R.G. Schnellmann, *Measurement of cell death in mammalian cells.* Curr Protoc Pharmacol, 2004. **Chapter 12**: p. Unit 12 8.